Observational Studies of the Chemical Evolution in the Galactic Thin and Thick Disks

Bensby, Thomas

2004

Observational Studies of the Chemical Evolution in the Galactic Thin and Thick Disks

Observational Studies of the Chemical Evolution in the Galactic Thin and Thick Disks

Thomas Bensby

Thesis for the degree of Doctor of Philosophy
(Avhandling för filosofie doktorsexamen)
Lund Observatory
Sweden
2004

LUND UNIVERSITY

To be publicly defended,
with permission of the Lund University Faculty of Science,
in the Lundmark lecture hall of Lund Observatory
on Saturday, the 27th of March 2004, at 10.15 a.m.

Thesis advisers:

Dr. Sofia Feltzing
Dr. Ingemar Lundström (assistant adviser)
Lund Observatory

Faculty Opponent:

Prof. Gerard Gilmore
Institute of Astronomy, University of Cambridge
United Kingdom

Evaluation Committee:

Dr. Vanessa Hill
Observatoire de Paris - Section de Meudon
France

Prof. Sveneric Johansson
Atomic Astrophysics, Lund Observatory

Prof. Poul Erik Nissen
Dep. of Physics and Astronomy, University of Aarhus
Denmark

LUNFD6/(NFAS 1028)/1-228/(2004)

ISBN 91-628-5954-4
Printed by KFS AB, Lund 2004

Organization **LUND UNIVERSITY** Lund Observatory Box 43 221 00 Lund, Sweden	**Document Name** **DOCTORAL DISSERTATION** **Date of issue** March 27, 2004 **CODEN:** LUNFD6/(NFAS 1028)/1-228/(2004)
Author(s) Thomas Bensby	**Sponsoring organization**

Title and subtitle

Observational Studies of the Chemical Evolution in the Galactic Thin and Thick Disks

Abstract

The origin and evolution of the thin and thick disks in the Galaxy have been studied by means of detailed stellar abundances. High-resolution spectra of 102 F and G dwarf stars have been obtained with the spectrographs on the ESO 3.6-m and ESO 1.5-m telescopes on La Silla (Chile), the Very Large Telescope (VLT) on Paranal (Chile), and the Nordic Optical Telescope (NOT) on La Palma (Canary Islands, Spain). Abundances for 14 elements (O, Na, Mg, Al, Si, Ca, Ti, Cr, Fe, Ni, Zn, Y, Ba, and Eu) have been determined. The following results were found: 1) Both the thin and the thick disks show distinct and well-defined abundance trends at sub-solar metallicities; 2) The thick disk shows signatures of chemical enrichment from Type Ia Supernovae; 3) [O/Fe] in the thin disk continues to decrease linearly at super-solar metallicities; 4) The abundance trends we see in the thick disk are invariant with distance from the Galactic plane ($Z_{\rm max}$) and galactocentric radius ($R_{\rm m}$); 4) The thick disk sample is in the mean older than the thin disk sample.

The thesis also includes an investigation of ages and metallicities in the thick disk. The results from this study are; 5) There is a possible age-metallicity relation present in the thick disk, 6) Star formation has been ongoing for several billion years in the thick disk.

Based on these findings, together with other constraints from the literature, we discuss different formation scenarios for the thick disk. We suggest that the currently most likely formation scenario is a violent merger event or a close encounter between the Galaxy and a companion galaxy.

Key words

Stars: fundamental parameters – Stars: abundances – Stars: kinematics – Galaxy: disk – Galaxy: formation – Galaxy: evolution – Galaxy: abundances – Galaxy: kinematics and dynamics – (Galaxy:) solar neighbourhood

Classification system and/or index terms (if any)

Supplementary bibliographical information	**Language** English
ISSN and key title	**ISBN** 91-628-5954-4
Recipient's notes	**Number of pages** 228 **Price**
	Security classification

Distribution by (name and address)

Thomas Bensby, Lund Observatory, Box 43, S-221 00 Lund, Sweden

To Jonna, Sofia, and Alva

Cover: An image that shows $\log(U_{\rm LSR}^2 + V_{\rm LSR}^2 + W_{\rm LSR}^2)$, which is a measure of the kinetic energy relative to LSR, versus the space velocities $U_{\rm LSR}$ (left panel), $V_{\rm LSR}$ (middle panel), and $W_{\rm LSR}$ (right panel) for thin disk (black dots), thick disk (brown dots), and stellar halo (blue dots). The stellar samples have been selected using the following kinematical criteria: $TD/D > 2$ and $TD/H > 1$ for the thick disk; $TD/D < 0.1$ and $TD/H > 1$ for the thin disk; and $TD/D > 1$ and $TD/H < 1$ for the halo stars (see also Chapter 2.2 and Fig. 8).

Image on previous page (p. vii): NGC 4038/4039, The Antennae Galaxies. Colliding galaxies that are located 63 million light-years away in the southern constellation Corvus. *Credit: Brad Whitmore (STScI) and NASA*

Research Articles

This thesis is based on the following research articles:

I. Bensby, T., Feltzing, S., & Lundström, I.:
Elemental abundance trends in the Galactic thin and thick disks as traced by nearby F and G dwarf stars
Astronomy and Astrophysics, **410**, 527–551 (2003)

II. Feltzing, S., Bensby, T., & Lundström, I.:
Signatures of SN Ia in the galactic thick disk – Observational evidence from α-elements in 67 dwarf stars in the solar neighbourhood
Astronomy and Astrophysics, **397**, L1–L4 (2003)

III. Bensby, T., Feltzing, S., & Lundström, I.:
Oxygen trends in the Galactic thin and thick disks
Astronomy and Astrophysics, **415**, 155–170 (2004)

IV. Bensby, T., Feltzing, S., Lundström, I., & Ilyin, I.:
α-, r-, and s-process element trends in the Galactic thin and thick disks
Astronomy and Astrophysics, in preparation

V. Bensby, T., Feltzing, S., & Lundström, I.:
A possible age-metallicity relation in the Galactic thick disk?
Astronomy and Astrophysics, submitted

VI. Feltzing, S., Bensby, T., Primas, F. & Ryan, S.G.:
A first study of the chemical composition in thick disk dwarf stars 1–1.5 kpc above the Galactic plane
DRAFT

Research articles and conference proceedings not included in this thesis:

i. Bensby, T., & Lundström, I.:
The distance scale of planetary nebulae
Astronomy and Astrophysics, **374**, 599–614 (2001)

ii. Bensby, T., Feltzing, S., & Lundström, I.:
Oxygen in the Galactic thin and thick disks
CNO in the Universe, ASP Conference Series, Vol. 304, C. Charbonnel, D. Schaerer, & G. Meynet, eds., pp. 175–178 (2003)

iii. Bensby, T., Feltzing, S., & Lundström, I.:
A differential study of the oxygen abundances in the Galactic thin and thick disks
Carnegie Observatories Astrophysics Series, Vol. 4: Origin and Evolution of the Elements, ed. A. McWilliam and M. Rauch (Pasadena: Carnegie Observatories, `http://www.ociw.edu/ociw/symposia/series/symposium4/proceedings.html`) (2003)

iv. Feltzing, S., Bensby, T., Gesse, S., & Lundström, I.:
Thin and thick disk results for α-, r-, and s-process elements
Carnegie Observatories Astrophysics Series, Vol. 4: Origin and Evolution of the Elements, ed. A. McWilliam and M. Rauch (Pasadena: Carnegie Observatories, `http://www.ociw.edu/ociw/symposia/series/symposium4/proceedings.html`) (2003)

Contents

Chapter 1
Introduction

The story so far:
In the beginning the Universe was created.
This has made a lot of people very angry and been widely regarded as a bad move.

Douglas Adams, The Restaurant at the End of the Universe, 1980

Astronomy is among the oldest of sciences and the observation of stars and celestial phenomena dates back several thousands of years. On a clear and dark night it is possible to see approximately 3000 stars with the naked eye. Looking more carefully it is also possible to see a diffuse band of brightness that stretches across the sky through several of the constellations, e.g., Sagittarius and Cassiopeia. This hazy band of light has since ancient times been imagined as a path of some kind. The Greeks, for instance, imagined it as a stream of milk, or a Milky Way. The Greek word for milk is *galaktos*, from which our modern term *galaxy* originates.

Many centuries later, in 1610, Galileo Galilei turned his telescope towards the Milky Way for the first time and discovered that it was made up of many stars that were too faint to be seen individually by the naked eye. This discovery changed the picture of the Milky Way; it was now "a mass of innumerable stars" instead of being made up of some obscure substance. In the late 18th century Sir William Herschel made the first map of the stars in the Milky Way by making extensive star counts (or "star gauging" as he called it) in various directions (see Fig. 1). He concluded that the Sun is located in the center of the Milky Way (and the Universe) and that the Milky Way is a flattened system of stars with a length roughly three times its height. His idea was based on the assumption that the greater number of stars in a given direction the greater the depth of the Milky Way in that direction. The concept of interstellar extinction was unknown to Herschel. This extinction obscures distant stars, making the observable depths into space roughly equal in all directions (at least in the plane of the Milky Way), which resulted in an apparently very central position for the Sun (see Fig. 1). In the early 20th century, the Dutch astronomer

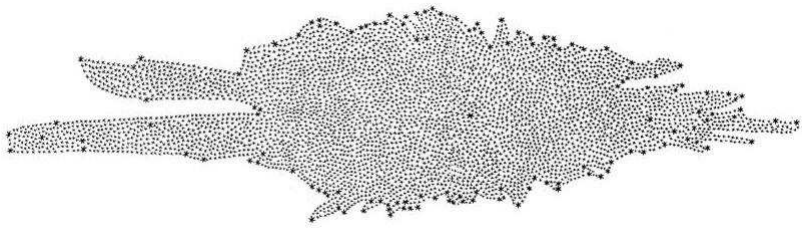

FIGURE 1: Sir William Herschel's map of the Milky Way (from Herschel 1785). The Sun is the brighter star just to the right of the middle. © *The Royal Society*

Jacobus C. Kapteyn extended the work of Herschel. By taking into account the distances to the stars that Herschel had counted, and by assuming that the average brightness of stars decreases as the inverse square of their distance, he came to the conclusion that the density of stars decreases with distance from the Sun in all directions. Since interstellar extinction was unknown to Kapteyn as well, he ended up with the same conclusion as Herschel: that the Sun is at the center of the Milky Way. Another astronomer, Harlow Shapley, was at the same time as Kapteyn studying the distribution of globular clusters in the Milky Way. He found that far more clusters were seen in the direction of Sagittarius than in any other direction. By assuming that all clusters were orbiting the Galactic center he concluded that the center must be in that direction, thousands of light years away from the Sun. Interstellar extinction was unknown to Shapley as well and he estimated the radius of the Milky Way to be about 50 kpc.

The discovery of general interstellar extinction (or reddening) awaited the works by Schalén in 1929 and Trumpler in 1930. The joint conclusion from their studies is that starlight travelling through space is dimmed and that this dimming (or absorption) is more in some regions and less in others. Directions in the plane of the Milky Way are especially affected. Because of this extinction, Herschel and Kapteyn (when they were looking in the plane of the Milky Way) were only seeing nearby stars, and hence their erroneous placement of the Sun.

The famous debate in 1920 between Shapley and Heber D. Curtis dealt with the question, "Are spiral nebulae part of our galaxy or external galaxies unto themselves?" The question was not settled until a few years later, in 1924, when Edwin Hubble discovered individual Cepheid stars in the Andromeda galaxy (at that time referred to as a "nebula"). By determining their distances (through the period-luminosity relation) he confirmed that they were well outside the Milky Way and that indeed these spiral nebulae were other galaxies or "island universes". The Milky Way had now become only one of several billion galaxies in the Universe.

The picture of the Galaxy[1] that has emerged since then, is that it is a flattened stellar

[1] From here on the Milky Way will generally be referred to as the Galaxy with a capital G.

FIGURE 2: A face-on view of the spiral galaxy NGC 1232 observed with the FORS1 instrument on the VLT/ANTU telescope. It is located in the direction of the constellation Eridanus (The River) and lies nearly 100 million light years away. *Credit: European Southern Observatory (ESO) - with whom the copyright rests.*

system where the central parts contain the highest concentration of stars. The Galaxy has also a grand spiral structure, and in this system, our star, the Sun, is located close to the Galactic plane in the Cygnus-Orion spiral arm, approximately 8 kpc from the Galactic center, which we orbit once every 200 million years. Figure 2 shows a face-on image of the spiral galaxy NGC 1232. This galaxy, beautifully displaying the spiral structure, is probably quite similar to the Milky Way. In a colour image, the inner regions of this galaxy looks reddish which is indicative of an old stellar population. The spiral arms, on the other hand, are bluish in colour representative of ongoing star formation. The edge-on appearance of a spiral galaxy is completely different from the face-on appearance. An example of a galaxy seen edge-on is NGC 891 which is shown in Fig. 3. The dark band seen along the disk of NGC 891 originates from the fact that gas and dust obscure parts of the galaxy and thereby

FIGURE 3: An edge-on view of the spiral galaxy NGC 891 which lies nearly 10 million light years from us in the direction of the constellation Andromeda. The individual stars that can be seen are nearby stars that are part of the Galaxy. *Credit: Adam Block/NOAO/AURA/NSF*

reduce the amount of light in our direction. The scattered stars seen in Fig. 3 do not belong to NGC 891 but are foreground stars in our Galaxy.

The Galaxy is now thought to be made up of four major structural components: the stellar halo (which should not be confused with the dark matter halo); the bulge; the thin disk; and the thick disk. Figure 4 shows a schematic edge-on view of the Galaxy.

The stellar halo: The stellar halo of the Galaxy is an essentially non-rotating spherical system of old and metal-poor stars that move on almost random orbits in their journeys around the Galactic center. As the stellar density in the halo is very low (compared to the other components) only 1–2 out of 1000 stars in the solar neighbourhood can be attributed to the halo (e.g., Fuhrmann 2002, and references therein). However, their extreme kinematical properties make them quite easy to identify, and in the solar neighbourhood they are represented by the high-velocity stars. Studies of such stars show that the halo stars are amongst the oldest dateable entities in the Galaxy (e.g., Unavane et al. 1996; Cayrel et al. 2001; Ortolani et al. 1995). Their absolute ages are, however, not easy to determine. Normally the uncertainties are of the order of a few billion years. Obviously, these stars can not be older than the Universe. According to the most recent estimates, the Universe has an age of 13.7 billion years (Spergel et al. 2003).

The metallicity[2] distribution of the halo stars peaks at [Fe/H] ≈ -1.6 with tails ranging from the lowest observed metallicities ([Fe/H] < -5) on one side, and to metallicities almost reaching solar values on the other (e.g., Laird et al. 1988; Wyse & Gilmore 1995).

[2]See Chapter 4 for a definition of the notation of elemental abundances

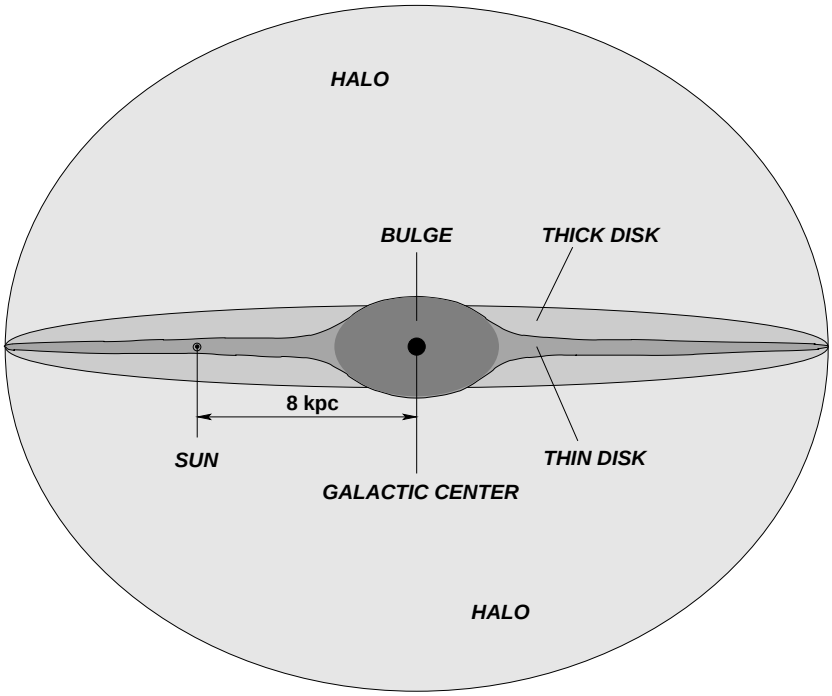

FIGURE 4: A schematic view of the Galaxy. The four major stellar components, the position of the Sun, and the Galactic center have been marked.

The bulge: The bulge is the stellar component in the central regions of the Galaxy (see, e.g., the review by Wyse et al. 1997). It is a flattened ellipsoid of stars that have a vertical scale height of ~ 350 pc. Its minor-to-major axis ratio is about 0.5. Bulge stars are generally believed to make up an old stellar population with ages greater than 10 Gyr and a metallicity distribution that peaks just below the solar value (e.g., McWilliam & Rich 1994). However, the metallicity distribution is rather broad, reaching below [Fe/H] $= -1$, and stars as young as a few hundred million years have been found (e.g., Gilmore 2003), which indicates a more complicated picture of the bulge population.

The thick disk: The thick disk stellar component was first discovered through star counts by Gilmore & Reid (1983). They found that the vertical density distribution of stars in the disk could not be well fitted by one single exponential profile. A better match was achieved by combining two independent exponential profiles with scale-heights of ~ 300 pc and ~ 1450 pc, respectively. The component with the small scale-height was identified as the Galactic thin disk, and the other component as a Galactic thick disk, which they estimated to make up approximately 2 % of the stellar content in the solar neighbourhood. The average Galactic rotational velocity of the thick disk is about ~ 170–180 km s^{-1}, i.e. it lags

behind the thin disk by some 40–50 km s^{-1}. The large scale-height means that the thick disk stellar population has a relatively high velocity dispersion in order for its stars to reach the large distances from the Galactic plane (see also Chapter 2.1).

All investigations more or less agree that the stellar population of the thick disk is old, ranging from ~ 7 Gyr all the way up to ages comparable to the oldest halo stars (i.e., well above 12 Gyr); see, e.g., Fuhrmann (1998). The metallicity distribution of the thick disk stars peaks somewhere in the interval $-0.7 \lesssim$ [Fe/H] $\lesssim -0.5$ (e.g., Wyse & Gilmore 1995). Stars with super-solar metallicities that have typical thick disk kinematical properties have also been found (see, e.g., Paper I). Whether or not these stars really belong to the thick disk stellar population is difficult to settle. They have in general quite large velocities in the direction towards or away from the Galactic center, implying a possible origin in the inner parts of the Galaxy or even in the bulge (compare, e.g., Pompéia et al. 2002).

The thin disk: The thin disk is the Galactic component in which active star formation currently is taking place. This generally happens in the regions of the spiral arms close to the Galactic plane that are especially rich in gas and dust. As a result the stellar population of the thin disk is young. Newly formed stars essentially follow almost circular orbits around the Galactic center with a very small vertical velocity component (i.e., they are confined to the plane). These stars make up what is sometimes referred to as the *extreme* thin disk (e.g., Buser 2000). In time the stars will interact gravitationally with other stars and, especially, molecular gas clouds. This will make their orbits more elliptical and with a larger vertical velocity component, and these more typical thin disk stars show a vertical scale height of 200–300 pc.

The majority of the stars in the thin disk are quite young and have formed out of interstellar gas that has been enriched by heavier elements from previous stellar generations. The thin disk stars therefore normally have higher metallicities than the halo and thick disk stars. The metallicity distribution peaks at [Fe/H] ≈ -0.2 and ranges from [Fe/H] ≈ -0.8 up to super-solar values of [Fe/H] $\approx +0.5$ (e.g., Wyse & Gilmore 1995).

Only recently have we started to understand how all these different stellar populations and Galactic structures formed and how they relate to each other. The picture is, however, still far from complete (e.g., Gilmore et al. 1989; Majewski 1993; Silk & Wyse 1993; McWilliam 1997; Freeman & Bland-Hawthorn 2002).

The relationships between the different stellar populations are unclear, showing overlaps in age and metallicity, as well as in the kinematical distributions. Studies of the specific angular momentum of the populations, however, indicate that the Galaxy can be divided into two discrete entities: the halo/bulge with low angular momentum, and the thick disk/thin disk with high angular momentum (Wyse & Gilmore 1992). This would lead to a picture where the halo evolves, while conserving angular momentum, directly into the bulge and then, somewhat later, the disk forms.

The questions why the Galaxy contains two disk populations, with apparently very different distributions in age and metallicity, and why the thick disk is thick, have several

proposed answers (see, e.g., the review by Gilmore et al. 1989). The main formation scenarios for the thick disk are: (1) First there was a thin disk and then as a result of a merger with a companion galaxy the stellar population in the old disk got "puffed" up and formed what we today see as the thick disk; (2) Kroupa (2002) has shown that galaxies do not have to merge during an encounter to produce a kinematical heating of a pre-existing gaseous galactic disk and increased star formation; (3) The thick and thin disks form an evolutionary sequence, i.e., in a dissipational collapse of the proto-galactic cloud the thick disk formed first and later the thin disk (e.g., Burkert et al. 1992).

Low-mass stars – fossils in the Milky Way

One way to put further constraints on possible thick disk formation scenarios is to compare the chemical compositions of large samples of thick and thin disk stars. Low-mass F and G dwarf stars are ideal tracers of the history of Galactic chemical evolution since the compositions of their atmospheres are representative of the interstellar medium out of which they formed, and because their expected life-times exceed the age of the Galaxy.

Since the overall metallicity is expected to increase with time (although low [Fe/H] does not necessarily mean high age) it is possible to analyze how the interstellar medium, and thereby the Galaxy, has evolved with time.

Unless dealing with the absolute first generation of stars (Pop III) one can expect that the low-mass stars we see today have been formed from gas that has been polluted by stars that existed earlier. This is reflected by the wealth of spectral lines from many different elements that can be seen in a stellar spectrum (see, e.g., the spectrum in Appendix D). But how were these elements formed and how were they dispersed into the interstellar medium?

Nucleosynthesis and the enrichment of the interstellar medium

Nuclei of heavy elements are built in the interiors of stars, where the temperature and pressure are high enough for nuclear fusion reactions to take place. These reactions also go under the term *stellar nucleosynthesis*. Except for hydrogen, helium and some lithium that were created in the fiery repercussions of the Big Bang (see, e.g., review by Boesgaard & Steigman 1985), all of the rest of the elements in the Universe have been produced in the interiors of stars (see, e.g., review by Wallerstein et al. 1997).

However, all types of elements are not made in all types of stars. Figure 5 shows the typical internal structures of evolved low-mass and high-mass stars. Very low-mass stars can only synthesize the second lightest element, helium. Stars that are as heavy as our own Sun and up to about eight solar masses ($8\,M_\odot$) can in their later phases synthesize heavier elements such as carbon and oxygen. Even more massive stars (i.e., $\mathcal{M} \gtrsim 8\,M_\odot$) can synthesize all elements with atomic numbers equal to or less than that of iron, e.g., O, Na, Mg, Al, Si, Ca, Ti, Cr, and Fe. This is as far as the chain of nuclear reactions can proceed in the build-up of elements during normal burning phases in the stellar interiors.

The production of elements heavier than iron requires environments with a considerable neutron flux. Such environments are created when massive stars run out of fuel and explode

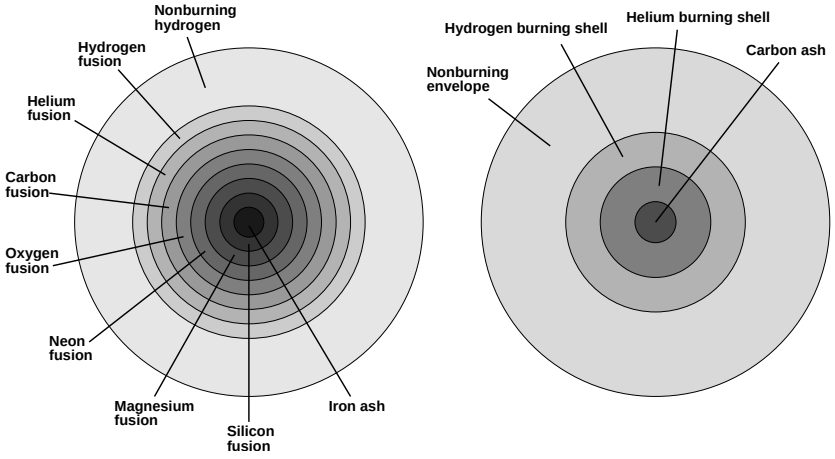

FIGURE 5: Schematic illustration (not to scale) of the "onion-skin" structure in the interior of highly evolved stars. To the left is shown a massive star ($\mathcal{M} \gtrsim 10\,\mathrm{M}_\odot$) and to the right a less massive star ($\mathcal{M} \lesssim 8\,\mathrm{M}_\odot$).

as core-collapse supernovae type II (SN II) (e.g., Arnett 1996), or in low and intermediate mass stars on the asymptotic giant branch, so-called AGB stars, (e.g., Busso et al. 1999). These elements will be dispersed into the interstellar medium through either supernovae explosions or the strong stellar winds that the AGB stars experience. Another production site of elements are supernovae type Ia (SN Ia). The exact mechanisms for these events are not known, but most likely they are binary stellar systems, that generally are thought to consist of a white dwarf and a red giant that loses mass onto the surface of the white dwarf. Eventually the white dwarf will be driven over the Chandrasekhar mass limit and undergo a thermal explosion (see, e.g., Livio 2001). SN Ia events mainly produce iron peak elements (e.g., Cr, Fe, Ni) and none or only very little of other elements (such as the α-elements, O, Mg, Si, Ca, and Ti); e.g., Thielemann et al. (2002). The intense winds from very massive stars, Wolf-Rayet stars, can also substantially contribute to the enrichment of the interstellar medium, especially for the CNO elements (e.g., Maeder 2000).

The above mentioned SN events and stellar winds cause heavy elements to be dispersed and mixed into the interstellar medium. Later generations of stars will then form from an enriched interstellar medium. Since the lifetimes of the progenitors of SN II are of the order 10–100 times shorter than those of the progenitors of the SN Ia, the chemical enrichment will be very different at different epochs in a stellar population. The massive stars will contribute early in the history (with large amounts of α-elements), while the contributions (e.g., of iron) from the low-mass stars will be delayed (see Tinsley 1979). The time-scale for the enrichment from AGB stars is (probably) of the same order as that for SN Ia, i.e., they will contribute considerably later than the high mass stars. By studying abundance ratios of various elements it is therefore possible to derive how chemical properties of a stellar

population have evolved with time (see also Chapter 5.2).

Aim and scope of thesis

The main purpose of this thesis work has been to investigate the chemical evolution of the thick disk, and to compare it with that of the thin disk, in order to put further constraints on their respective origins. Another major aim has been to define the oxygen trend above solar metallicity. When selecting stars for the different studies we have solely relied on kinematical criteria, since they are what ultimately defines the Galactic thick disk.

In a way, the projects presented in this thesis followed from a three-week project assignment during the first months of my PhD work, in the Spring of 1999, where I investigated the errors in [O/Fe] for different signal-to-noise ratios and resolutions. This three-week project resulted in an ESO observation proposal (#65.L-0019), which was accepted, and the first observations were carried out in September 2000.

The idea behind the studies was to establish the oxygen trends in the thin and thick disk. The results presented in Paper III are actually the joint results from two observational projects where we aimed to study (1) the oxygen trends in the metal-rich thin disk (i.e., [Fe/H] > 0), and (2) the differences between the the thin and thick disks at sub-solar metallicities (i.e., [Fe/H] < 0). In order to derive as accurate oxygen abundances as possible we wanted to observe the stars with two different instruments: (1) the ESO 3.6-m and the CES spectrograph with its very high resolution enabling proper modeling of the faint forbidden [O I] line at 6300 Å, and (2) the ESO 1.5-m and the FEROS spectrograph with its complete wavelength coverage from about 3800 Å to 9000 Å, which allowed us to derive accurate iron and nickel abundances by measuring hundreds of spectral lines. The FEROS spectra were then also utilized for other elemental abundances (Papers I and II). The results presented in those papers inspired us to apply for observing time at the NOT telescope to observe a northern sample of thin and thick disk stars in order to verify and strengthen the abundance trends, especially at sub-solar metallicities, from the southern FEROS sample (Paper IV). The stars for the observing runs in Chile and on the Canary Islands were selected from a larger catalogue of stars containing ~ 4500 stars. This catalogue was then used for a study where we probe the thick disk for an age-metallicity relation that is presented in Paper V.

This thesis work consists of the 6 research articles (Papers I–VI). The following chapters serve as a short summary of the work and results that are presented in the articles. Also, some further background information are given.

Chapter 2
The stellar sample

If it looks like a duck, and quacks like a duck, we have at least to consider the possibility that we have a small aquatic bird of the family anatidae on our hands.

Douglas Adams, Dirk Gently's Holistic Detective Agency, 1987

All stars used in this thesis have been selected from a catalogue of approximately 4500 stars that was prepared for the studies by Feltzing & Holmberg (2000) and Feltzing et al. (2001). The stars in the catalogue have been selected from the Hipparcos catalogue (ESA 1997) with the following constraints: the relative errors in their parallaxes should be less than 25% (note that all stars flagged as either binaries or likely binaries have been rejected, nevertheless, previously unknown binaries remain, see Table A2); the stars should have measured radial velocities in the compilation by Barbier-Brossat et al. (1994). This resulted in a sample of $\sim$ 12600 stars. By adding the constraint that the stars should have Strömgren *uvby* photometry, and hence estimates of their metallicities [Me/H][3], from the compilation by Hauck & Mermilliod (1998) the sample further shrinks to about 4500 stars.

Since the stars in the catalogue have distances of approximately 100–200 parsecs from the Sun, they are all more or less located in the Galactic plane. The definition of the thick disk is that the orbits of its stars are likely to reach larger distances from the plane than those in the thin disk. This will be reflected in that thick disk stars typically have higher velocities when they cross the Galactic plane than the thin disk stars. The thick disk stellar orbits are also less circular than the thin disk ones, and the thick disk is also known to have a lower average Galactic rotation than the thin disk. As our main purpose is to investigate the chemical properties of the two disks we will not use chemical criteria but simply rely on kinematical criteria in order to distinguish between stars from the two populations in the solar neighbourhood.

[3]Metallicities derived from photometry, [Me/H], are usually measures of the content of all elements heavier than helium, whereas spectroscopic metallicities, [Fe/H], are measures of the content of iron atoms.

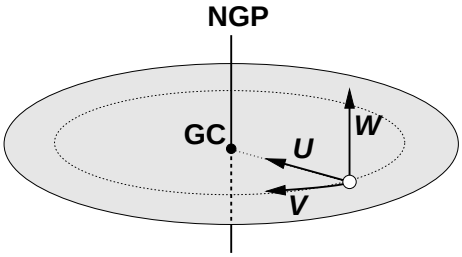

FIGURE 6: Illustration of the U, V, and W velocity components. The Galactic Center (GC) and the North Galactic Pole (NGP) have been marked.

Before describing the kinematical selection criteria some kinematical terms and typical data for the different stellar populations will be summarized.

2.1 Some kinematical terms

Galactic space velocities

When describing kinematical properties of stellar populations in the Galaxy it is convenient to use velocities that have the Galaxy itself as the reference. Such a system can be obtained by decomposing the velocity of a star into the following three velocity components (see Fig. 6):

- $U_{\rm LSR}$: Velocity component in the direction of the Galactic center. The definition used here is that positive velocities are directed towards the Galactic center. The opposite definition can also be found in the literature.
- $V_{\rm LSR}$: Velocity component in the direction of the Galactic rotation.
- $W_{\rm LSR}$: Velocity component perpendicular to the Galactic plane. Positive towards the North Galactic Pole.

The sub-script "LSR" indicates that the velocities are given relative to the local standard of rest (LSR) which is the current velocity of a fictional particle in the Galactic plane that moves around the Galactic center on a perfect circular orbit that passes through the present location of the Sun (see, e.g., Binney & Merrifield 1998). The total space velocity relative to the LSR, or the *peculiar* velocity, is given by:

$$v_{\rm pec} = \sqrt{U_{\rm LSR}^2 + V_{\rm LSR}^2 + W_{\rm LSR}^2}. \quad (1)$$

The $U_{\rm LSR}$, $V_{\rm LSR}$, and $W_{\rm LSR}$ velocities can be determined if the positions on the sky (RA and DEC), the distances (or parallaxes), the proper motions (μ_α and μ_δ), and the radial velocities ($v_{\rm r}$) of the stars are known (see Eqs. (A.1) – (A.4) in Paper I). The Sun is assumed

TABLE 1: Characteristic velocity dispersions (σ_U, σ_V, and σ_W) in the thin disk, thick disk, and stellar halo. X is the observed fraction of stars for the populations in the solar neighbourhood and $V_{\rm asym}$ is the asymmetric drift. Values are taken from Papers I and IV.

	X	σ_U	σ_V	σ_W	$V_{\rm asym}$
		—— [km s^{-1}] ——			
Thin disk (D)	0.90	35	20	16	-15
Thick disk (TD)	0.10	67	38	35	-46
Halo (H)	0.0015	160	90	90	-220

to move with $(U_\odot, V_\odot, W_\odot) = (+10.00, +5.25, +7.17)$ km s^{-1} relative to the LSR (Dehnen & Binney 1998).

Velocity dispersions

Stellar systems, or populations, can be kinematically characterized by the velocity dispersions, or the size of the "scatter" around the mean velocity of all stars in the system. The dispersions for the $U_{\rm LSR}$, $V_{\rm LSR}$, and $W_{\rm LSR}$ velocities are denoted by σ_U, σ_V, and σ_W, respectively. The velocity dispersions that we have assumed for the different stellar populations are given in Table 1.

Larger dispersions indicate "hotter" kinematics. The dispersion of a stellar population is expected to increase with time due to the gravitational interaction that the stars experience with neighbouring stars and due to "collisions" with molecular clouds as they rotate around the Galactic center. However, it should be noted that simulations show that such events do not produce the sufficient heating in order to account for the hot kinematics that is observed in today's thick disk stellar population (e.g., Hänninen & Flynn 2002).

Asymmetric drifts

The asymmetric drift ($V_{\rm asym}$) is how much a stellar population lags behind the LSR in the general Galactic rotation. The LSR rotates around the Galactic center at approximately 220 km s^{-1}. The stellar halo is essentially a non-rotating system and therefore its stars have an asymmetric drift of -220 km s^{-1}. The values for the asymmetric drifts used here for the different stellar populations are given in Table 1.

Solar neighbourhood stellar density

The stellar content of the solar neighbourhood is a mixture of stars from the thin disk, thick disk, and halo (and bulge?). Figure 7 shows a schematic picture of how the densities of the different populations change as one goes to greater distances from the Galactic plane. Since the scale heights for the thin disk, thick disk, and halo populations are different, their respective stellar density will drop off at different rates. The thin disk is the dominant

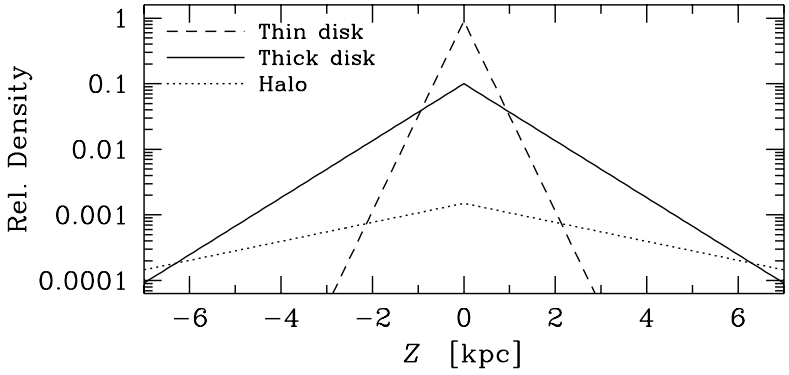

FIGURE 7: Sketch of the stellar densities of the thin disk, thick disk, and halo stellar populations as functions of vertical distance (Z) from the Galactic plane. For simplicity, exponential distributions have been assumed in the figure. The densities in the solar neighbourhood are here taken to be 0.9, 0.10, and 0.0015 for the thin disk, thick disk, and halo, respectively, and their respective scale heights are 0.3, 1.0, and 3.0 kpc.

population in the solar neighbourhood, making up about 90 % of its stellar content, whereas the thick disk make up about 10 % (see the Appendix of Paper IV for a further discussion). But, as can be seen in Fig. 7, already at 1000 pc the thick disk population starts to dominate over the thin disk due to the larger scale height of the thick disk. Halo stars are rare in the solar neighbourhood. The distance where the halo stars start to dominate is dependent on the scale height for the halo but lies most probably somewhere beyond 5 kpc from the Galactic plane (see Fig. 7).

2.2 Kinematical selection criteria

Since the thick disk stellar population have much hotter kinematics and larger asymmetric drift than the thin disk stellar population it is possible to distinguish the two populations by looking at their space velocities. Stars that for instance have high $W_{\rm LSR}$ velocities in the solar neighbourhood reach large vertical distances from the Galactic plane and should be regarded as thick disk stars. Stars that move in highly elongated orbits around the Galactic center (i.e., high $U_{\rm LSR}$ velocities) are also more likely to belong to the thick disk than the thin disk. Since the rotation of the thick disk lags behind the LSR by some 40 km s^{-1} those stars with low $V_{\rm LSR}$ are also more likely to belong to the thick disk. By assuming that the space velocities have Gaussian distributions for each stellar population component it is possible to calculate a "probability" for each star that it belongs to either the thin disk, the thick disk, or the halo (see also Fig. 1 in Paper I):

$$f(U,\,V,\,W) = k \cdot \exp\left(-\frac{U_{\rm LSR}^2}{2\,\sigma_U^2} - \frac{(V_{\rm LSR} - V_{\rm asym})^2}{2\,\sigma_V^2} - \frac{W_{\rm LSR}^2}{2\,\sigma_W^2}\right), \qquad (2)$$

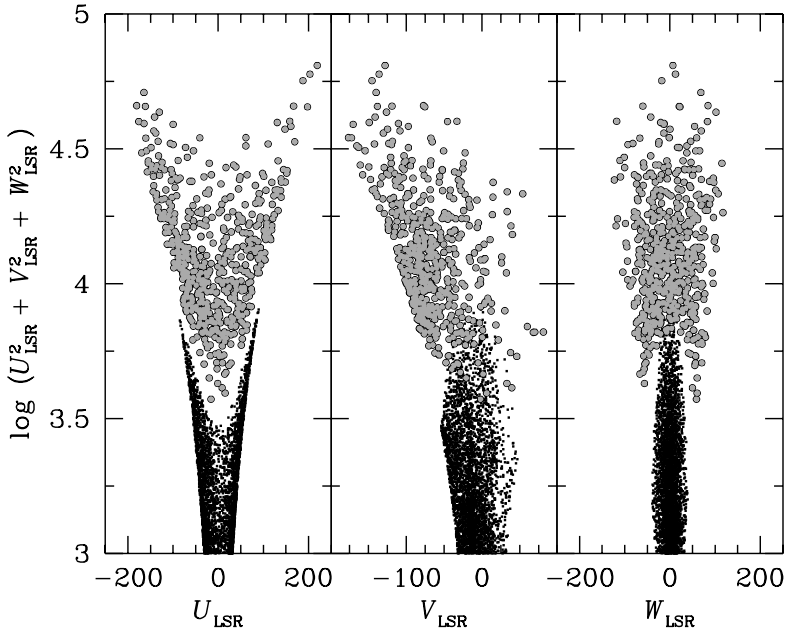

FIGURE 8: The kinetic energy distribution for thin and thick disk stellar samples using the kinematical criteria $TD/D > 2$ and $TD/H > 1$ for the thick disk (gray filled circles) and $TD/D < 0.1$ and $TD/H > 1$ for the thin disk (black dots). All stars in the catalogue of ~ 12600 stars that fulfill the criteria have been plotted.

where

$$k = \frac{1}{(2\pi)^{3/2}\,\sigma_U \sigma_V \sigma_W}, \tag{3}$$

normalizes the expression.

When randomly picking a star in the solar neighbourhood it also has a probability, independent of its kinematical properties, of being a thin disk star, a thick disk star, or a halo star, based on the local number densities of the populations. If for instance 90 % of all nearby stars belong to the thin disk, the thin disk probability, that was calculated from kinematics only, should be multiplied by this percentage, and similarly for the thick disk and halo probabilities (i.e., multiply Eq. (2) with the X-values given in Table 1).

Finally, by dividing the probability for thick disk membership (TD) with the probabilities for thin disk membership (D) and the halo membership (H), respectively, two dimensionless ratios that express how much more likely it is that a star belongs to the thick disk than the thin disk and the halo, respectively, can be constructed:

$$TD/D = \frac{X_{TD}}{X_D} \cdot \frac{f_{TD}}{f_D}, \qquad TD/H = \frac{X_{TD}}{X_H} \cdot \frac{f_{TD}}{f_H}. \tag{4}$$

$X_{TD,\,D,\,H}$ denote the solar neighbourhood normalizations of the different populations. The parameters that have most influence on these ratios (and thereby also on the classification of the stars) are these normalization parameters. For instance, by increasing the normalization of the thick disk stars from 6 % (which is the number that we used for Papers I – III) to 10 % (which is the number we used for Papers IV and V), and consequently lowering the thin disk normalization to 90 %, the TD/D ratios increase by a factor of ~ 1.7 (see Appendix of Paper IV for a discussion of the value for the thick disk normalization). Other parameters, such as the velocity dispersions, of course also influence the TD/D ratio. They are however better known.

In order to select our thick disk sample we have used $TD/D > 2$ and $TD/H > 1$ (assuming the 10 % normalization). This will ensure that the probability of belonging to the thick disk always will be greater than the probability of belonging to the thin disk (i.e. $TD/D > 1$), even if the true value for normalization of the thick disk actually is as low as 2 % or as high as 14 %. To select thin disk stars we used $TD/D < 0.1$ and $TD/H > 1$ (see Papers I and IV for further discussions).

Figure 8 (see also cover image) shows the distribution of the kinetic energies (which is proportional to the square of the total velocity) as a function of the three Galactic velocity components. It is apparent that the kinematically selected thin and thick disk samples ($TD/D < 0.1$ and $TD/D > 2$, respectively) are kinematically separated even though there are overlaps in $V_{\rm LSR}$ and $W_{\rm LSR}$, when using the kinematical criteria described above.

2.3 Properties of the stellar sample

All astrometric and kinematical data for the stellar sample that was used for the spectroscopic studies (Papers I–IV) are gathered in Table A3 and the stellar atmosphere parameters in Table A4. In total we have 38 stars with kinematics typical for the thick disk and 60 stars with kinematics typical for the thin disk. 4 stars have kinematics that are intermediate to the thin and thick disks and their classifications will depend on the assumed value of the stellar densities in the solar neighbourhood. These stars will be referred to as “transition objects”.

Kinematics

The kinematical characteristics of the total stellar sample in our spectroscopic studies are shown in a Toomre diagram in Fig. 9. In such a diagram the concentric half circles represent curves of constant kinetic energy with respect to the LSR. As a consequence of our selection criteria, the thin disk stars have peculiar velocities less than about 70 km s^{-1}, whereas the thick disk stars are more or less confined to peculiar velocities in the range 80–180 km s^{-1}. The appearance of this Toomre diagram is similar to the one that Fuhrmann (1998) presented for his thin and thick disk samples, even though he used different criteria for selecting his stars.

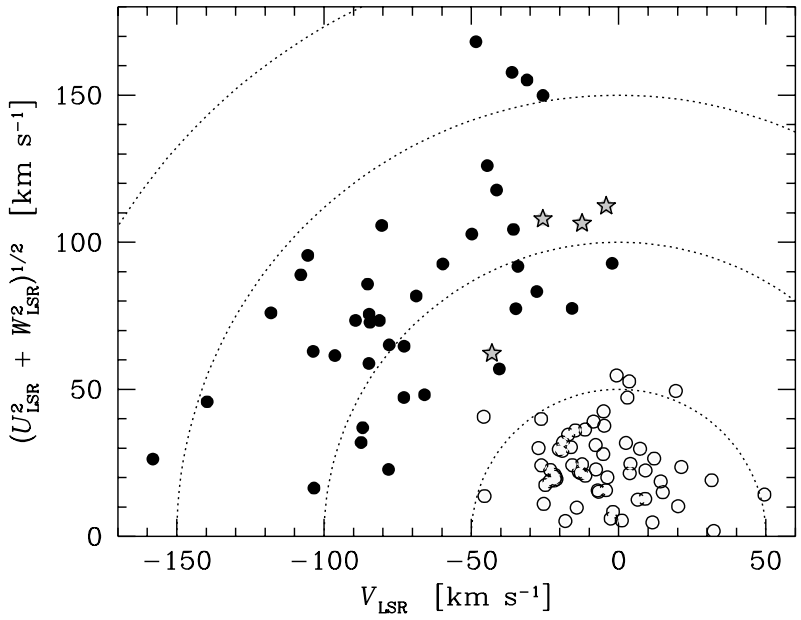

FIGURE 9: Toomre diagram for the total stellar sample (102 stars) (Papers I–IV). Thick and thin disk stars are marked by filled and open circles, respectively. "Transition objects" are marked by grey coloured stars. Dotted lines indicate constant peculiar space velocities in steps of 50 km s^{-1}.

Metallicity distribution

Figure 10 shows how our thin and thick disk samples are distributed in [Fe/H] (the four stars with intermediate kinematics have not been included in the histograms). The distribution for the thin disk is heavily weighted towards stars with super-solar metallicities ([Fe/H] > 0). This distribution is not representative for the thin disk stellar population in general but is an effect of our selection since we wanted to observe the oxygen trend in the metal-rich thin disk. Otherwise our thin disk stars trace the thin disk fairly well down to [Fe/H] ≈ -0.5 with at least 3 stars in each 0.1 dex bin.

Our thick disk sample is rather well distributed in metallicity below solar values, with the exception of the metallicity bin around -0.2 dex where we have fewer stars. This is somewhat unfortunate since this is a really interesting range of [Fe/H] for the thick disk (see Chapter 5.3). Originally, we selected stars for observation that were evenly distributed in metallicity. Those metallicities were based on Strömgren *uvby* photometry and the uneven distribution arose after determining [Fe/H] spectroscopically. It should, however, be noted that in general we have good agreement between the photometric metallicities and our

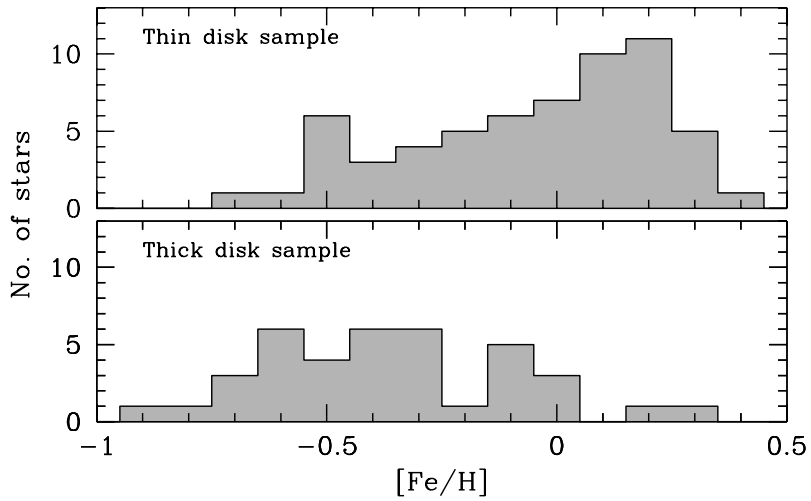

FIGURE 10: Histograms showing the [Fe/H] distribution for the thin and thick disk samples. The four stars with intermediate kinematics have not been included.

[Fe/H] (see Paper I).

Kinematics versus metallicities

In Fig. 11 the peculiar velocity $v_{\rm pec}$, as well as the individual space velocities components $U_{\rm LSR}$, $V_{\rm LSR}$, and $W_{\rm LSR}$ are plotted versus [Fe/H]. Regarding $v_{\rm pec}$ and $V_{\rm LSR}$, the thin and thick disk samples are well separated, whereas there is some overlap in the other two ($U_{\rm LSR}$ and $W_{\rm LSR}$). What is interesting is that four stars that are marked as "transition objects" resemble the thick disk in their $v_{\rm pec}$ and the thin disk if looking at the $V_{\rm LSR}$ component. This means that they have either high $U_{\rm LSR}$ and/or $W_{\rm LSR}$ velocities in order to attain the high $v_{\rm pec}$. Three of them have high $U_{\rm LSR}$ and moderate $W_{\rm LSR}$ (meaning shallow and elongated galactic orbits), and the fourth high $W_{\rm LSR}$ and moderate $U_{\rm LSR}$ (meaning an orbit that reaches higher $Z_{\rm max}$ and is less elongated). Which of the Galactic stellar populations that these stars belong to is difficult to determine since they also have elemental abundances that are intermediate to the thin and thick disks (see Chapter 5 and discussion in Paper IV).

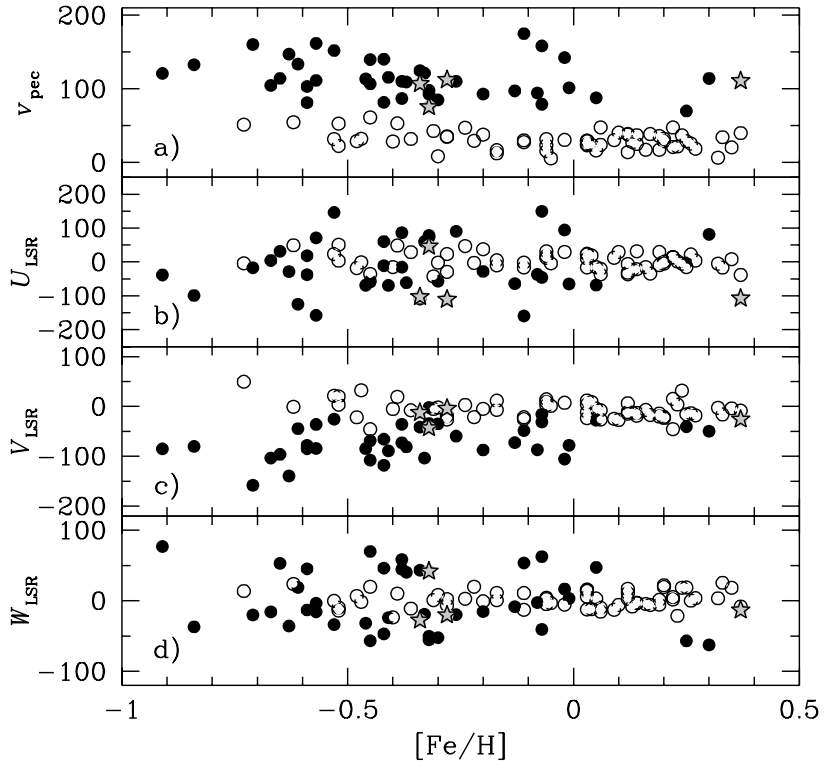

FIGURE 11: Kinematics versus [Fe/H] for the full sample (102 stars). Thick and thin disk stars are marked by filled and open circles, respectively. "Transition objects" are marked by grey coloured stars.

Chapter 3
Observations and data reductions

The lowest of all employments is mere observation. No intellect and very little skill are required for it. An idiot with a few days' practice may observe very well.

George Biddell Airy (1801-1892), Astronomer Royal 1835-1881[4]

Observations were carried out during several runs from August 2000 to September 2003 (see Table 2). Since spectroscopy is doable even under conditions that are far from perfect (photometric) we were in general granted with observing time under a full Moon. The majority of our stars are relatively bright and we had a large catalogue to select targets from, so observing under a full Moon was of less significance for the success of our runs. The observed stars and their dates of observation are listed in Table A1.

ESO 1.5-m telescope and FEROS

The ESO 1.5-m telescope on La Silla in Chile (see Fig. 13) has a primary mirror with a diameter of 1524 mm. The telescope is mounted in an English cradle and can be positioned either west or east of the pier. Changing positioning requires extreme care and is usually not done during the observing night. This results in a severe limitation of the available pointing directions. Observations of stars with declinations $\delta \leq -40^\circ$ and $\delta \geq +20^\circ$ are especially effected.

FEROS[5] (Fiber Extended Range Optical Spectrograph) is a fiber-fed echelle spectrograph that, during our observations, was used together with the ESO 1.5-m telescope. In a single exposure it is possible to obtain a spectrum with a resolving power of $\sim$48 000 of the whole optical region (3560–9200 Å). The spectrum is recorded in 39 spectral orders on a CCD with a size of 2048×4096 pixels.

[4] Source: British Astronomical Association, http://www.britastro.org/iandi/quotns.htm
[5] The FEROS spectrograph has now been moved to the ESO 2.2-m telescope

FIGURE 12: An aerial view of the ESO observatories on La Silla in Chile (From ESO messenger March 1989). *Credit: European Southern Observatory (ESO) - with whom the copyright rests.*

In order to reduce the data we used the context FEROS which is available under the ESO-MIDAS[6] software program. The software allows several parameters to be varied, as how to extract and merge the different orders. An example of a reduced one-dimensional spectrum, ranging from 4500 to 8800 Å, is shown in Appendix D.

ESO 3.6-m telescope and CES

The ESO 3.6-m telescope on La Silla (see Fig. 13) has an equatorial mount in a horseshoe fork. The diameter of the primary mirror is 3566 mm. The CES (Coudé Echelle Spectrometer) on the ESO 3.6-m telescope is the spectrograph with the highest spectral resolution at any ESO telescope. For our observing runs we used the highest resolution, $R \sim 215\,000$, which splits the spectrum into 12 slices (see Fig. 1 in Paper III). Since only a part of a single spectral order is recorded on the CCD (2048×4096 pixels) the spectral bandwidth is limited. For our observations the setting was centered on the forbidden oxygen line at 6300 Å which resulted in spectra with a wavelength coverage of ~ 40 Å. An example of a spectrum

[6]ESO-MIDAS is the acronym for the European Southern Observatory Munich Image Data Analysis System which is developed and maintained by the European Southern Observatory.

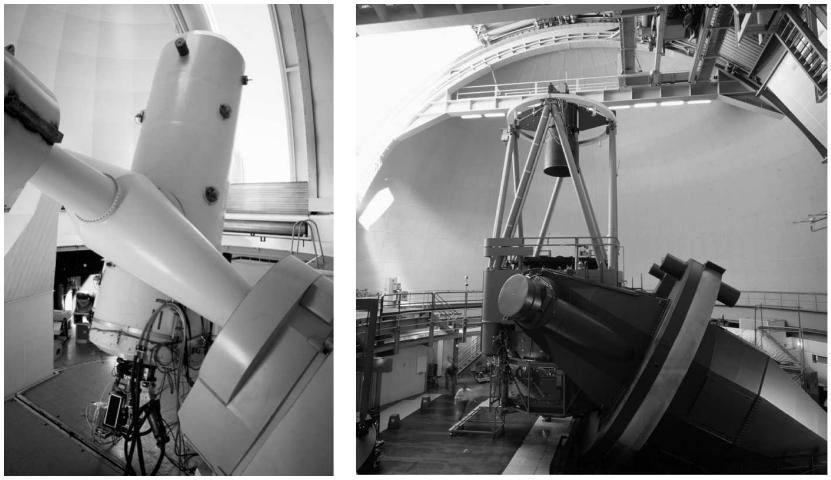

FIGURE 13: The ESO 1.5-m telescope (left) and the ESO 3.6-m telescope (right) on La Silla in Chile. *Credit: European Southern Observatory (ESO) - with whom the copyright rests.*

is shown in Fig. 14 (see also Figs. 3 and 6 in Paper III).

For the reduction of the CES spectra we used standard MIDAS routines for background subtraction, flatfielding and wavelength calibration. There are however a few peculiarities with the CES spectra that demand special care, such as the presence of a straylight pedestal and a weak interference pattern in the continuum. These properties and the difficulties they impose are further discussed in Paper III. Furthermore, since the forbidden oxygen line lies in a region of the spectrum where telluric lines are common we also had, for some stars, to divide out these telluric lines from the stellar spectrum in order to get a clean oxygen line (see Paper III).

Very Large Telescope Kueyen and UVES

The Very Large Telescope (VLT) on the Paranal observatory in Chile consists of an array of four 8-m telescopes that can be used individually or in combination. The Kueyen (UT2) telescope is the second of these four telescopes and was taken into use during the second half of 1999. UVES (UV-Visual Echelle Spectrograph) is a cross-dispersed echelle spectrograph that is located at the Kueyen telescope. The light coming from the telescope is split into two arms (Blue and Red) within the instrument. These arms can be operated individually or in parallel. The maximum resolutions are 80 000 and 110 000 for the Blue and Red arm, respectively. For our observations we have used the Red arm only. In order to minimize the loss of light we choose to use an image slicer instead of a narrow slit for the higher resolutions. For the three stars in Papers III and IV we used a resolution of 110 000 and for the *in situ* dwarfs in Paper VI a resolution of 60 000. The lower resolution was used for the *in situ* dwarfs because they are so faint that a higher resolution would incur too long

TABLE 2: Summary of the observations.

Site	Telescope	Instr.	Proposal No.	Time	Date	Observer
La Silla	ESO 1.5-m	FEROS	65.L-0019(B)	1n	16 Sep. 2000	TB, SF
		FEROS	67.B-0108(B)	1n	28 Aug. 2001	TB
	ESO 3.6-m	CES	65.L-0019(A)	3n	13–15 Sep. 2000	TB, SF
		CES	67.B-0108(A)	4n	29 Aug. – 2 Sep. 2001	TB
		CES	67.B-0141(A)	2n	3–4 Sep. 2001	TB
		CES	69.B-0468(A)	10h	1 Apr. – 31 Sep. 2002	Service mode
Paranal	VLT/UT2	UVES	69.B-0277(A)	2n	20–21 Jul. 2002	TB
		UVES	71.B-0298(A)	72h	1 Apr. – 31 Sep. 2003	Service mode
La Palma	NOT	SOFIN		3n	20 Aug. – 1 Sep. 2002	IL, BS, II
		SOFIN		5n	11 Nov. – 27 Nov. 2002	TB, SF, II

BS = Björn Stenholm, II = Ilya Ilyin, IL = Ingemar Lundström,
SF = Sofia Feltzing, TB = Thomas Bensby

exposure times.

The reductions of the UVES spectra were performed with the UVES pipeline that runs under ESO-MIDAS and is described by Ballester et al. (2003).

Nordic Optical Telescope and SOFIN

The Nordic Optical Telescope (NOT) is located on the Roque de los Muchachos on the La Palma island. It has a primary mirror with a diameter of 2560 mm and the telescope has an alt-az mounting. First light was in late 1988 and regular observing started in 1989. The SOFIN (SOviet FINnish) (or SO FINe) spectrograph is a high-resolution echelle spectrograph that dates back to 1992. It allows three different resolutions ($R \sim 30\,000$, 80 000, and 170 000). For our observations we have used the intermediate resolution.

The data reductions were performed by Ilya Ilyin using the 4A software (Ilyin 2000) and are briefly described in Paper IV.

Chapter 4
Abundance determination

We understand the possibility of determining their shapes, their distances, their sizes and their movements; whereas we would never know how to study by any means their chemical composition . . .
. . . I persist in the opinion that every notion of the true mean temperatures of the stars will necessarily always be concealed from us.

August Comte, Cours de Philosophie Positive, 1835

Contrary to the statements by August Comte in the 19th century, it is now widely known that the stellar spectrum contains a wealth of information about the properties of the star. The amount of spectral lines, and the strengths of the lines present, are sensitive to the conditions in the star's atmosphere and make it possible to determine fundamental parameters such as effective temperature ($T_{\rm eff}$), surface gravity ($\log g$), and chemical composition. These parameters can then be used to determine the age and the mass of the star.

The (absolute) abundance of an element, $\epsilon(E)$, is given as the difference between the logarithm of the number density of atoms from that element ($N_{\rm E}$) and the logarithm of the number density of hydrogen ($N_{\rm H}$) atoms (a constant value of 12 is normally added to all abundances in order to avoid negative numbers). It is convenient to use elemental abundances that are related to a star whose chemical composition is known, i.e., a standard star. The Sun is the natural reference in studies of chemical evolution. Especially in studies of the type presented here it is a good reference since its physical properties ($T_{\rm eff}$, $\log g$) are similar to the stars that we have analyzed (F and G dwarf stars). Elemental abundances given relative to the solar standard abundances are usually written within square brackets:

$$[{\rm E/H}] = \log\left(\frac{N_{\rm E}}{N_{\rm H}}\right)_{\star} - \log\left(\frac{N_{\rm E}}{N_{\rm H}}\right)_{\odot}, \qquad (5)$$

where the sub-scripts $\star$ and $\odot$ indicate the star and the Sun, respectively. By definition the Sun will always have $[{\rm E/H}]_{\odot} = 0$. Stars that have $[{\rm E/H}] > 0$ are consequently more

abundant in the element E than the Sun and stars that have $[\mathrm{E/H}] < 0$ are less abundant in the element E than the Sun. As an example, the most metal-poor star known to date is HE 0107-5240 that has $[\mathrm{Fe/H}] = -5.3$ (Christlieb et al. 2002). This means that the abundance of iron atoms in the atmosphere of this star is only 1/200 000 of that in the Sun.

4.1 Equivalent widths and synthetic spectra

Absorption lines in a stellar spectrum form when atoms in the stellar atmosphere absorb photons and re-emit them in random directions. This will make light "disappear" at certain wavelengths. The wavelengths are coupled to the difference between certain energy levels in the atom. The likeliness for an atom or ion to absorb a photon with a specific energy (wavelength) is dependent on the effective temperature and electron pressure (surface gravity) in the stellar atmosphere, as well as the properties of the atom. By measuring the strengths of spectral lines it is possible to determine the chemical composition of the stellar atmosphere. One has to be aware of that there are further processes, such as stellar rotation and micro- and macroturbulence, that broadens the line. Since these parameters, as well as the effective temperature and surface gravity, are not known *a priori* one has to make assumptions and then iterate until there are consistency between atmospheric parameters and abundances. The iterative process that we have applied is described in Paper I.

The strength of a spectral line (and hence the elemental abundance) can be determined either by equivalent width measurements or by fitting models to observed line profiles. Both methods have been applied in this work.

Equivalent widths

The use of equivalent widths is in principle very appropriate for determining abundances from a stellar spectrum since several mechanisms that only broadens a spectral line, without changing the total absorption, can be neglected. Such profile broadening originates from the macroturbulent motions (or radial-tangential motions, ζ_{RT}), stellar rotation ($v \sin i$), and the instrument. Microturbulence (ξ_{t}) on the other hand affects the amount of absorption and should be included (see Sect. 4.2).

The actual measurement of equivalent widths was done by fitting Gaussian line profiles, for which we have used the IRAF[7] task SPLOT. There are several uncertainties involved in the actual measuring process, such as the placement of the continuum and avoiding possible blends. These and other uncertainties are discussed in Paper I. In total the abundance analysis presented here involves approximately 40 000 equivalent width measurements. The number of lines that have been used for each element in every star is listed in Table B2.

[7] IRAF is distributed by National Optical Astronomy Observatories, operated by the Association of Universities for Research in Astronomy, Inc., under contract with the National Science Foundation, USA.

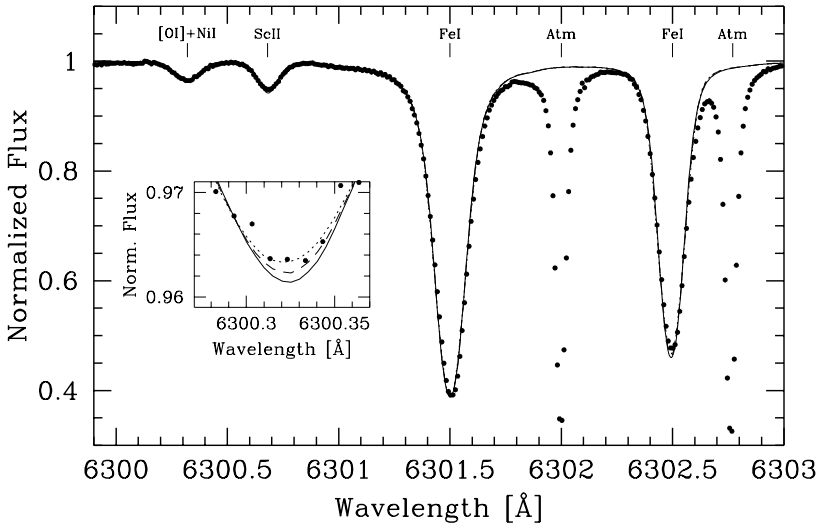

FIGURE 14: Synthetic spectra of the [O I] line at 6300 Å in the Sun. The observed spectrum (dots) was obtained with the CES spectrograph on the ESO 3.6-m telescope on La Silla (see Paper III). The joint macroscopic broadenings (rotation and macroturbulence) have been modelled by a single broadening profile in three different ways: Gaussian line profile (dashed line); elliptical line profile (dotted line) which was the adopted profile in this case (Paper III); radial-tangential line profile (solid line). There is almost no difference between the three different convolutions and therefore a zoom-in on the line bottom of the [O I] line, where small differences are present, is also included.

Line synthesis

Sometimes it is difficult to measure the equivalent width of a spectral line with high precision. This is especially the case when the line is blended with other spectral lines, or when the line shows structure due to hyperfine splitting and/or isotopic shifts. The forbidden oxygen line at 6300 Å is for instance blended with two Ni I lines whose contribution to the joint line profile increase with metallicity (see Fig. 6 in Paper III). Our very high-resolution spectra obtained with the CES spectrograph enabled an accurate modelling of this line which also is reflected in the tight [O/Fe] vs [Fe/H] trends that we found for the thin and thick disks (see Figs. 9 and 10 in Paper III).

When calculating the synthetic spectra it is necessary to have more detailed information about the mechanisms that shape the line profiles. The instrument broadening is set by the resolution (R) of the spectrograph and is usually assumed to be Gaussian in shape. For the CES spectra with $R \sim 215\,000$ we convolved the synthetic spectra with a Gaussian line profile having FWHM = 30 mÅ (FWHM = $\Delta\lambda = \lambda/R = 6300/215\,000$ Å). The broadening due to the rotational velocity ($v \sin i$) of the star has an elliptical line profile.

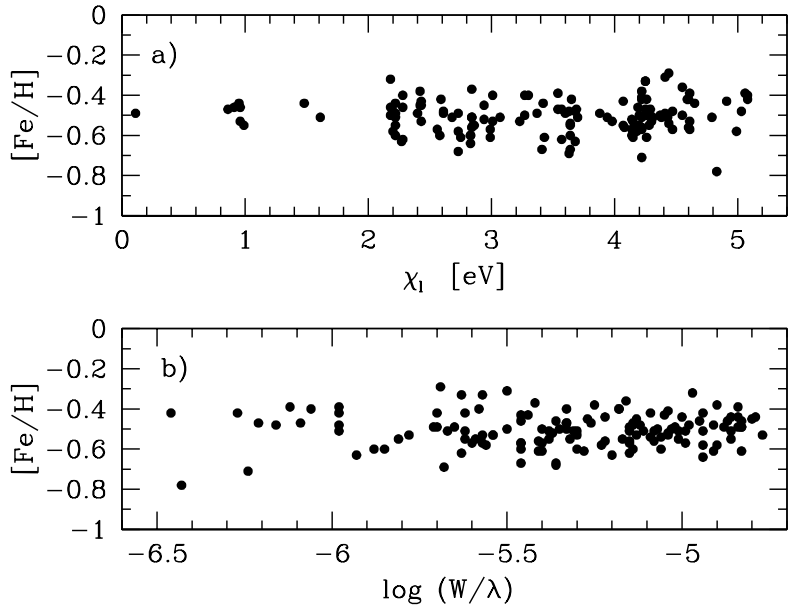

FIGURE 15: **a)** Excitation balance in the determination of $T_{\rm eff}$ for Hip 83229. **b)** Iron abundance versus reduced line strength for the determination of microturbulence for the same star.

The macroturbulent broadening ($\zeta_{\rm RT}$) is neither Gaussian nor elliptical in shape. Instead it is more narrowly peaked and with wider wings than the Gaussian distribution (see, e.g., Fig. 18.4 in Gray 1992). In cool stars the macroturbulent and rotational broadening are of comparable sizes, i.e. $v \sin i/\zeta_{\rm RT} \approx 1$, and their joint contribution to the broadening of the spectral line is close to Gaussian in shape (e.g. Gray 1992). This means that satisfactory modelling could probably be done by assuming Gaussian line profiles only (which actually usually is done when measuring equivalent widths). Fig. 14 shows the differences by using different types of profiles (Gaussian, Elliptical, and Rad-Tan, respectively) for the joint macroscopic broadening which is made up of rotation and macroturbulence. As can be seen the differences are small.

In Paper III we used rotational (elliptical) line profiles to produce the macroscopic broadening of the synthetic spectra. In Paper IV we used macroturbulent line profiles (Rad-Tan) for the same purpose. The difference in the resulting abundances are small, and is reflected by a slight shift of the zero-point in the absolute abundances. Since we always normalize our abundances to the solar abundances that we derive from our own solar analysis this means that our [O/H] abundances and [O/Fe] (or [Fe/O]) trends with metallicity (either [Fe/H] or [O/H]) are negligbly affected.

4.2 Stellar atmosphere parameters

In order to determine elemental abundances a model of the stellar atmosphere that details how temperature and pressure varies with depth is needed. We have used the Uppsala MARCS code for the generation of the model stellar atmospheres. These models are one-dimensional and constructed under the assumption of local thermodynamic equilibrium (LTE). The code was originally developed by Gustafsson et al. (1975) and has been extensively updated by Edvardsson et al. (1993) and Asplund et al. (1997). In order to produce the model atmospheres the code needs input in the form of $T_{\rm eff}$, $\log g$, and [Fe/H]. The choice of starting values and the iterative process that follows to tune the parameters are detailed in Paper I.

Determination of effective temperature

The strengths of different spectral lines (from a given element) depends on the number of atoms as well as the temperature. Since the number of atoms of the element in the stellar atmosphere is independent on which line of the element that is analyzed one can, by forcing all lines from the element to give the same abundance, determine $T_{\rm eff}$. This is most easily done by plotting the abundances from individual lines as a function of the lower excitation potential ($\chi_{\rm l}$) of the lines. If the temperature is correct there should be no observed trends in this plot, i.e., one has *excitation balance*.

Since Fe I lines are by far the most common spectral lines in stellar spectra, and since they span a large range in $\chi_{\rm l}$, they are especially suited for this analysis. Figure 15a shows an example of a [Fe/H] versus $\chi_{\rm l}$ plot for HIP 83229 where we use 138 Fe I lines. If we had assumed an erroneous temperature we would see that different lines give different abundances depending on their lower energy levels. A too high temperature would for example predict too many electrons in higher energy levels in the model as compared to the measured numbers (line strengths). The measured lines with higher excitation potentials will therefore give abundances that are too low which can be seen as a trend with negative slope in the [Fe/H] versus $\chi_{\rm l}$ plot. A too low temperature will work in the opposite direction.

Determination of surface gravity

The surface gravity can be derived by forcing the abundances derived from lines arising from an neutral element and an ionized element (e.g., Fe I and Fe II) to be equal, i.e. *ionization balance*. There are however indications that derived abundances for Fe I are sensitive to departures from the assumption of LTE, which Fe II is not (e.g., Thévenin & Idiart 1999). If large departures from LTE are present it is therefore possible that the $\log g$-values derived from ionization balance of Fe I and Fe II are erroneous.

Knowing the distance to the star it is, however, possible to determine $\log g$ from physics. Combining that the luminosity of the star can be written as $L = 4\pi\sigma T_{\rm eff}^4 R^2$, that the surface gravity is given by $g = G\mathcal{M}R^{-2}$ (G is the gravitation constant, $\mathcal{M}$ is the stellar mass, and R is the stellar radius), and that the luminosity of a star, relative to the Sun, can be

expressed as $\log(L_\odot/L) = 0.4(M_{\rm bol} - M_{\rm bol\odot})$ (where $M_{\rm bol}$ is the bolometric magnitude), we obtain the following fundamental relation:

$$\log\frac{g}{g_\odot} = \log\frac{\mathcal{M}}{\mathcal{M}_\odot} + 4\log\frac{T_{\rm eff}}{T_{\rm eff\,\odot}} + 0.4(M_{\rm bol} - M_{\rm bol\odot}), \quad (6)$$

where

$$M_{\rm bol} = V + BC + 5\log\pi + 5. \quad (7)$$

All our stars have parallaxes (π) measured by the Hipparcos satellite (ESA 1997) that were used in the calculation of $\log g$. The bolometric corrections (BC) in Eq. (7) were found by interpolating in the grids by Alonso et al. (1995).

The good agreement between the derived Fe I and Fe II abundances (see Fig. 7 in Paper I and Fig. 2 in Paper IV) indicates that NLTE effects for Fe I probably are not severe for the types of stars that we study (late F and G dwarfs) and that it probably would have been safe to assume ionization balance when deriving $\log g$.

Determination of microturbulence

The movements of the gas in the stellar atmosphere introduce slight wavelength (doppler) shifts of the emitted radiation. Motions in a stellar atmosphere related to volume sizes that are small compared to the mean free path of a photon are usually referred to as microturbulence, $\xi_{\rm t}$ (e.g., Gray 1992). The effect of $\xi_{\rm t}$ is to make spectral lines wider than they would normally be (i.e., when only broadened by thermal motions, pressure, and the natural line width due to the uncertainty principle). The presence of microturbulence mainly affects strong lines that, in the absence of microturbulence, would have been saturated or close to saturation. Such lines are de-saturated since microturbulence will allow for a wider range in wavelength for absorption and hence make those lines proportional to variations in the abundance again.

Since the derived abundance should be the same regardless of which line that is being considered, and how strong this line is, it is possible to determine the microturbulence by forcing all spectral lines from an element to give the same abundances. Figure 15b shows an example where the abundances from 138 Fe I lines have been plotted as a function of the strength of the line, $\log(W_\lambda/\lambda)$. For a correct value of $\xi_{\rm t}$ there should be no trend (slope) in this plot, i.e., one strives for "line strength balance".

4.3 Stellar ages and masses

Determination of ages

When deriving stellar ages we have made use of α-enhanced isochrones for stars with chemical compositions such that [α/Fe] > 0. Two sets of the Yale-Yoshii (Y^2) isochrones (Yi et al. 2001; Kim et al. 2002) are shown in Fig. 16. Both sets have the same metallicity but different α-enhancements. Taking α-enhancement into consideration results in ages that are

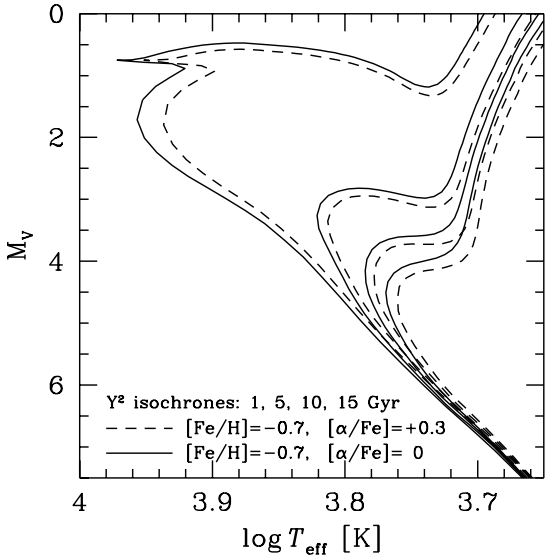

FIGURE 16: The Y^2 stellar isochrones with α-enhancement (dashed lines) and without α-enhancement (solid lines) for a metallicity of [Fe/H] $= -0.7$ (Yi et al. 2001; Kim et al. 2002). Each set has four isochrones representing stellar ages of 1, 5, 10, and 15 Gyr (ages increase to the right).

lower than if solar-scaled isochrones are used. In Paper II where we used ages that were determined by Feltzing et al. (2001), who did not take α-enhancement into consideration. In Paper I we used α-enhanced isochrones from Salasnich et al. (2000) or, depending on the degree of α-enhancement, the solar-scaled isochrones from Girardi et al. (2000). The difference was a lowering of the mean age from 12.1 Gyr to 11.2 Gyr for the thick disk stars, whereas the mean age for the thin disk stars was mainly unaffected.

In Paper IV we changed to the Y^2-isochrones (Yi et al. 2001; Kim et al. 2002) since these come with interpolation routines to construct sets of isochrones with your own choice of metallicity and α-enhancement. In Paper IV we also re-derived the ages for the stellar samples in Paper I in order to get a consistent age determination for all samples. No large differences were found between the ages based on the Girardi/Salasnich isochrones and the Y^2-isochrones. However, the extended sample in Paper IV also included some younger thick disk stars which lead to a mean age of the thick disk stellar sample of 9.7 ± 3.1 Gyr. This should be compared to the mean age of 4.3 ± 2.6 Gyr for the thin disk sample.

More sophisticated methods to derive stellar ages from isochrones exist. However, our age estimates are virtually identical to those obtained with more sophisticated methods. On the other hand, our method probably underestimates the uncertainties of the derived ages (Rosenkilde Jørgensen private comm.).

Determination of masses

The stellar masses used in the determination of $\log g$ (see Eq. 6) were obtained by fitting evolutionary tracks to the stellar data points in the $\log T_{\rm eff}$ - $M_{\rm V}$ plane. Figure 5 in Paper I illustrates the procedure. In that paper we used the evolutionary tracks from Girardi et al. (2000) and Salasnich et al. (2000), whereas in Paper IV we instead used the Y^2 evolutionary tracks from (Yi et al. 2003), for the same reasons as discussed above.

4.4 Atomic line data

In order to derive elemental abundances from equivalent width measurements, or to produce synthetic spectra, one needs data that describe how likely it is for an atom to absorb a photon with a specific energy (wavelength). One such property is the oscillator strength, or $\log gf$-value, which is a measure of how likely it is that an electron will jump between two given energy levels. Since the derived abundance is inversely proportional to the gf-value it is important to have accurate and homogeneous sets of $\log gf$-values in order to derive trustworthy abundances. In Paper I we therefore performed an extensive investigation of the $\log gf$-values. This set of $\log gf$-values was then used in the other papers. The main conclusion from this "sidestep" was that in some cases we had to rely on astrophysical $\log gf$-values (see Paper I), and that in the optical region, good laboratory data are missing for certain very important elements such as Si, Mg, and Al.

Other atomic data needed to determine elemental abundances are the parameters for the broadening of atomic lines by radiation damping ($\gamma_{\rm rad}$) and the collisional Van der Waals broadening. For these parameters we adopted values in the literature (see further discussion and references in Paper I).

4.5 Solar normalization

All elemental abundances have been normalized with respect to the Sun. To do this we have determined solar abundances from spectra from the afternoon sky or the Moon, obtained with the same equipment as used for the stellar spectra. These abundances were then compared to standard solar photospheric values given in Grevesse & Sauval (1998). Depending on which instrument that was used we got slightly different values for the solar abundances. This has probably its origin in that the spectrographs have different wavelength coverage (meaning that the number of lines available for abundance analysis varies). Another possible cause could be the different spectral resolutions. When measuring equivalent widths it is easier to avoid blending lines and other artefacts in the spectra with the higher resolutions. This could be the reason why the equivalent widths in the SOFIN solar spectrum are slightly smaller than those measured in the FEROS solar spectrum (see Paper IV). However, this difference is indeed small. Our solar abundances and the values that have been subtracted from the abundances derived with the different spectrographs are given in Table B1 (see also discussion in Sect. 6.1.2 of Paper I, as well as in Paper IV). *The abundances in Tables B2–B4 are corrected values expressed relative to the solar abundances.*

Chapter 5
Results and discussion

The history of the Galaxy has got a little muddled, for a number of reasons: partly because those who are trying to keep track of it have got a little muddled, but also because some very muddling things have been happening anyway.

Douglas Adams, Mostly Harmless, 1992

5.1 Main results

The detailed appearance of our resulting abundance trends for the individual elements are discussed in Papers I–IV and VI, and the possible age-metallicity relation in Paper V. In the context of the chemical evolution of the Galaxy, the following are our key results:

- ★ **Distinct and well-defined elemental abundance trends for the thin and thick disks at [Fe/H] < 0:** This is found not only for the α-elements (O, Mg, Si, Ca, Ti), but also for the r- and s-process elements (Y, Ba, Eu) as well as Al and Na. This indicates that both the thin and thick disks formed from interstellar gas that were reasonably homogeneous and that the chemical histories of the two disks are different, even if linked (see Papers I–IV).

- ★ **Signatures of SN Ia in the thick disk:** The down-turn in [α/Fe] at [Fe/H] $= -0.4$, from being essentially flat at lower metallicities, is most likely a signature from the peak in the SN Ia rate (see Papers I–IV).

- ★ **The abundance trends in the thick disk seem to be invariant with $Z_{\rm max}$ and $R_{\rm m}$:** Splitting the solar neighbourhood thick disk sample into sub-samples whose stars move in orbits of different galactocentric radii ($R_{\rm m}$, the mean of the apo- and peri-galactic distances), or that reach different heights above the Galactic plane ($Z_{\rm max}$), we see that the abundance trends are similar for the different sub-samples (see Fig. 17 in

Paper I and Fig. 9 in Paper IV, respectively). The invariance of the abundance trends with $Z_{\rm max}$ is further verified by the preliminary results in Paper VI. In that paper we have analyzed four dwarf stars situated 1–1.5 kpc above the Galactic plane which make them very likely to belong to the thick disk. Note, however, that this does *not* imply that the metallicity *distribution* of the thick disk is invariant with either $Z_{\rm max}$ nor $R_{\rm m}$.

★ **An age-metallicity relation in the thick disk:** The tentative evidence for an age-metallicity relation (AMR) in the thick disk presented in Paper V implies that star formation in the thick disk has been an ongoing process for several billion years. The AMR suggests that it took at least 2–3 billion years to reach [Fe/H] $= -0.4$ (see Paper V).

★ **The thick disk is older than the thin disk:** We find that our thick disk sample, on average, is older than our thin disk sample: 9.7 ± 3.1 Gyr and 4.3 ± 2.6 Gyr, respectively (see Paper IV).

★ **The evolution of the thin disk has been moderate in comparison to the thick disk:** The shallow decline of the thin disk [α/Fe] trends with [Fe/H], without a flat plateau, indicates that the thin disk has not experienced such an initially fast enrichment by SN II as the thick disk.

★ **The declining trend of [O/Fe] in the thin disk continues [Fe/H] > 0:** In contrast, previous studies found that the [O/Fe] versus [Fe/H] trend levels out at solar [Fe/H] (see Paper III).

5.2 Abundance ratios a tracers of chemical evolution

Before discussing our elemental abundance trends in terms of Galactic chemical evolution, let us briefly recap the interpretaion of such trends.

Oxygen is an α-element that is believed to be produced solely in supernovae type II (SN II) and its evolution has been extensively modelled for the Galaxy, as well as for other galaxies. When comparing oxygen to an element such as iron, which is produced in both SN Ia and SN II, one can diagnose fundamental and intrinsic properties of a chemically evolving system of stars, such as the stellar halo, the bulge, or the thin and the thick disks. The [O/Fe] ratio can for instance be used to trace the initial mass function (IMF), the star formation rate (SFR), and the formation time scales for the system in question (see, e.g., McWilliam 1997; Matteucci 2001).

Figure 17 is a schematic illustration of how the [α/Fe] versus [Fe/H] trend is affected by variations in the IMF and in the SFR. The flat, horizontal portion of the trend below [Fe/H] < -0.4 represents times when large amounts of α-elements (oxygen, for instance) were expelled into the interstellar medium through the explosions of SN II. Since SN II produce over-abundances of α-elements compared to iron, there will be a positive [α/Fe] ratio. As long as time does not allow SN Ia to contribute to the enrichment, and as long

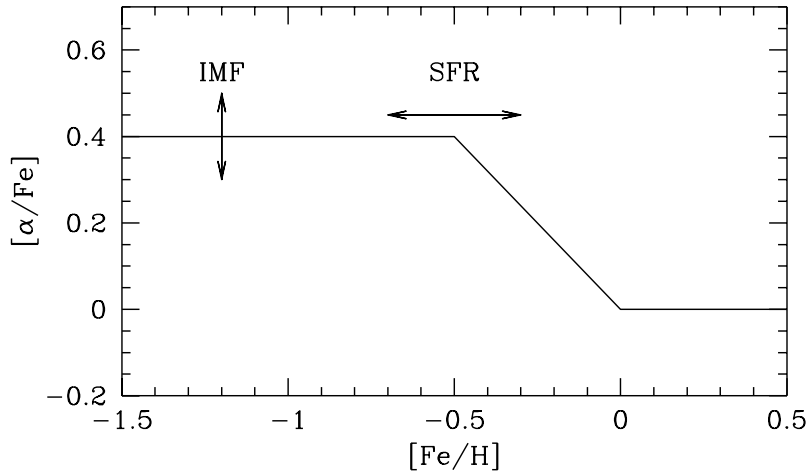

FIGURE 17: Schematic illustration of how the α-element-to-iron ratio might evolve with metallicity and how the trend changes for differing IMFs and/or SFRs.

as star formation is an ongoing process, SN II will continue to enrich the next generations of stars with their ejecta. The [α/Fe] ratio will continue on a high and roughly constant overabundance of the α-elements to higher metallicities ([Fe/H]).

The ratio at which this flat plateau is located depends on the IMF. The IMF is the relative frequency of masses of stars that are born in a stellar generation and has generally been found (empirically) to be approximately constant over time. However, if the IMF is skewed towards stars with higher masses (more SN II) the yields from these stars will increase and the vertical position of the flat plateau in the [α/Fe] vs [Fe/H] diagram would be shifted upwards, and vice versa if the IMF is skewed towards stars with lower masses (fewer SN II).

After some time SN Ia start to enrich the interstellar medium. The peak in the SN Ia rate will be reflected in a lowering of the [α/Fe] ratio as a consequence of the large amounts of iron (and no α-elements) that these events eject into the interstellar medium. In the [α/Fe] versus [Fe/H] diagram this will be reflected by a down-turn in the run of [α/Fe] with [Fe/H].

The horizontal position of this down-turn (or "knee") depends on the SFR. A high SFR will allow many generations of massive stars (SN II) to contribute to the enrichment before the SN Ia start to contribute. This means that the "knee"will be shifted towards higher [Fe/H], and vice versa if the SFR is low.

If, where, and when the [α/Fe] trend will level out depend on the time when there is an equilibrium between SN Ia and SN II. It might also be that the relative fraction of expelled elements from either of the two SN changes with metallicity, i.e., the yields are metallicity dependent. If this is the case, the interpretation of the abundance trends at high [Fe/H] will

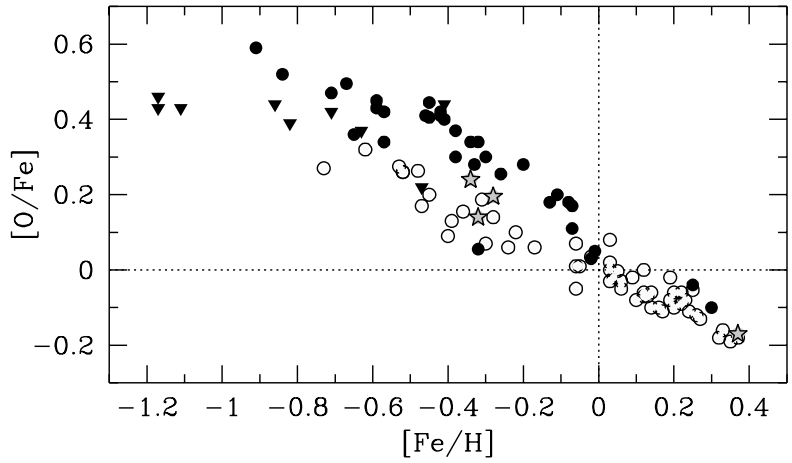

FIGURE 18: [O/Fe] versus [Fe/H]. Thin and thick disk stars are marked by open and filled symbols, respectively. "Transition objects" have been marked by grey coloured stars. Those thick disk stars that are marked by filled triangles have been taken from Nissen et al. (2002) and were selected with the same criteria as our thick disk stars (see Chapter 2.2).

be further complicated.

5.3 A possible origin for the thick disk

Given our observations (see, e.g., Fig. 18 for oxygen), the star formation in the thick disk must initially have been fast in order to produce the large over-abundances of oxygen relative to iron. From being mainly flat at a level of [O/Fe] ~ 0.4 at [Fe/H] $\lesssim -0.4$ we then see a lowering of [O/Fe]. This down-turn can most likely be interpreted as being due to the delayed enrichment of iron from SN Ia to the interstellar medium. That we easily find stars (with kinematics typical of the thick disk population) with metallicities higher than [Fe/H] $= -0.4$ is a sign that star formation has continued in the thick disk for at least as long as the time-scale for SN Ia to contribute to the chemical enrichment. Whereas the time-scale for a single SN Ia is very uncertain (e.g., Livio 2001), we can see from our tentative age-metallicity relation (Fig. 20) that it has taken about 2–3 billion years for the thick disk stellar population to reach a metallicity of [Fe/H] $= -0.4$, and that it might have continued to form stars for 2–3 billion years after that in order to reach roughly solar metallicities. The main conclusion from this is that the thick disk has most probably formed during an interval spanning several ($>$ 2–3) billion years. The well-defined abundance trends, that we see for the thick disk, with internal small scatter, also implies that the material from which the thick disk stars formed was well-mixed.

But how did the thick disk stellar population achieve the "hot" kinematics that we

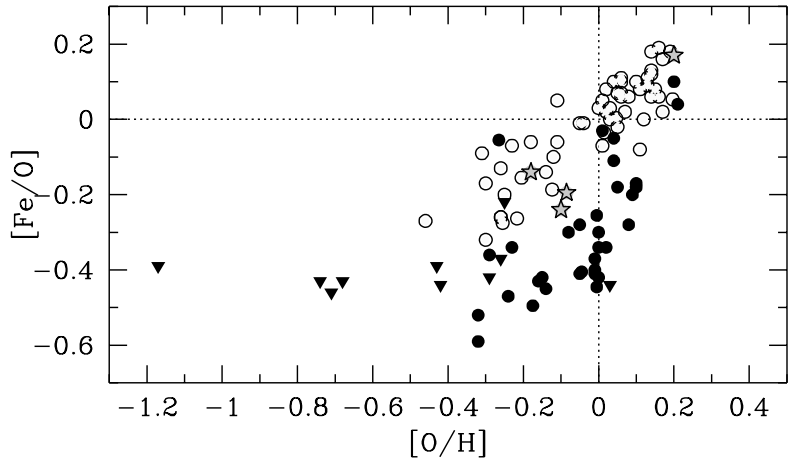

FIGURE 19: [Fe/O] versus [O/H]. Symbols as in Fig. 18.

see today? The observational results presented above appear to favour a merging and/or interaction scenario between the Galaxy and a companion (dwarf?) galaxy. We are lead to this conclusion not so much by what is in favour of a merger scenario as by what is against the alternative scenarios. There are essentially five main formation scenarios for the thick disk (see, e.g., Gilmore et al. 1989) and I will start by discussing the most likely one and then turn to a discussion about what makes the others less probable.

The most likely scenario(s):

Violent heating by a merger: In this scenario the Galaxy cannibalizes on another companion stellar system. As a result the stellar disk that was present at the time of the merger event "puffs up" and forms a thick disk. Gradually the remaining interstellar gas, maybe enriched or diluted by the merger, will settle and star formation will start again, forming today's thin disk. The merger scenario has been modelled with N-body simulations (e.g., Quinn et al. 1993; Walker et al. 1996; Huang & Carlberg 1997; Velázquez & White 1999). Although the consequences of such events are not fully understood, it is clear from the simulations that some heating will occur. A shortcoming of N-body simulations is that they do not include hydrodynamic processes. In order to inflate the old thin disk to the velocity dispersions that today's thick disk exhibits, the simulations require that the merging satellite is quite massive ($\sim$ 0.1–0.2 of the Galaxy disk). Dwarf galaxies in the Local Group with masses of that order are today rare (e.g., Mateo 1998).

The merger scenario does not in itself put any constraints on the time-scale for the formation of the stars that make up today's thick disk. Depending on the structure of the stellar disk that was the predecessor of the thick disk, and the amount of gas and stars that

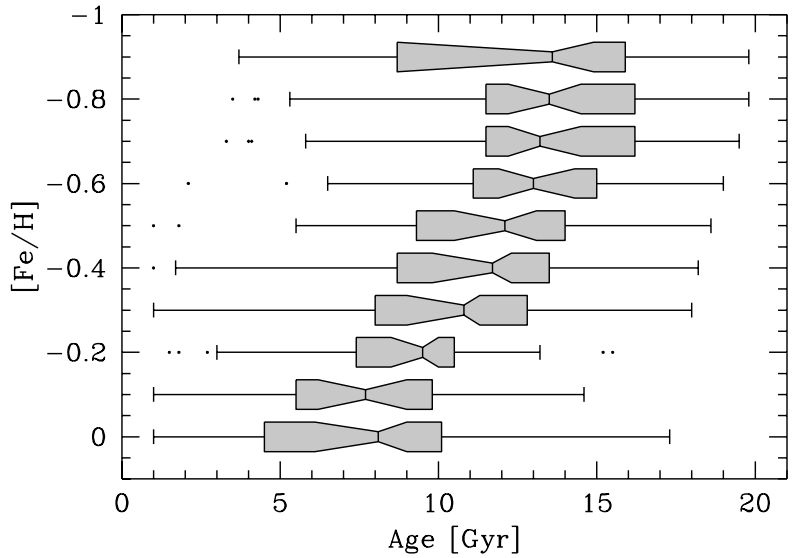

FIGURE 20: Age-metallicity diagram for the thick disk (see Paper V). In the boxplots the central vertical line represents the median value. The lower and upper quartiles are represented by the outer edges of the boxes, i.e. the box encloses 50 % of the sample. The notches (waists) indicate the 95 % confidence intervals for the median value. The whiskers extend to the farthest data point that lies within 1.5 times the inter-quartile distance. Those stars that do not fall within the reach of the whiskers are regarded as outliers and are marked by solid circles. A common rule is that, samples for which the boxplot notch intervals do not overlap are likely to be different in their distributions.

comes with the merging galaxy, the constraints on the abundance and age distributions in today's thick disk may vary. The overall picture can be quite complex, but it is reasonable to expect that the distributions of today's thin and thick disks, in terms of kinematics, ages, and abundances, should be distinct. Especially, we expect the thick disk to be older and more heated. This is what we see. We also see that the elemental abundance trends appear to be invariant with $Z_{\rm max}$ and $R_{\rm m}$ (see Fig. 17 in Paper I and Fig. 9 in Paper IV). Also, Gilmore et al. (1989) found no evidence for a gradient in the metallicity distribution for the thick disk with height above the Galactic plane.

Further evidence in favour of a merger event comes from a spectroscopic survey of $\sim$ 2000 F and G dwarf stars by Gilmore et al. (2002). They claim to have identified a stellar population in the Galaxy that might come from a disrupted satellite that merged with the Galaxy, and that this merger happened some 10–12 Gyr ago.

Extra-galactic studies have also found that thick disks in spiral galaxies are more com-

mon in environments where the host galaxies are merging and/or interacting with companion galaxies (e.g., Schwarzkopf & Dettmar 2000; Reshetnikov & Combes 1997; Dalcanton & Bernstein 2002). Even though these studies are not evidence for the origin of the Galactic thick disk, they do point at the kind of environments in which thick disks are likely to appear.

Heating by a passing satellite: Kroupa (2002) shows that the merging with another galaxy is not necessary in order to produce a kinematical heating of a galactic disk. An episode of kinematical heating and increased star formation may also be caused by a passing satellite. The resulting abundance trends are difficult to predict. It is however likely that they could be similar to those of the merging scenario, and in that case also be cleaner since no extragalactic stars and gas have been received.

The less likely scenarios

The thick disk formation scenarios that we find less likely are the following:

Slow, pressure supported collapse: As the pre-galactic cloud slowly contracts and loses energy through dissipation, star formation is continuously ongoing. Enrichment from the ejecta of SN II results in later stellar generations to be born from interstellar gas with higher elemental abundances. Vertical abundance gradients will have time to build up in the thick disk and the age distributions for the two disk populations will be a continuous distribution. The abundance trends in the thick disk, being the older and more metal-poor, will also be followed smoothly by the abundance trends in the thin disk.

This scenario fails on the fact that there are no vertical gradients in the metallicity distribution of the thick disk (Gilmore et al. 1995). Also, the abundance trends in the thick and thin disk do not follow smoothly upon each other. If the thin disk formed after the thick disk, one has to put very tight constraints on the possible time spans for infall of pristine interstellar gas to occur. This is necessary since we see that the first stars in the thin disk have formed from interstellar gas that is considerably more metal-poor than the gas forming the (metal-rich) thick disk (down to [Fe/H] ~ -0.7 for the thin disk and up to solar metallicities for the thick disk).

Fast collapse due to increased dissipation: This scenario has been modelled in detail by Burkert et al. (1992) and their results indicate that this kind of collapse could produce thin and thick disk populations that do not have overlapping age, metallicity, and kinematical distributions. Also, there is not enough time to build up vertical abundance gradients since the star formation in the thick disk ceases after only ~ 400 Myr in their model.

This scenario fails on the fact that we see that the thick disk formed under a substantially longer time period than what usually can be accommodated in a fast collapse. Also, as in the case of a slow collapse, there have to be tight constraints on the infall of material.

Direct accretion of material: Extragalactic debris on suitable orbits might end up in the Galaxy, and their joint contributions can form a larger entity, in this case the thick disk. The consequences of such a scenario would be mixed age and abundance trends in the disks, reflecting the properties of the accreted debris.

This scenario fails on the fact that we see distinct and well-defined abundance trends in the thin and thick disks, and essentially non-overlapping age distributions.

Kinematic diffusion of stellar orbits: Stars are influenced by their surroundings and their orbits will change with time due to interaction with e.g. giant molecular clouds or "collisions" with other stars. If such effects are responsible for the kinematic properties of the thick disk then the stars of the thin and the thick disks come from the same stellar population. The age and abundance distributions of the two populations would then be continuously connected.

Modelling by Hänninen & Flynn (2002) shows that diffusion effects are not sufficient to be responsible for the kinematics that today's thick disk possess. Also, as in the previous cases, very tight (and unlikely) constraints have to be set on the infall of pristine gas in order to produce the low-metallicity thin disk stars.

5.4 The evolution of the thin disk

The thin disk does not show the flat [O/Fe] trend (see Fig. 18) with large over-abundances of oxygen that the thick disk exhibits. This indicates that the thin disk has not had such an intense star formation history as the thick disk. The shallow decline in the [O/Fe] trend from an oxygen overabundance of [O/Fe] ~ 0.2–0.3 at [Fe/H] ~ -0.8 to an oxygen under-abundance of [O/Fe] ≈ -0.2 at [Fe/H] ~ 0.4 indicates a more continuous star formation with no fast initial enrichment from SN II. Instead the observed [O/Fe] trend favours a chemical evolution in the thin disk where both SN Ia and SN II in a steady rate contribute to the enrichment of the interstellar medium, thereby producing a shallow decline in [O/Fe] with [Fe/H] (see Fig. 18).

Previous studies have found that the [O/Fe] trend levels out at [Fe/H] > 0 instead of the downward trend that we find (see Paper III and references therein). The studies that have used the forbidden [O I] line usually neglected the blending Ni I lines and/or assumed that [Ni/Fe] ≈ 0 for all [Fe/H], which we have seen not to be the case at [Fe/H] > 0 (see Papers II, III, and IV). This resulted in oxygen abundances in those studies that in general were too high for stars with super-solar metallicities. The downward trend that we see now is also in better agreement with models of Galactic chemical evolution (see, e.g., Chiappini et al. 2003).

How can we explain the trend observed in the thin disk? The thin disk stars, on average, are younger than the thick disk stars. However, the low-metallicity tail in the metallicity distribution of the thin disk stars overlap with the metallicity distribution of the thick disk stars. A possible scenario would be that once star formation in the thick disk stops, there is a pause in the star formation. During this time in-falling fresh gas accumulates in the Galactic

plane, forming a new thin disk. Also, if there is any remaining gas from the thick disk it will settle down onto the new disk. Once enough material is collected, star formation is restarted in the new thin disk. The gas, though, has been diluted by the metal-poor in-falling gas. This means that the first stars to form in the thin disk will have lower metallicities than the last stars that formed in the thick disk.

Chapter 6
Ongoing and future studies

There are limitless futures stretching out in every direction from this moment - and from this moment and from this. Billions of them, bifurcating every instant! Every possible position of every possible electron balloons out into billions of probabilities! Billions and billions of shining, gleaming futures!

Douglas Adams, Mostly Harmless, 1992

Carbon in the Galactic thin and thick disks

The success with the analysis of the forbidden oxygen line at 6300 Å (Paper III) encouraged us to apply for observing time on the ESO 3.6-m/CES to study the weak forbidden carbon line at 8727 Å for the same set of stars (ESO proposal #073.B-0620). The proposal was granted six nights of observations that will be carried out September 4–10, 2004. The C/O ratio derived from these two forbidden lines is insensitive to departures from LTE as well as to the surface gravity of the stars. The C/O ratio will therefore be of very high accuracy and will give insights into which types of objects that contribute carbon to the chemical enrichment. There are at the moment two theories, where one favours carbon to come mainly from massive metal-rich stars, and the other that carbon comes from low- and intermediate mass stars. Our observations will help to clarify this picture.

Establishing the chemical properties of stars with kinematics intermediate to those of the thin and thick disks

In our studies of nearby dwarf stars we have relied on kinematical criteria to distinguish between stars in the thin and thick disks. In doing so we have excluded stars that have kinematics intermediate to the two disks. We have, however, observed four such stars and first results show that they also have chemical compositions intermediate to the thin and thick disk populations (see Paper IV). To further constrain the origin of these stars (where

did they form?) would require observations of more stars in order to improve the statistics of the abundance trends and equally important their kinematical properties (i.e., their combination of U, V, and W velocities). An observing proposal is in preparation.

Continuation of the study of thick disk *in situ* dwarf stars

Since only a small part of our observations of thick disk *in situ* dwarf stars with UVES on VLT/UT2 were carried out we plan to apply for more observing time. These observations will serve as an important comparison to the observations of the solar neighbourhood thick disk dwarf stars that we already have studied. This study will give very real constraints on vertical changes in the abundance trends.

Metallicity distribution functions at different heights above the Galactic plane

In order to further constrain the formation scenario for the thick disk we want to observe F and G dwarf stars at various distances from the Galactic plane to look for vertical gradients in the metallicity distribution of the thick disk. The only study that has done this is Gilmore et al. (1995) who determined [Fe/H] for $\sim$ 210 stars, using low-resolution spectra with low signal-to-noise ratios where they defined narrow band photometric indices around strong Fe lines. Their abundance distributions of stars at distances 500-3000 pc from the plane are consistent with no metallicity gradients in the thick disk, which implies that the thick disk did not form in a slow dissipational collapse. As this is the only study of its kind, the results need to be extended and checked. FLAMES would be a suitable instrument to use for this investigation. For example one of the Gilmore et al. (1995) areas can be covered with a few pointings with FLAMES. Note that with FLAMES we would be able to obtain good data for much fainter stars than in Gilmore et al. (1995). The richness of Fe lines in the stellar spectrum would allow accurate [Fe/H] determinations, using detailed abundance analysis, even with the limited wavelength coverage of FLAMES. Proposals are being planned.

Establishing the abundance trends for r- and s- process elements in the Galactic thin and thick disks

We have started a project in order to establish the abundance trends for r- and s-process elements (e.g., Ba, Eu, Y, Sr, Nd) in the thin and thick disks. As a start we have used our FEROS and SOFIN spectra (see Paper IV). We have also been granted 24 hours of observing time in Period 72 (ESO proposal #072.B-0179) with the VLT/UVES to observe a further $\sim$ 70 stars. These observations will have implications for the formation of the thick disk, nucleosynthesis in AGB stars, and to some extent SN Ia lifetimes.

Old and metal-rich – real or fake?

A significant number of old dwarf stars that are more metal-rich than the Sun was found in Feltzing et al. (2001). The presence of such stars is unexpected, since generally models of Galactic chemical evolution predict that older stars should be less abundant in metals

than younger ones. Could these stars be binaries? Are their metallicities erroneous? In order to find out we have, in June 2003, observed a number of such stars with the SOFIN spectrograph on the Nordic Optical Telescope. A second observing run was scheduled for February 2004. The resulting abundances in these stars will be compared to the abundance trends that have been presented in Papers I–IV, and will give insights into the possible origin of these stars. Do they form a chemically separate entity in the Galactic disk? If they do, one may speculate on their origin – could they, e.g., be part of an accretion event, or scattered from the inner disk?

Chapter 7
Comments on research articles

I here give a short summary and comments on individual papers. Some comments on my contributions to the Papers are also given, but unless otherwise indicated, all data analysis and preparation of manuscripts has been done by the first author.

Paper I:

Bensby, T., Feltzing, S., & Lundström, I.:
Elemental abundance trends in the Galactic thin and thick disks as traced by nearby F and G dwarf stars
Astronomy and Astrophysics, **410**, 527–551 (2003)

This paper includes a detailed abundance analysis of 66 stars in the solar neighbourhood that were observed with the FEROS spectrograph on La Silla in Chile. The stellar sample was divided into two sub-samples consisting of 21 thick disk stars and 45 thin disk stars, respectively. The analyzed elements were Na, Mg, Al, Si, Ca, Ti, Cr, Fe, Ni, and Zn using equivalent width measurements of ~ 450 spectral lines for each star, or in total $\sim 34\,000$ lines.

Special effort was put into the atomic data ($\log gf$-values in particular) in order to not only determine accurate abundances, but also put the derived abundances on a baseline that was as general as possible. The atomic data that were collected in this paper have been used in all the succeeding papers in this thesis work.

Paper II:

Feltzing, S., Bensby, T., & Lundström, I.:
Signatures of SNIa in the galactic thick disk – Observational evidence from α-elements in 67 dwarf stars in the solar neighbourhood
Astronomy and Astrophysics, **397**, L1–L4 (2003)

This letter briefly highlights the results and discussions that later appeared in Paper I. It focuses on the four α-elements Mg, Si, Ca and Ti. A few of the observed stars were not fully analyzed and were left to Paper I. Also, a few stars with intermediate kinematics that were included in this letter were instead discussed in Paper IV, where more stars with similar kinematics were included. Further, two of the stars in the letter do not have the right classification, due to a minor error in calculating the TD/D probabilities. The appearance of the abundance trends does not change however and the discussion in the letter is not affected. The reader is directed to the corresponding figures in Paper I when reading the text.

The data analysis is the same as in Paper I and was done by T. Bensby. The manuscript was prepared by S. Feltzing.

Paper III:

Bensby, T., Feltzing, S., & Lundström, I.:
Oxygen trends in the Galactic thin and thick disks
Astronomy and Astrophysics, **415**, 155–170 (2004)

This paper contains a detailed analysis of the oxygen abundances in 72 F and G dwarf stars, divided into thin and thick disk sub-samples. The analysis was mainly based on spectra of the forbidden [O I] line at 6300 Å obtained with extremely high spectral resolution ($R \sim 215\,000$) and very high signal-to-noise ratios ($S/N > 400$) on the CES spectrograph at La Silla in Chile. The stars are the same as in Papers I and II with three additional stars from Paper IV included (since we had CES and UVES spectra, but no FEROS spectra for these stars). Two conference proceeding papers concerning oxygen abundances in these stars have also been presented. The analysis in these proceeding papers differ in the details (although the results do not) from that in the final paper and they are not included in this thesis (see however "Research articles and conference proceedings not included in this thesis" on page x for references).

Paper IV:

Bensby, T., Feltzing, S., Lundström, I., & Ilyin, I.:
α-, r-, and s-process element trends in the Galactic thin and thick disks
Astronomy and Astrophysics, in preparation

This paper contains a detailed abundance analysis of a further 36 F and G dwarf stars. Thirty of the stars were observed with the SOFIN spectrograph on Roque de los Muchachos, La Palma, Spain, and the remaining six were taken from the previous observing runs at Paranal and La Silla in Chile. The stars were selected to populate metallicities below solar in order to confirm the abundance trends that we found from the FEROS spectra (Paper I). The paper also includes a further analysis of the assumptions of the density of thick disk stars in the solar neighbourhood, on which the selection of the stellar samples partly depend.

This paper extends the elemental abundance analysis in the thin and thick disks by including the *r*- and *s*-process elements Y, Ba, and Eu. The 66 stars from Paper I were also included in the new analysis of the *r*- and *s*-process elements.

The reductions of the raw data from the SOFIN spectrograph to un-normalized one-dimensional spectra was performed by I. Ilyin.

Paper V:

Bensby, T., Feltzing, S., & Lundström, I.:
A possible age-metallicity relation in the Galactic thick disk?
Astronomy and Astrophysics, submitted

By selecting stars from the Hipparcos catalogue with accurate parallaxes, measured radial velocities, and measured Strömgren $uvby$ photometry, we ended up with a thick disk stellar sample consisting of 229 stars. For these stars we determined new ages from isochrone fitting. These stars were then used to investigate if there is an age-metallicity relation present in the thick disk, which we found to be very likely. The possible age-metallicity relation indicates that star formation has continued for at least 2–3 Gyr in the thick disk.

The stars were selected from the stellar catalogue that was prepared for the studies by Feltzing & Holmberg (2000) and Feltzing et al. (2001). The [Fe/H]-values used in the age-metallicity relation were also taken from that catalogue, as well as the magnitudes and colour-indices that were needed for the age determinations.

Paper VI:

Feltzing, S., Bensby, T., Primas, F., & Ryan, S.G.:
A first study of the chemical composition in thick disk dwarf stars 1–1.5 kpc above the Galactic plane
DRAFT

In this draft we present a first analysis of five dwarf stars situated 1–1.5 kpc above the Galactic plane. Such stars are very likely members of the thick disk as the thick disk stellar population dominates at these heights. Hence, determining the elemental abundance trends for such stars is an important test of our findings in Papers I and IV. Although our sample is very small we, nevertheless, find preliminary evidence that the elemental abundance trends at these heights are similar to those found for kinematically selected thick disk stars in the solar neighbourhood.

The data analysis and the preparation of the manuscript has been done by S. Feltzing.

Chapter 8
Popular summary in Swedish

Vintergatans kemiska utveckling

Vår galax, Vintergatan, är en spiralgalax som innehåller bortåt 200 miljarder stjärnor. En mörk natt kan man urskilja ca 3000 av dessa på himlavalvet. Tittar man noggrant så kan man också se ett diffust ljusband som sträcker sig genom, bland andra, stjärnbilderna Skytten och Cassiopeia. Detta diffusa band är det samlade ljuset från alla de miljarder stjärnor i Vintergatans skiva som antingen är för ljussvaga eller för avlägsna för att kunna ses som individuella objekt med blotta ögat. Figur 21 visar en handmålad karta av Vintergatan, innehållande ca 7000 stjärnor.

Man kan dela upp Vintergatan i olika komponenter (se Fig. 4): den tunna skivan (thin disk), den tjocka skivan (thick disk), den centrala ansvällningen (bulge), och halon. Egenskaperna hos stjärnorna i dessa olika populationer skiljer sig åt.

De äldsta stjärnorna finns i halon och har i många fall daterats till en bra bit över 12 miljarder år. Det som är karaktäristiskt för halostjärnor är att de rör sig med höga hastigheter relativt *lokala vilostandarden* (local standard of rest, LSR). Deras banor runt Vintergatans centrum är mer eller mindre slumpvisa, vilket också medför att halon som helhet i stort sett inte deltar i den allmänna galaktiska rotationen (som är ca $220\,\mathrm{km\,s^{-1}}$). Halostjärnorna innehåller också mycket lite av tyngre grundämnen såsom järn (man säger att de är metallfattiga[8]). Generellt sett har halostjärnorna järnhalter (relativt vätehalten i stjärnan) som är mindre än 1/10 av vad som finns i solen. Den mest metallfattiga halostjärnan som observerats har en järnhalt som endast är 1/200000 av solens.

Den tjocka skivan innehåller också mestadels äldre stjärnor. Det finns dock en betydligt större spridning i åldersfördelningen hos dessa stjärnor och man kan relativt lätt hitta stjärnor vars åldrar inte är mer än 7–8 miljarder år. Andelen av tyngre grundämnen är också högre hos stjärnorna i den tjocka skivan än för halostjärnorna. Metallhaltsfördelningen

[8] Astronomer använder av hävd ofta beteckningen "metaller" för alla grundämnen förutom väte och helium

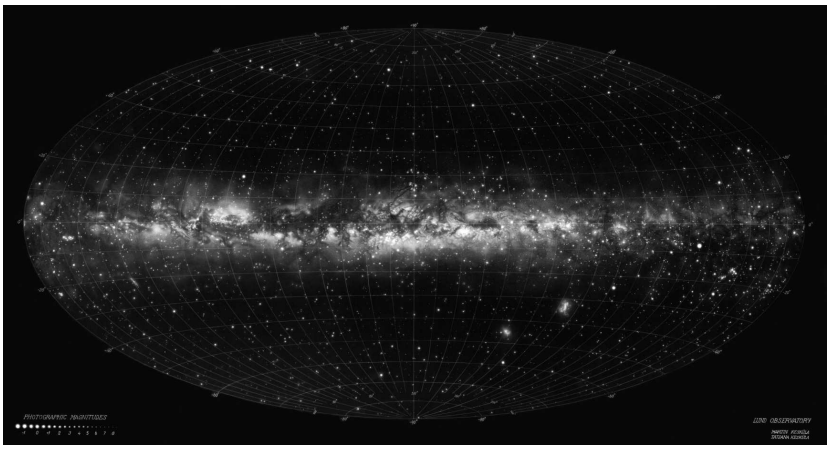

FIGURE 21: Denna karta visar hela den visuella stjärnhimlen i galaktiska koordinater där 7000 stjärnor med kända koordinater inprickats i exakta positioner. Även det diffusa ljuset från Vintergatan har åskådliggjorts genom sprutmålning. Originalkartan har dimensionerna 2×1 meter och tillhör Institutionen för astronomi i Lund. © *Lund Observatory*

sträcker sig från ungefär 1/10 av solens järnhalt och upp till solhalten. Stjärnorna i den tjocka skivan rör sig också med relativt höga hastigheter relativt LSR. Detta gör att "formen" på den tjocka skivan är en ellipsoid med en exponentiell skalhöjd på ungefär 1000–1500 pc. Till skillnad från halostjärnorna deltar den tjocka skivans stjärnor i den galaktiska rotationen. Dock så "släpar" de efter den allmänna rotationshastigheten i Vintergatsplanet med ungefär 40–50 km s^{-1}.

Den tunna skivan innehåller mestadels stjärnor som är unga och har betydligt mer tyngre grundämnen än stjärnorna i halon och den tjocka skivan. Deras metallhalter spänner från ungefär 1/10 och upp till ungefär 3 gånger solens metallhalt.

Syftet med denna avhandling är att studera hur den tjocka skivan har utvecklats i jämförelse med den tunna skivan och på så sätt söka förklaringar till deras respektive uppkomster. Eftersom den kemiska sammansättningen i atmosfärerna hos sollika stjärnor (s.k. huvudseriestjärnor av F- och G-typ) i stort sett inte har påverkats under de miljarder år som gått sedan de bildades, kan man genom att spektroskopiskt analysera sådana stjärnor bestämma vad deras atmosfärer består av och således vad de gas- och stoftmoln som stjärnan bildades ur bestod av. Detta leder i sin tur till att man kan spåra den kemiska utvecklingen i Vintergatan och dess olika komponenter. Skillnader och likheter i ymnigheterna, av speciellt utvalda grundämnen, mellan de båda stjärnpopulationerna kan då användas för att få en bättre uppfattning om deras respektive uppkomst. Speciellt uppkomsten av den tjocka skivan har många tänkbara förklaringar.

Noggranna undersökningar av sollika stjärnor kräver stjärnspektrum med hög upplösning och högt signal/brus-förhållande. För att få observationstid för en sådan undersökning av

ett stort antal stjärnor så är det nödvändigt att observationerna kan utföras under en rimlig tidsperiod. Det bästa sättet är då att observera stjärnor som är befinner sig i solens närhet och är relativt ljusstarka. Att de är närbelägna medför vissa problem i urskiljandet av stjärnor tillhörande de två olika skivkomponenterna. Stjärnorna i solens närhet består nämligen av en blandning av stjärnor från den tunna skivan ($\sim$ 90 %), den tjocka skivan ($\sim$ 10 %), och halon ($\sim$ 0.1–0.2 %) och det finns ingen definitiv metod för att särskilja dem. Den metod som anammats i denna avhandling är att använda stjärnornas kinematik (hastigheter) då denna torde vara det mest fundamentala som skiljer komponenterna åt. Ytterligare egeneskaper såsom metallhalt och åldrar skulle också kunna användas men eftersom syftet är att studera de kemiska egenskaperna i de två skivorna så skulle sådana urvalskriterier underminera syftet med undersökningen.

Utifrån de kinematiska kriterier som beskrivs i kapitel 2 så har vi valt ut och observerat drygt hundra stjärnor vars hastigheter gör att de med stor sannolikhet tillhör antingen den tunna eller den tjocka skivan. Observationerna har utförts vid det Europeiska Sydobservatoriets (European Southern Observatory, ESO) anläggningar på La Silla och Paranal i Chile och vid det Nordiska teleskopet (Nordic Optical Telescope, NOT) på La Palma.

Resultaten som presenteras i denna avhandling (artiklar I–VI) angående halttrender av olika grundämnen visar på att det finns tydliga skillnader mellan stjärnor tillhörande den tjocka och den tunna skivan. De skillnader vi ser tyder på att bildandet av stjärnorna i dessa komponenter har skett under skilda epoker. Formen på de halttrender vi ser ger också information om bildandet av de olika komponenterna gått fort eller långsamt. Tecken på en intensiv och snabb stjärnbildning finns i den tjocka skivan, medan stjärnbildningen i den tunna skivan skett i långsammare takt. Våra resultat i artikel V tyder också på att själva bildandet av stjärnorna i den tjocka skivan fortgick under flera miljarder år, uppskattningsvis 2–3 miljarder. Frågan om varför Vintergatan har två skivkomponenter kan dock inte entydigt förklaras. Våra resultat pekar på att den mest troliga förklaringen till den tjocka skivans uppkomst är en kollision mellan Vintergatan och en annan (antagligen mindre) galax. Som ett resultat av denna kollision så blev det en kinematisk “upphettning” av en redan existerande stjärnpopulation (antagligen i form av en tunn skiva). Vid kollisionen är det möjligt att Vintergatan även berikades med stjärnor och gas från den andra galaxen. Den kvarvarande gasen kom med tiden att koncentreras mot Vintergatans plan. Ur denna gas började sedan stjärnor åter bildas, och det är dessa som vi idag ser som den tunna skivan.

Acknowledgements

Finally, but not the least, I would like to put together some words for the people that have made it possible for me to complete this thesis.

First I want to thank my thesis adviser Sofia Feltzing for being the one who dragged me into this particular field of astrophysics. Without her eager outlook for submitting observing proposals whenever possible I do not think that this thesis could have been realized. Now I have so much data (still not analyzed) that I easily could produce one or even two more PhD theses, and more observations are coming... I would also like to thank my second thesis adviser Ingemar Lundström, with whom I early on in my PhD work tried to delve deeper into the field of planetary nebulae. Those observing proposals were, however, not as well received as the ones about the thin and thick disks.

The Uppsala group, including Bengt Edvardsson, Kjell Eriksson, Bengt Gustafsson, and Martin Asplund (now i Australia), are thanked for giving us access to the Uppsala MARCS models and software programs to calculate stellar abundances and synthesize spectral lines.

Poul Erik Nissen and Sean Ryan are thanked for writing loads of reference letters for my postdoc applications. I would also like to thank Poul Erik for the time he has put into reading early versions of several of our papers which gave us a lot of valuable input. Bengt Gustafsson and Bengt Edvardsson are also thanked for reading early versions of Papers I and III.

I also thank Kungl. Fysiografiska Sällskapet in Lund. Without their financial support I would not have been able to go on my first observing trip to Chile in September 2000, or to go to the IAC Winter School of Astrophysics on Tenerife in November 2001, or to go to the "Origin of the Elements" conference in Pasadena in February 2003.

I would also like to thank the ESO staff, both in Garching and in Chile, for making my three trips to Chile really something to remember.

Fredrik Boberg is thanked for numerous everlasting discussions about irrational subjects and scenarios.

The staff and personnel at Lund Observatory are thanked for making my five years run smoothly. Also, the staff and PhD students of the Atomic Astrophysics Department are thanked for their efforts in trying to discuss and explain the origin and structure of spectral lines with a blissfully ignorant person.

I would like to dedicate a special thank to my parents, my sister, my parents in law, and all other relatives for their support, and their efforts to understand what my goals in life are.

Most of all I want to thank my wife Jonna whom I met in the Spring of 1992. During these five last years *we* not just have managed to put this thesis together but also to get married and started to raise the next generation of astrophysicists: our two beloved daughters Sofia and Alva. Thank You! I Love You!

Appendix A
Observations, kinematics, and atmospheric parameters

This appendix consists of the following tables:

Table A1: Summary of observations: Columns 1–4 give different identifications for the stars; col. 5 gives the spectral class as given in the Simbad database; cols. 6 and 7 give the RA and DEC coordinates as given in the Hipparcos catalogue (ICRS J1991.25); col. 8 gives the visual magnitude as given in the Hipparcos catalogue; col. 9 indicates with which instruments the star has been observed (F=FEROS, C=CES, S=SOFIN, U=UVES); col. 10 indicates which year the star was observed (02 = UVES july 2002, 02a = SOFIN August 2002, 02b = SOFIN November 2002) (see also Table 2).

Table A2: Rejected stars: Column 1 gives the Hipparcos identification; col. 2 gives the instrument(s) the star was observed with; col. 3 gives the year the star was observed; col. 4 gives comments on why the star was rejected from the abundance analysis.

Table A3: Distances and kinematics: Column 1 gives the Hipparcos identification; cols. 2, 3, 4, give the parallax (π) and the proper motions (μ_α and μ_δ, ICRS for epoch J1991.25), all taken from the Hipparcos catalogue; col. 5 gives the radial velocity; cols. 7–9 give the three Galactic velocity components ($U_{\rm LSR}$, $V_{\rm LSR}$, and $W_{\rm LSR}$); cols. 10 and 11 give the TD/D and TD/H ratios (calculated with the 10% normalization for the thick disk, see Eqs. 4).

Table A4: Stellar atmospheric parameters: Column 1 give the Hipparcos identification; col. 2 gives the metallicity [Fe/H]; col. 3 gives the effective temperature $T_{\rm eff}$; col. 4 gives the surface gravity $\log g$; col. 5 gives the bolometric correction BC; col. 6 gives the microturbulence $\xi_{\rm t}$; col. 7 gives the stellar mass; col. 8 gives the stellar age.

Table A1: Summary of observations

IDENTIFICATIONS					RA	DEC	V	Inst.	DATE
HIP	HD	HR	Name		h m s	d am as	mag		YY
				THICK DISK STARS					
3086	3628			G2V	00 39 12.81	+03 07 59.5	7.34	F/C	00/01
3185	3795	173		G3/G5V	00 40 32.40	−23 48 14.4	6.14	F/C	00/01
3497	4308			G5V	00 44 39.04	−65 38 51.8	6.55	F/C	01/01
3704	4597			F7/F8V	00 47 30.89	−36 56 21.6	7.85	F/C	00/01
5315	6734			K0IV	01 07 59.58	+01 59 38.7	6.44	F/C	01/01
11309	15029			F5	02 25 34.01	+11 58 18.9	7.36	S	02b
12306	16397			G0V	02 38 28.19	+30 49 03.2	7.36	S	02b
14086	18907	914	ϵ For	G5IV	03 01 37.45	−28 05 25.7	5.88	F/C	01/01
15510	20794	1008	82 Eri	G8V	03 19 55.65	−43 04 11.2	4.26	U	02
16788	22309			G0	03 36 03.35	+16 28 05.1	7.65	S	02b
17147	22879			F9V	03 40 21.66	−03 12 59.3	6.68	F/C	01/01
18235	24616			G8IV/V	03 53 59.25	−23 08 10.9	6.68	S	02b
20242	27485			G0	04 20 14.57	−03 45 02.3	7.87	S	02b
21832	29587			G2V	04 41 35.90	+42 07 10.1	7.29	S	02b
26828	37739			F5	05 41 46.63	+22 52 14.4	7.92	S	02b
36874	60298			G2V	07 34 50.33	+24 57 19.2	7.37	S	02b
37789	62301			F8V	07 44 56.17	+39 33 28.9	6.74	S	02b
40613	69611			F8	08 17 29.43	−03 59 18.8	7.74	S	02b
44075	76932	3578		F8IV/V	08 58 43.78	−16 07 59.7	5.80	S	02b
44860	78558			G3V	09 08 25.56	−15 08 39.5	7.29	S	02b
75181	136352	5699	ν 2Lup	G4V	15 21 49.57	−48 19 01.1	5.65	F/C	01/01
79137	145148	6014		K1.5IV	16 09 11.06	+06 22 49.8	5.93	F/C	01/01
82588	152391			G8V	16 52 59.22	−00 01 22.1	6.65	F/C	01/01
83229	153075			G1V	17 00 31.82	−57 17 47.0	6.99	F	01
84905	157089			F9V	17 21 07.15	+01 26 32.6	6.95	F/C	01/01
88622	165401			G0V	18 05 37.47	+04 39 28.6	6.80	F/C	01/01
96124	183877			G5IV	19 32 40.28	−28 01 04.8	7.14	F/C	01/01
98767	190360	7670		G6IV	20 03 36.95	+29 53 53.1	5.73	F/C	01/01
103458	199288			G0V	20 57 40.49	−44 07 37.2	6.52	F/C	01/01
108736	208998			G0V	22 01 36.47	−53 05 32.5	7.12	F/C	01/01
109450	210483			G1V	22 10 25.94	+18 47 49.8	7.57	F	00
109821	210918	8477		G5V	22 14 38.21	−41 22 47.1	6.23	F/C	00/01
110512	212231			G2V	22 23 14.23	−25 50 31.4	7.87	F/C	00/01
112151	215110			G5	22 42 57.87	+00 24 08.2	7.73	S	02b
116421	221830			F9V	23 35 28.53	+31 00 59.6	6.86	S	02a
116740	222317			G2V	23 39 30.77	+28 14 45.4	7.04	S	02b
118010	224233			G0	23 56 11.21	+59 46 00.9	7.67	S	02b
118115	224383			G2V	23 57 33.25	−09 38 49.8	7.89	F/C	00
				THIN DISK STARS					
699	400	17		F8IV	00 08 41.02	+36 37 38.7	6.21	S	02a
910	693	33	6 Cet	F5V	00 11 15.91	−15 28 02.4	4.89	S	02b
2235	2454	107		F6V	00 28 20.03	+10 11 25.2	6.05	S	02a
2787	3229	143	14 Cet	F5IV	00 35 32.75	−00 30 19.7	5.94	S	02a

Table A1: Summary of observations - *continued*

IDENTIFICATIONS					RA	DEC	V	Inst.	DATE
HIP	HD	HR	Name		h m s	d am as	mag		YY
3142	3735	170		F8V	00 39 57.59	−33 57 40.3	6.68	F/C	01/01
3909	4813	235	19ϕ2Cet	F7IV/V	00 50 07.72	−10 38 37.6	5.17	S	02a
5862	7570	370	ν Phe	F8V	01 15 11.12	−45 31 54.0	4.97	U	02
7276	9562	448		G2IV	01 33 42.73	−07 01 30.5	5.75	F/C	00/00
9085	12042	573		F6.5V	01 56 59.66	−51 46 00.7	6.10	F/C	00/01
10306	13555	646	17η Ari	F5V	02 12 47.98	+21 12 39.5	5.23	S	02a
10798	14412	683		G5V	02 18 58.65	−25 56 48.4	6.33	F/C	01/01
12186	16417	772	λ2For	G5IV	02 36 58.62	−34 34 38.4	5.78	F/C	00/00
12611	17006	807		K1III	02 42 08.44	−46 31 27.2	6.09	F/C	00/01
12653	17051	810	ι Hor	G0V	02 42 33.16	−50 48 03.0	5.40	F/C	00/00
14954	19994	962	94 Cet	F8V	03 12 46.32	−01 11 45.4	5.07	F/C	01/01
15131	20407			G1V	03 15 06.39	−45 39 53.4	6.75	U	02
17378	23249	1136	23δ Eri	K0IV	03 43 14.96	−09 45 54.7	3.52	F/C	00/00
18833	25322			F5V	04 02 15.32	+22 25 20.8	7.82	S	02b
22263	30495	1532	58 Eri	G3V	04 47 36.21	−16 56 05.5	5.49	F/C	00/00
22325	30606	1538	59 Eri	F8V	04 48 32.53	−16 19 46.5	5.76	F/C	00/01
23555	32820	1651		F8V	05 03 53.94	−41 44 43.2	6.30	F/C	00/01
23941	33256	1673	68 Eri	F2V	05 08 43.67	−04 27 22.5	5.11	F	00
24829	35072	1767	ζ Pic	F7IV	05 19 22.11	−50 36 23.5	5.44	F/C	00/00
29271	43834	2261	α Men	G6V	06 10 14.20	−74 45 09.1	5.08	F/C	00/00
30480	45701	2354		G3IV-V	06 24 26.57	−63 25 43.1	6.45	F/C	00/00
30503	45184	2318		G2IV	06 24 43.99	−28 46 47.3	6.37	F/C	00/01
72673	130551			F5V	14 51 31.66	−60 55 51.8	7.16	F/C	01/01
78955	144585	5996		G5V	16 07 03.53	−14 04 16.8	6.32	F/C	01/01
80337	147513	6094		G5V	16 24 01.24	−39 11 34.8	5.37	F/C	00/00
80686	147584	6098	ζ TrA	F9V	16 28 27.80	−70 05 04.8	4.90	F/C	01/01
81520	149612			G3V	16 39 04.39	−58 15 27.0	7.01	F	01
83601	154417	6349		F9IV-V	17 05 16.83	+00 42 12.1	6.00	F/C	00/00
84551	156098	6409		F6IV	17 17 03.71	−32 39 45.7	5.53	F/C	00/00
84636	156365			G3V	17 18 07.07	−24 04 22.2	6.59	F/C	00/01
85007	157466			F8V	17 22 27.61	+24 52 47.4	6.88	F/C	01/01
85042	157347	6465		G5IV	17 22 51.26	−02 23 16.5	6.28	F/C	00/00
86731	161239	6608	84 Her	G2IIIb	17 43 21.64	+24 19 39.5	5.73	F/C	01/01
86796	160691	6585	μ Ara	G3IV-V	17 44 08.72	−51 50 00.9	5.12	F/C	01/01
87523	162396	6649		F8IV-V	17 52 52.47	−41 59 45.8	6.19	F/C	01/01
88945	166435			G0	18 09 21.33	+29 57 05.6	6.84	S	02a
90485	169830	6907		F9V	18 27 49.48	−29 49 00.8	5.90	F/C	00/00
91438	172051	6998		G5V	18 38 53.45	−21 03 05.4	5.85	F/C	01/01
92270	174160	7079		F8V	18 48 16.39	+23 30 53.2	6.19	S	02a
93185	176377			G0	18 58 50.97	+30 10 48.6	6.80	S	02a
94645	179949	7291		F8V	19 15 33.15	−24 10 44.8	6.25	F/C	00/00
96258	184960	7451		F7V	19 34 19.76	+51 14 13.5	5.71	S	02a
96536	184985	7454		F7V	19 37 34.48	−14 18 05.2	5.46	F/C	00/00
98785	190009	7658		F7V	20 03 44.33	−22 35 44.3	6.44	F/C	00/01
99240	190248	7665	δ Pav	G7IV	20 08 41.86	−66 10 45.6	3.55	F/C	00/00
102264	197214			G5V	20 43 16.03	−29 25 24.3	6.95	F/C	01/01

Table A1: Summary of observations - *continued*

IDENTIFICATIONS					RA	DEC	V	Inst.	DATE
HIP	HD	HR	Name		h m s	d am as	mag		YY
103682	199960	8041	11 Aqr	G1V	21 00 33.81	−04 43 47.7	6.21	F/C	00/01
105858	203608	8181	γ Pav	F6V	21 26 26.49	−65 22 05.3	4.21	F/C	01/01
107975	207978	8354	15 Peg	F6IV-V	21 52 29.96	+28 47 37.3	5.52	S	02b
109378	210277			G0	22 09 29.82	−07 32 51.2	6.54	F/C	01/01
110341	211976	8514		F6V	22 20 55.77	+08 11 12.1	6.18	F/C	01/01
113137	216437	8701	ρ Ind	G2.5IV	22 54 39.56	−70 04 26.0	6.04	F/C	00/00
113174	216756	8718		F5II	22 55 02.58	+37 04 36.5	5.91	S	02a
113357	217014	8729	51 Peg	G3IVa	22 57 27.85	+20 46 07.3	5.45	F/C	00/00
113421	217107	8734		G8IV	22 58 15.54	−02 23 43.2	6.17	F/C	01/01
117880	224022	9046		F8IV	23 54 38.34	−40 18 00.5	6.03	F/C	00/01
"TRANSITION OBJECTS"									
3170	3823	176		G1V	00 40 24.66	−59 27 20.5	5.89	F/C	01/01
44441	77408			F6IV	09 03 16.03	+32 52 53.2	7.03	S	02b
95447	182572	7373	31 Aql	G8IV..	19 24 57.77	+11 56 34.3	5.17	F/C	01/01
100412	193307	7766		G0V	20 21 41.36	−49 59 55.7	6.26	F/C	01/01

Table A2: Summary of observations (Rejected stars)

NAME	Instrument	Year	Comment
HIP 238	FEROS/CES	2001	fast rotator
HIP 3641	SOFIN	2002	fast rotator
HIP 4989	SOFIN	2002	fast rotator
HIP 5034	SOFIN	2002	fast rotator
HIP 6669	SOFIN	2002	fast rotator, binary
HIP 6706	SOFIN	2002	fast rotator
HIP 13679	FEROS/CES	2001	fast rotator
HIP 17651	CES	2000	fast rotator
HIP 17732	SOFIN	2002	fast rotator
HIP 18859	SOFIN	2002	fast rotator
HIP 20284	FEROS	2000	fast rotator
HIP 21861	CES	2000	bad exposure
HIP 24109	SOFIN	2002	fast rotator
HIP 24162	FEROS	2000	fast rotator
HIP 45879	SOFIN	2002	fast rotator
HIP 85397	FEROS/CES	2000	fast rotator
HIP 86736	FEROS/CES	2001	fast rotator
HIP 87958	SOFIN	2002	fast rotator
HIP 96556	CES	2000	fast rotator
HIP 102485	CES	2000	fast rotator
HIP 104680	FEROS/CES	2000	fast rotator
HIP 109422	CES	2000	fast rotator
HIP 109652	SOFIN	2002	fast rotator, binary?
HIP 114081	FEROS	2000	fast rotator
HIP 115713	CES	2000	fast rotator
HD 3010	UVES	2002	fast rotator

Table A3: Distances and kinematics

OBJECT	π	μ_α	μ_δ	v_r	U_{LSR}	V_{LSR}	W_{LSR}	TD/D	TD/H
	["]	[mas/yr]	[mas/yr]	———	[km/s]	———			
THICK DISK STARS									
HIP 3086	21.79	781.34	296.76	−25.5	−159.4	−48.4	53.6	8960	213.5
HIP 3185	35.02	635.49	−363.28	−44.7	−37.5	−84.8	45.3	132.3	768
HIP 3497	45.76	157.92	−742.38	94.1	60.0	−103.7	−19.0	418.5	447.3
HIP 3704	19.99	−182.57	−350.64	−36.9	86.5	−35.7	58.4	41.2	1174
HIP 5315	21.53	143.39	−432.84	−95.8	60.3	−118.0	46.3	1e+05	104.3
HIP 11309	15.05	−123.59	−281.65	−8.5	73.3	−34.2	−55.3	11.7	1647
HIP 12306	27.89	−487.55	−387.37	−99.7	146.0	−25.7	−33.9	46.1	819.4
HIP 14086	32.94	282.98	−440.90	41.9	18.6	−78.1	−13.1	2.05	2147
HIP 15510	165.00	3037.21	726.52	90.3	−69.4	−89.3	−24.0	73.7	765.3
HIP 16788	22.25	−284.52	−276.33	−29.1	78.0	−2.2	−50.3	2.68	2220
HIP 17147	41.07	689.67	−214.34	119.2	−99.0	−80.4	−37.0	295.7	542.2
HIP 18235	15.87	336.31	−297.71	100.7	−17.0	−158.1	−20.1	5e+07	13.4
HIP 20242	14.79	−10.23	−318.42	−31.6	90.5	−59.7	−19.8	3.31	1826
HIP 21832	35.31	536.05	−416.89	111.5	−124.6	−44.6	18.9	7.26	1374
HIP 26828	12.32	194.34	−125.43	75.8	−61.4	−81.2	40.2	80.9	837.9
HIP 36874	25.42	129.72	−352.76	−134.9	149.7	−31.1	−40.7	178.8	584.3
HIP 37789	29.22	27.78	−683.88	−5.4	4.5	−103.4	−15.8	115.3	656.5
HIP 40613	20.46	−145.07	−438.72	113.4	−28.4	−139.7	−35.9	2e+06	41.0
HIP 44075	46.90	244.35	213.46	119.5	−38.2	−85.2	76.8	54310	198.2
HIP 44860	27.27	−534.34	−200.01	66.8	−58.9	−68.7	−56.7	172.7	795.6
HIP 75181	68.70	−1622.71	−275.10	−69.7	−109.5	−41.4	43.3	21.1	1197
HIP 79137	32.84	258.17	−746.68	−4.3	81.5	−49.8	−62.6	193.1	806.2
HIP 82588	59.04	−711.75	−1483.65	44.4	94.1	−105.5	16.6	2427	257.6
HIP 83229	31.77	−165.20	−298.01	98.5	71.1	−84.4	−15.6	22.5	1046
HIP 84905	25.88	−165.01	269.80	−163.1	−157.7	−36.2	−3.5	38.7	765.4
HIP 88622	41.00	−30.66	−322.06	−119.9	−68.6	−84.7	−31.7	68.9	818.9
HIP 96124	38.38	71.64	−748.43	−43.6	−28.0	−87.4	−15.4	9.84	1359
HIP 98767	62.92	683.32	−524.06	−46.3	−2.6	−40.5	−56.9	4.64	2283
HIP 103458	46.26	−515.51	−975.63	−9.2	31.3	−96.3	52.9	2273	359.9
HIP 108736	27.96	51.86	−504.00	−28.0	−15.6	−72.9	44.6	16.7	1409
HIP 109450	20.58	353.19	−29.57	−71.8	−64.1	−72.8	−8.4	2.68	1927
HIP 109821	45.19	570.33	−791.08	−17.7	−36.9	−86.9	−2.5	7.58	1428
HIP 110512	18.77	376.34	−94.31	7.2	−57.2	−34.9	−52.2	3.90	2219
HIP 112151	11.30	146.54	−161.09	−8.3	−10.9	−65.9	−46.9	9.62	1690
HIP 116421	30.93	540.21	253.77	−112.1	−55.1	−107.9	69.8	8e+05	78.2
HIP 116740	20.27	303.04	227.05	−32.0	−68.5	−27.8	47.3	1.95	2531
HIP 118010	20.01	195.30	282.18	3.3	−45.9	−15.8	62.5	7.96	1975
HIP 118115	20.98	455.25	−146.26	−29.6	−65.0	−77.9	3.3	4.92	1602
THIN DISK STARS									
HIP 699	30.26	−114.72	−124.60	−14.9	37.6	−4.9	−0.8	0.013	8250
HIP 910	52.84	−84.20	−269.31	15.0	29.0	−7.8	−11.1	0.014	8360
HIP 2235	27.51	32.79	−203.14	−9.9	23.2	−26.2	−6.7	0.018	8059
HIP 2787	17.97	143.36	−61.94	11.7	−16.5	−21.7	−12.9	0.017	8243
HIP 3142	24.12	330.05	−108.27	−13.2	−35.5	−45.8	19.9	0.122	4901

Table A3: Distances and kinematics - *continued*

OBJECT	π	μ_α	μ_δ	v_r	U_{LSR}	V_{LSR}	W_{LSR}	TD/D	TD/H
	["]	[mas/yr]	[mas/yr]	———	[km/s]	———			
HIP 3909	64.69	−224.67	−228.44	7.6	31.4	2.5	−4.8	0.013	8265
HIP 5862	66.43	664.46	178.14	14.3	−34.1	−17.1	−6.0	0.016	8182
HIP 7276	33.71	176.82	−81.49	−13.3	1.1	−21.1	19.5	0.021	7882
HIP 9085	37.97	348.83	249.36	5.7	−42.5	−5.1	1.0	0.015	7960
HIP 10306	33.19	162.52	4.07	5.9	−10.3	−6.8	11.2	0.011	8932
HIP 10798	78.88	−218.07	444.51	6.2	−0.7	32.3	−1.7	0.028	5897
HIP 12186	39.16	−18.27	−259.92	13.0	31.8	−18.9	−3.2	0.015	8288
HIP 12611	24.47	9.99	−94.30	14.4	22.0	−13.5	0.1	0.011	8946
HIP 12653	58.00	333.73	219.21	18.5	−21.3	−12.8	−3.1	0.011	8958
HIP 14954	44.69	193.43	−69.23	18.1	−9.7	−14.2	1.2	0.010	9246
HIP 15131	41.05	−132.56	141.62	6.7	3.6	20.2	−9.6	0.017	7243
HIP 17378	110.58	−91.71	742.23	−4.0	−4.8	31.6	18.5	0.045	5317
HIP 18833	11.47	−68.93	−50.78	−29.5	50.8	3.6	−14.0	0.027	6676
HIP 22263	75.10	130.41	169.20	23.9	−15.4	−4.3	3.1	0.010	9151
HIP 22325	24.06	7.09	39.68	36.4	−20.5	−7.7	−9.9	0.012	8765
HIP 23555	31.93	22.82	159.17	32.8	−23.1	−12.4	−8.2	0.012	8726
HIP 23941	39.99	55.62	16.03	12.2	−2.0	−1.9	8.1	0.010	9106
HIP 24829	27.70	23.00	227.39	46.6	−36.8	−26.3	−15.5	0.031	6981
HIP 29271	98.54	121.84	−212.82	38.2	29.5	−27.2	−5.8	0.020	7766
HIP 30480	31.46	19.37	−116.00	29.4	29.1	−20.3	−5.5	0.015	8280
HIP 30503	45.38	−164.83	−120.68	−1.8	19.0	9.1	−11.9	0.014	7969
HIP 72673	20.94	54.43	113.14	32.4	49.3	−0.7	23.8	0.044	6097
HIP 78955	34.60	−261.22	11.77	−14.7	−16.6	−16.2	25.4	0.030	7219
HIP 80337	77.69	72.64	3.41	13.4	24.0	4.0	5.8	0.012	8467
HIP 80686	82.61	199.89	110.77	1.7	18.5	14.3	2.5	0.013	7887
HIP 81520	46.13	−226.99	−285.49	−9.9	−17.8	−21.8	6.7	0.014	8555
HIP 83601	49.06	−15.67	−335.11	−16.2	12.0	−24.9	−12.7	0.018	8129
HIP 84551	19.80	−99.18	−55.48	−38.8	−31.9	−14.7	16.8	0.021	7693
HIP 84636	21.20	97.01	−73.75	−12.1	1.7	3.8	−21.4	0.019	7715
HIP 85007	33.54	62.67	−160.22	33.1	48.4	19.4	10.2	0.033	5898
HIP 85042	51.39	49.94	−107.54	−35.2	−16.5	−11.3	−12.4	0.013	8693
HIP 86731	26.13	−116.66	72.26	−24.4	−15.3	−15.7	18.8	0.019	8034
HIP 86796	65.46	−15.06	−191.17	−10.4	−5.0	−2.7	3.5	0.009	9283
HIP 87523	30.55	141.81	−190.53	−18.1	−14.9	−5.2	−23.7	0.023	7582
HIP 88945	39.62	71.12	60.54	−14.4	−4.3	1.1	−3.3	0.009	9144
HIP 90485	27.53	−0.84	15.16	−16.4	−6.1	6.5	10.9	0.012	8474
HIP 91438	77.02	−74.88	−151.87	36.0	47.1	3.0	2.9	0.018	7395
HIP 92270	34.85	25.30	−6.78	3.6	12.0	9.0	4.4	0.011	8490
HIP 93185	42.68	56.25	194.66	−40.4	−29.0	−19.1	2.2	0.014	8424
HIP 94645	36.97	114.78	−101.81	−23.0	−15.0	−7.1	−4.5	0.010	9165
HIP 96258	39.08	31.72	−188.14	1.0	29.3	7.3	−5.4	0.013	8050
HIP 96536	32.36	−104.36	−146.68	−14.3	9.9	−23.4	16.0	0.020	8008
HIP 98785	17.38	−38.45	23.36	9.9	22.6	12.1	13.8	0.017	7484
HIP 99240	163.73	1210.29	−1130.34	−21.1	−38.2	−8.5	−8.2	0.015	8054
HIP 102264	44.57	−43.54	−207.55	−22.9	−2.6	−21.4	20.0	0.022	7807
HIP 103682	37.80	47.64	−138.75	−16.0	3.8	−18.1	3.6	0.011	9116

Table A3: Distances and kinematics - *continued*

OBJECT	π	μ_α	μ_δ	v_r	U_{LSR}	V_{LSR}	W_{LSR}	TD/D	TD/H
	["]	[mas/yr]	[mas/yr]	———	[km/s]	———			
HIP 105858	108.50	81.08	800.68	−31.0	−3.8	49.5	13.7	0.144	3415
HIP 107975	36.15	−58.67	−63.26	19.3	23.6	21.3	−0.3	0.018	6985
HIP 109378	46.97	85.48	−449.82	−22.0	13.6	−45.5	1.8	0.047	6237
HIP 110341	31.45	43.67	21.60	7.5	4.7	11.5	0.7	0.011	8417
HIP 113137	37.71	−43.19	73.20	−1.4	14.1	15.0	5.2	0.013	7862
HIP 113174	24.24	88.52	9.25	−28.1	−1.8	−25.4	10.9	0.017	8317
HIP 113357	65.10	208.06	60.96	−31.8	−5.2	−23.2	22.0	0.027	7461
HIP 113421	50.71	−6.05	−16.03	−14.3	8.3	−3.8	18.3	0.015	8294
HIP 117880	35.86	367.44	30.51	−7.4	−36.2	−11.4	2.8	0.014	8311
"TRANSITION OBJECTS"									
HIP 3170	39.26	883.26	443.01	1.9	−102.8	−12.4	−27.6	0.71	2729
HIP 44441	19.85	−419.82	−3.94	72.8	−110.5	−4.2	−20.2	0.62	2654
HIP 95447	66.01	721.27	643.60	−101.3	−107.1	−25.7	−13.3	0.55	2835
HIP 100412	30.84	−359.84	−250.36	17.0	46.1	−43.0	41.8	1.04	3002

Table A4: Stellar atmospheric parameters

OBJECT	[Fe/H]	$T_{\rm eff}$ [K]	$\log g$ [cgs]	BC [mag]	$\xi_{\rm t}$ [km/s]	$\mathcal{M}$ $M_\odot$	Age [Gyr]
HIP 699	−0.20	6250	4.19	−0.09	1.35	1.27	3.8
HIP 910	−0.36	6220	4.07	−0.10	1.43	1.10	5.5
HIP 2235	−0.28	6645	4.17	−0.07	1.75	1.30	2.5
HIP 2787	−0.11	6620	3.86	−0.06	1.70	1.68	1.8
HIP 3086	−0.11	5840	4.15	−0.12	1.15	1.07	7.7
HIP 3142	−0.45	6100	4.07	−0.12	1.50	1.12	6.6
HIP 3170	−0.34	5970	4.11	−0.12	1.40	1.05	7.1
HIP 3185	−0.59	5320	3.78	−0.24	0.70	0.88	10.9
HIP 3497	−0.33	5636	4.30	−0.17	0.80	0.85	11.8
HIP 3704	−0.38	6040	4.30	−0.12	1.08	0.98	6.0
HIP 3909	−0.06	6270	4.41	−0.08	1.12	1.17	1.0
HIP 5315	−0.42	5030	3.46	−0.32	0.86	1.10	5.9
HIP 5862	0.17	6100	4.26	−0.08	1.10	1.04	2.0
HIP 7276	0.20	5930	3.99	−0.09	1.35	1.22	3.8
HIP 9085	−0.31	6200	4.25	−0.10	1.30	1.06	4.0
HIP 10306	−0.17	6560	4.04	−0.07	1.75	1.48	2.5
HIP 10798	−0.47	5350	4.57	−0.23	0.20	0.84	13.5
HIP 11309	−0.32	6210	3.98	−0.10	1.40	1.12	4.6
HIP 12186	0.14	5800	4.04	−0.11	1.20	1.10	6.5
HIP 12306	−0.53	5765	4.20	−0.16	0.90	0.78	12.3
HIP 12611	0.26	5250	3.66	−0.24	1.35	1.46	3.0
HIP 12653	0.14	6150	4.37	−0.07	1.25	1.15	1.0
HIP 14086	−0.59	5110	3.51	−0.30	0.87	0.81	8.8
HIP 14954	0.19	6240	4.10	−0.06	1.60	1.33	2.5
HIP 15131	−0.52	5834	4.35	−0.15	1.00	0.85	9.9
HIP 15510	−0.41	5480	4.43	−0.20	0.75	0.82	12.4
HIP 16788	−0.32	5920	4.24	−0.13	1.00	0.89	7.3
HIP 17147	−0.84	5920	4.33	−0.16	1.20	0.82	11.2
HIP 17378	0.24	5020	3.73	−0.33	0.80	1.18	6.9
HIP 18235	−0.71	5000	3.13	−0.33	0.95	0.79	10.5
HIP 18833	−0.52	6370	3.99	−0.10	1.75	1.19	4.6
HIP 20242	−0.26	5650	3.94	−0.16	1.00	1.02	8.3
HIP 21832	−0.61	5570	4.27	−0.19	0.65	0.72	18.0
HIP 22263	0.05	5850	4.50	−0.11	0.95	1.10	
HIP 22325	0.06	6250	3.91	−0.07	1.80	1.55	2.6
HIP 23555	0.13	6300	4.29	−0.06	1.50	1.23	1.7
HIP 23941	−0.30	6427	4.04	−0.08	1.90	1.24	3.1
HIP 24829	0.06	6360	3.93	−0.06	1.70	1.54	2.3
HIP 26828	−0.37	6410	4.15	−0.09	1.50	1.31	3.7
HIP 29271	0.10	5550	4.38	−0.16	0.80	0.90	6.3
HIP 30480	0.19	5890	4.15	−0.10	1.20	1.09	4.2
HIP 30503	0.04	5820	4.37	−0.12	0.90	1.00	5.0
HIP 36874	−0.07	5730	4.22	−0.14	0.90	0.98	9.3
HIP 37789	−0.67	5900	4.09	−0.15	1.20	0.88	11.1
HIP 40613	−0.63	5740	4.11	−0.16	0.92	0.84	12.9

Table A4: Stellar atmospheric parameters - *continued*

OBJECT	[Fe/H]	$T_{\rm eff}$ [K]	$\log g$ [cgs]	BC [mag]	$\xi_{\rm t}$ [km/s]	$\mathcal{M}$ $M_\odot$	Age [Gyr]
HIP 44075	−0.91	5875	4.10	−0.17	1.10	0.86	13.2
HIP 44441	−0.28	6260	4.11	−0.09	1.48	1.13	4.0
HIP 44860	−0.45	5690	4.19	−0.16	0.82	0.90	12.4
HIP 72673	−0.62	6350	4.18	−0.11	1.60	1.03	5.4
HIP 75181	−0.34	5650	4.30	−0.17	0.78	0.85	11.4
HIP 78955	0.33	5880	4.22	−0.09	1.12	1.20	3.8
HIP 79137	0.30	4900	3.62	−0.39	0.60	1.30	4.9
HIP 80337	0.03	5880	4.49	−0.11	1.10	1.09	0.5
HIP 80686	−0.06	6090	4.45	−0.09	1.01	1.15	1.2
HIP 81520	−0.48	5680	4.53	−0.17	0.65	0.90	6.8
HIP 82588	−0.02	5470	4.55	−0.19	0.90	0.95	
HIP 83229	−0.57	5770	4.17	−0.16	0.97	0.79	13.5
HIP 83601	0.09	6167	4.48	−0.07	1.21	1.20	
HIP 84551	0.12	6475	3.79	−0.05	2.00	1.85	1.8
HIP 84636	0.23	5820	3.91	−0.11	1.30	1.27	4.5
HIP 84905	−0.57	5830	4.06	−0.15	1.20	0.91	10.9
HIP 85007	−0.39	6050	4.37	−0.12	1.10	0.98	5.3
HIP 85042	0.03	5720	4.40	−0.13	1.00	0.98	5.8
HIP 86731	0.25	5840	3.79	−0.10	1.43	1.40	3.6
HIP 86796	0.32	5800	4.30	−0.10	1.05	1.31	4.3
HIP 87523	−0.40	6070	4.07	−0.12	1.36	1.11	6.3
HIP 88622	−0.46	5720	4.35	−0.16	0.80	0.88	12.0
HIP 88945	−0.05	5690	4.37	−0.15	1.33	0.95	6.8
HIP 90485	0.12	6339	4.05	−0.06	1.55	1.35	2.5
HIP 91438	−0.24	5580	4.42	−0.17	0.55	0.78	6.2
HIP 92270	−0.06	6370	4.32	−0.07	1.50	1.20	2.3
HIP 93185	−0.28	5810	4.40	−0.14	0.90	0.84	6.6
HIP 94645	0.16	6200	4.35	−0.07	1.20	1.18	0.5
HIP 95447	0.37	5600	4.13	−0.14	1.10	0.98	8.9
HIP 96124	−0.20	5590	4.37	−0.17	0.78	0.84	9.0
HIP 96258	−0.02	6380	4.25	−0.08	1.48	1.25	2.4
HIP 96536	0.03	6397	4.06	−0.06	1.65	1.43	2.5
HIP 98767	0.25	5490	4.23	−0.17	0.66	0.90	9.3
HIP 98785	0.03	6430	3.97	−0.06	1.90	1.61	2.3
HIP 99240	0.37	5585	4.26	−0.15	0.98	0.98	5.6
HIP 100412	−0.32	5960	4.06	−0.12	1.20	1.07	6.7
HIP 102264	−0.22	5570	4.37	−0.17	0.60	0.77	8.7
HIP 103458	−0.65	5780	4.30	−0.16	0.90	0.77	13.7
HIP 103682	0.27	5940	4.26	−0.09	1.25	1.16	3.1
HIP 105858	−0.73	6067	4.27	−0.14	1.17	0.88	8.8
HIP 107975	−0.53	6460	4.06	−0.10	1.50	1.10	4.5
HIP 108736	−0.38	5890	4.24	−0.13	1.05	0.96	8.9
HIP 109378	0.22	5500	4.30	−0.17	0.78	0.90	9.0
HIP 109450	−0.13	5830	4.18	−0.13	1.10	1.05	7.8
HIP 109821	−0.08	5800	4.29	−0.13	1.05	0.99	7.3
HIP 110341	−0.17	6500	4.29	−0.07	1.70	1.28	2.1

Table A4: Stellar atmospheric parameters - *continued*

OBJECT	[Fe/H]	$T_{\rm eff}$ [K]	$\log g$ [cgs]	BC [mag]	$\xi_{\rm t}$ [km/s]	$\mathcal{M}$ $M_\odot$	Age [Gyr]
HIP 110512	−0.30	5770	4.15	−0.14	1.05	0.95	10.3
HIP 112151	−0.42	5035	3.43	−0.32	0.85	1.15	5.3
HIP 113137	0.22	5800	4.10	−0.11	1.16	1.10	5.3
HIP 113174	−0.11	6870	4.14	−0.05	1.95	1.51	1.7
HIP 113357	0.20	5789	4.34	−0.11	1.00	1.07	4.2
HIP 113421	0.35	5620	4.29	−0.14	0.97	0.95	5.0
HIP 116421	−0.45	5700	4.15	−0.16	0.95	0.93	13.2
HIP 116740	0.05	5740	3.96	−0.13	1.15	1.12	
HIP 117880	0.12	6100	4.21	−0.08	1.30	1.21	3.3
HIP 118010	−0.07	5795	4.17	−0.13	1.00	1.03	8.4
HIP 118115	−0.01	5800	4.30	−0.12	1.00	1.00	6.7

Appendix B
Elemental abundances

This appendix consists of the following tables:

Table B1: Solar abundances: Column 1 gives the element and degree of ionization; an asterisk ($*$) in col. 2 indicates that astrophysical log gf-values have been used, an asterisk in parenthesis indicate that astrophysical log gf-values have been used for part of the lines (see Paper I for further discussion); col. 3 gives the standard elemental abundances in the solar photosphere as given in Grevesse & Sauval (1998); cols. 4–6 give the solar analysis based on FEROS spectra; cols. 7–9 give the solar analysis based on SOFIN spectra; cols. 10–12 give the solar analysis based on SOFIN spectra. For each set we give the number of analyzed lines ($N_{\rm lines}$), the absolute abundance ($\epsilon(X)$), and the difference between the derived abundance and the standard solar photospheric value from Grevesse & Sauval (1998) in col. 3.

Table B2: Abundances - Na, Mg, Al, Si, Ca, Ti, Cr, Fe, Ni, Zn, Y, Ba: Column 1 gives the Hipparcos identification; the remaining columns give the derived elemental abundances as indicated. All abundances have been normalized with respect to our solar abundances (by subtracting the differences listed in Table B1). Each star has three rows: row 1 – elemental abundance (the mean value from all analyzed lines); row 2 – the spread (1σ) around the mean value; row 3 – the number of lines that were used in the calculation of the mean value.

Table B3: Abundances - Oxygen and Europium Column 1 gives the Hipparcos identification; cols. 2–6 give the normalized oxygen abundances as derived from the different oxygen lines; col. 7 gives the NLTE correction term (interpolated from the tables of Gratton et al. 1999) that have been applied to the abundances from the O I triplet at ~ 7770 Å; col. 8 gives the empirical NLTE correction based on Eq. (1) in Paper III; cols. 9 and 10 give the europium abundances from the 4129 Å and 6645 Å lines.

Table B1: Solar abundances

Ion		Phot	FEROS/CES			SOFIN			UVES		
		$\epsilon(X)$	$N_{\rm lines}$	$\epsilon(X)$	Diff.	$N_{\rm lines}$	$\epsilon(X)$	Diff.	$N_{\rm lines}$	$\epsilon(X)$	Diff.
Fe I		7.50	147	7.56	+0.06	86	7.53	+0.03	62	7.56	+0.06
Fe II		7.50	29	7.58	+0.08	19	7.53	+0.03	13	7.59	+0.09
Na I		6.33	4	6.27	−0.06	4	6.27	−0.06	4	6.25	−0.08
Mg I	*	7.58	7	7.58	0.00	4	7.57	−0.01	1	7.58	0.00
Al I	*	6.47	6	6.47	0.00	6	6.47	0.00	2	6.50	+0.03
Si I	(*)	7.55	32	7.54	−0.01	15	7.54	−0.02	18	7.54	−0.01
Ca I	*	6.36	22	6.36	0.00	10	6.35	−0.01	12	6.37	+0.01
Ti I		5.02	31	4.92	−0.10	12	4.90	−0.12	7	4.93	−0.09
Ti II		5.02	18	4.91	−0.11	8	4.88	−0.11	0		
Cr I	*	5.67	14	5.67	0.00	6	5.64	−0.03	2	5.76	+0.09
Cr II	*	5.67	9	5.67	0.00	6	5.60	−0.07	0		
Ni I	(*)	6.25	54	6.25	−0.01	36	6.24	−0.01	23	6.24	−0.01
Zn I	*	4.60	2	4.60	0.00	1	4.58	−0.02	1	4.55	−0.05
Y II		2.24	7	2.20	−0.04	4	2.05	−0.19	0		
Ba II		2.13	4	2.29	+0.16	4	2.27	+0.14	3	2.34	+0.21
[O I]	6300	8.83		8.71	−0.12		8.74	−0.09			
[O I]	6363	8.83		9.06	+0.23						
O I	7771	8.83		8.83	±0.00						
O I	7773	8.83		8.88	+0.05						
O I	7774	8.83		8.82	−0.01						
Eu II	4129	0.51		0.47	−0.04		0.46	−0.05			
Eu II	6645	0.51		0.56	+0.05						

Table B2: Abundances – Na, Mg, Al, Si, Ca, Ti, Cr, Fe, Ni, Zn, Y, and Ba

HIP	Fe I	Fe II	Na I	Mg I	Al I	Si I	Ca I	Ti I	Ti II	Cr I	Cr II	Ni I	Zn I	Y II	Ba II
699	–0.20	–0.19	–0.13	–0.13	–0.21	–0.16	–0.17	–0.20	–0.16	–0.23	–0.21	–0.25	–0.24	–0.25	0.00
	0.06	0.06	0.04	0.06	0.03	0.07	0.05	0.07	0.10	0.07	0.06	0.07	0.00	0.10	0.03
	79	16	4	3	3	15	10	9	8	5	5	33	1	4	4
910	–0.36	–0.34	–0.25	–0.28	–0.31	–0.29	–0.28	–0.30	–0.26	–0.42	–0.36	–0.40	–0.41	–0.44	–0.17
	0.07	0.05	0.05	0.09	0.04	0.06	0.12	0.07	0.08	0.07	0.06	0.08	0.00	0.10	0.11
	68	14	4	4	6	15	10	9	8	5	5	30	1	4	4
2235	–0.28	–0.25	–0.13	–0.18	–0.30	–0.22	–0.21	–0.16	–0.23	–0.37	–0.30	–0.33	–0.34	0.31	0.54
	0.07	0.06	0.07	0.02	0.00	0.06	0.10	0.14	0.10	0.07	0.07	0.08	0.00	0.14	0.06
	65	16	4	2	1	11	10	5	7	2	6	23	1	3	4
2787	–0.11	–0.09	–0.08	–0.08	–0.10	–0.11	–0.04	–0.06	–0.09	–0.16	–0.13	–0.19	–0.25	–0.14	0.35
	0.07	0.05	0.07	0.10	0.11	0.06	0.14	0.09	0.12	0.07	0.11	0.08	0.00	0.13	0.15
	74	17	4	3	5	15	10	8	8	4	5	29	1	4	4
3086	–0.11	–0.18	–0.10	0.03	0.03	–0.05	–0.02	0.01	–0.01	–0.09	–0.20	–0.12	–0.03	–0.24	–0.11
	0.09	0.07	0.03	0.05	0.05	0.07	0.06	0.12	0.13	0.08	0.03	0.09	0.07	0.24	0.05
	145	24	4	6	5	32	22	29	18	13	8	52	2	6	4
3142	–0.45	–0.45	–0.33	–0.27	–0.32	–0.33	–0.32	–0.34	–0.33	–0.45	–0.44	–0.47	–0.47	–0.57	–0.34
	0.09	0.08	0.04	0.05	0.03	0.10	0.10	0.09	0.13	0.06	0.07	0.11	0.05	0.18	0.02
	131	25	4	7	6	31	22	24	18	10	9	50	2	7	4
3170	–0.34	–0.35	–0.34	–0.14	–0.13	–0.23	–0.23	–0.20	–0.21	–0.25	–0.32	–0.37	–0.28	–0.57	–0.34
	0.10	0.09	0.05	0.06	0.04	0.12	0.08	0.16	0.15	0.10	0.11	0.13	0.00	0.23	0.08
	117	23	4	5	5	30	22	23	16	9	9	42	1	5	4
3185	–0.59	–0.66	–0.43	–0.28	–0.24	–0.37	–0.35	–0.30	–0.31	–0.58	–0.56	–0.57	–0.41	–0.52	–0.50
	0.10	0.10	0.04	0.04	0.03	0.08	0.05	0.17	0.15	0.16	0.07	0.08	0.05	0.22	0.11
	140	21	4	6	6	31	22	30	18	13	7	51	2	7	4
3497	–0.33	–0.36	–0.28	–0.09	–0.04	–0.16	–0.19	–0.13	–0.12	–0.30	–0.34	–0.31	–0.17	–0.45	–0.39
	0.09	0.09	0.05	0.01	0.04	0.06	0.06	0.16	0.14	0.05	0.06	0.07	0.06	0.21	0.08
	142	24	4	6	6	29	22	30	18	13	9	52	2	7	4
3704	–0.38	–0.41	–0.32	–0.31	–0.32	–0.34	–0.31	–0.30	–0.30	–0.41	–0.41	–0.40	–0.31	–0.56	–0.30
	0.11	0.10	0.10	0.08	0.06	0.09	0.09	0.12	0.15	0.04	0.09	0.11	0.01	0.16	0.08
	132	24	4	5	3	29	22	26	17	11	8	47	2	7	4
3909	–0.06	–0.04	–0.14	–0.06	–0.07	–0.11	–0.09	–0.08	–0.06	–0.11	–0.07	–0.14	–0.16	–0.03	0.16
	0.07	0.05	0.06	0.04	0.08	0.04	0.16	0.08	0.09	0.06	0.05	0.07	0.00	0.12	0.06
	76	18	4	3	5	15	10	10	8	5	5	35	1	4	4
5315	–0.42	–0.48	–0.24	–0.07	–0.08	–0.20	–0.20	–0.06	–0.12	–0.39	–0.42	–0.37	–0.20	–0.36	–0.50
	0.11	0.12	0.05	0.04	0.06	0.08	0.05	0.20	0.17	0.11	0.07	0.11	0.02	0.29	0.09
	143	22	4	6	6	30	22	30	18	14	7	52	2	7	4
5862	0.17	0.19	0.23	0.23	0.18	0.23	0.19	0.12	0.11	0.16	0.00	0.16	0.10	0.44	0.26
	0.07	0.07	0.05	0.08	0.03	0.07	0.04	0.03	0.00	0.03	0.00	0.05	0.00	0.00	0.01
	70	16	4	2	2	21	14	7	0	4	0	30	1	1	3
7276	0.20	0.15	0.35	0.31	0.31	0.27	0.22	0.16	0.19	0.18	0.14	0.24	0.26	0.09	0.18
	0.10	0.10	0.08	0.03	0.09	0.11	0.09	0.15	0.16	0.15	0.06	0.10	0.14	0.26	0.05
	146	26	4	6	5	32	22	30	18	13	9	52	2	6	4
9085	–0.31	–0.27	–0.29	–0.22	–0.27	–0.23	–0.21	–0.27	–0.19	–0.35	–0.31	–0.37	–0.40	–0.33	–0.08
	0.27	0.08	0.09	0.09	0.05	0.05	0.08	0.06	0.15	0.11	0.08	0.11	0.16	0.14	0.05
	123	25	4	6	4	24	18	18	17	10	9	38	2	7	4
10306	–0.17	–0.13	–0.09	–0.08	–0.12	–0.12	–0.13	–0.12	–0.11	–0.21	–0.16	–0.21	–0.25	–0.15	0.23
	0.08	0.07	0.07	0.13	0.09	0.07	0.08	0.10	0.08	0.05	0.10	0.10	0.00	0.13	0.08
	74	14	4	2	3	14	10	8	8	3	5	28	1	3	4

Table B2: Abundances – Na, Mg, Al, Si, Ca, Ti, Cr, Fe, Ni, Zn, Y, and Ba - *continued*

HIP	Fe I	Fe II	Na I	Mg I	Al I	Si I	Ca I	Ti I	Ti II	Cr I	Cr II	Ni I	Zn I	Y II	Ba II
10798	–0.47	–0.46	–0.49	–0.40	–0.36	–0.42	–0.45	–0.37	–0.36	–0.46	–0.46	–0.48	–0.41	–0.45	–0.34
	0.10	0.12	0.04	0.07	0.04	0.09	0.03	0.15	0.13	0.08	0.08	0.09	0.07	0.23	0.10
	147	25	4	7	6	30	22	31	17	13	8	51	2	7	4
11309	–0.32	–0.32	–0.23	–0.19	–0.25	–0.27	–0.28	–0.31	–0.28	–0.36	–0.35	–0.34	–0.36	–0.44	–0.15
	0.08	0.06	0.04	0.10	0.05	0.06	0.06	0.04	0.11	0.05	0.06	0.09	0.00	0.08	0.05
	73	18	4	3	4	14	10	9	8	4	5	30	1	4	4
12186	0.14	0.12	0.10	0.17	0.28	0.19	0.21	0.10	0.20	0.10	0.12	0.14	0.09	0.02	0.19
	0.10	0.07	0.03	0.04	0.05	0.10	0.13	0.18	0.18	0.12	0.06	0.10	0.16	0.20	0.02
	149	27	4	6	6	32	22	32	18	13	9	54	2	7	4
12306	–0.53	–0.58	–0.47	–0.23	–0.30	–0.38	–0.37	–0.37	–0.42	–0.55	–0.56	–0.53	–0.46	–0.74	–0.62
	0.07	0.07	0.03	0.07	0.05	0.07	0.08	0.06	0.12	0.03	0.06	0.05	0.00	0.08	0.05
	80	19	4	3	4	17	8	8	9	6	5	33	1	4	4
12611	0.26	0.28	0.38	0.28	0.41	0.37	0.30	0.29	0.31	0.28	0.25	0.33	0.34	0.25	0.17
	0.12	0.12	0.03	0.05	0.05	0.10	0.16	0.24	0.26	0.15	0.17	0.14	0.18	0.32	0.07
	149	24	4	6	6	31	22	31	18	14	9	53	2	7	4
12653	0.14	0.12	0.13	0.15	0.13	0.17	0.23	0.14	0.14	0.16	0.15	0.12	0.05	0.18	0.33
	0.10	0.08	0.04	0.06	0.09	0.09	0.14	0.15	0.18	0.13	0.06	0.11	0.18	0.22	0.06
	143	26	4	6	6	32	22	26	17	13	9	52	2	7	4
14086	–0.59	–0.67	–0.51	–0.22	–0.20	–0.37	–0.31	–0.23	–0.31	–0.51	–0.64	–0.53	–0.49	–0.62	–0.62
	0.10	0.10	0.04	0.07	0.06	0.08	0.07	0.16	0.15	0.08	0.08	0.13	0.08	0.29	0.06
	144	22	4	7	6	32	22	32	18	14	9	51	2	8	4
14954	0.19	0.10	0.39	0.29	0.31	0.29	0.23	0.24	0.16	0.19	0.16	0.22	0.22	0.01	0.21
	0.12	0.11	0.06	0.04	0.05	0.12	0.09	0.13	0.16	0.07	0.10	0.11	0.10	0.21	0.09
	137	27	4	5	5	29	21	19	15	10	9	45	2	4	4
15131	–0.52	–0.53	–0.38	–0.34	–0.43	–0.43	–0.50	–0.46	0.11	–0.52	0.00	–0.52	–0.46	–0.36	–0.40
	0.07	0.07	0.04	0.02	0.01	0.06	0.10	0.02	0.00	0.01	0.00	0.06	0.00	0.00	0.23
	69	11	4	2	2	21	14	6	0	4	0	28	1	1	3
15510	–0.41	–0.42	–0.32	–0.05	–0.05	–0.24	–0.25	0.00	0.11	–0.32	0.00	–0.36	–0.22	0.09	–0.56
	0.08	0.21	0.08	0.04	0.04	0.05	0.07	0.05	0.00	0.08	0.00	0.04	0.00	0.00	0.08
	69	10	4	2	2	21	14	6	0	5	0	28	1	1	3
16788	–0.32	–0.32	–0.28	–0.18	–0.21	–0.31	–0.27	–0.27	–0.27	–0.34	–0.34	–0.35	–0.20	0.45	0.63
	0.07	0.08	0.02	0.08	0.05	0.05	0.12	0.14	0.08	0.06	0.07	0.06	0.00	0.12	0.06
	78	17	4	3	4	15	10	9	8	5	6	32	1	4	4
17147	–0.84	–0.88	–0.75	–0.44	–0.50	–0.57	–0.58	–0.53	–0.55	–0.75	–0.92	–0.83	–0.72	–0.88	–0.81
	0.09	0.12	0.04	0.04	0.01	0.10	0.12	0.10	0.12	0.13	0.07	0.14	0.04	0.16	0.06
	120	24	4	6	4	29	22	25	18	10	7	42	2	6	4
17378	0.24	0.26	0.26	0.24	0.27	0.29	0.20	0.32	0.32	0.25	0.24	0.31	0.38	0.29	0.22
	0.14	0.15	0.08	0.05	0.03	0.10	0.09	0.30	0.19	0.17	0.21	0.17	0.05	0.44	0.10
	147	22	4	7	6	32	22	32	17	14	9	53	2	7	4
18235	–0.71	–0.75	–0.61	–0.31	–0.33	–0.43	–0.40	–0.38	–0.43	–0.72	–0.68	–0.68	–0.52	–0.60	–0.71
	0.08	0.09	0.04	0.12	0.05	0.08	0.06	0.10	0.09	0.04	0.05	0.08	0.00	0.11	0.07
	81	14	4	5	6	16	10	11	8	5	5	35	1	4	3
18833	–0.52	–0.50	–0.39	–0.42	–0.32	–0.43	–0.44	–0.37	–0.39	–0.62	–0.48	–0.50	–0.57	–0.60	–0.29
	0.07	0.08	0.07	0.02	0.22	0.07	0.08	0.06	0.12	0.08	0.09	0.09	0.00	0.14	0.08
	57	15	4	2	2	12	9	5	8	2	3	19	1	3	4
20242	–0.26	–0.29	–0.25	–0.08	–0.02	–0.24	–0.11	–0.19	–0.22	–0.26	–0.25	–0.30	–0.23	–0.43	–0.23
	0.08	0.09	0.05	0.05	0.03	0.10	0.09	0.09	0.07	0.08	0.07	0.07	0.00	0.07	0.06
	82	18	4	3	5	16	8	8	8	4	6	32	1	4	4
21832	–0.61	–0.62	–0.56	–0.30	–0.33	–0.44	–0.44	–0.42	–0.43	–0.63	–0.59	–0.60	–0.47	–0.79	–0.64
	0.08	0.07	0.04	0.13	0.02	0.07	0.04	0.07	0.09	0.04	0.07	0.07	0.00	0.07	0.13
	76	16	4	3	4	15	10	10	8	6	5	32	1	4	3

Table B2: Abundances – Na, Mg, Al, Si, Ca, Ti, Cr, Fe, Ni, Zn, Y, and Ba - *continued*

HIP	Fe I	Fe II	Na I	Mg I	Al I	Si I	Ca I	Ti I	Ti II	Cr I	Cr II	Ni I	Zn I	Y II	Ba II
22263	0.05	0.02	–0.06	0.01	0.02	0.02	0.12	0.04	0.09	0.07	0.03	–0.01	–0.06	0.16	0.32
	0.10	0.09	0.01	0.04	0.05	0.08	0.06	0.13	0.19	0.11	0.08	0.10	0.11	0.20	0.06
	148	26	4	5	5	32	22	29	17	14	9	52	2	7	4
22325	0.06	0.00	0.14	0.17	0.12	0.15	0.15	0.09	0.10	0.09	0.03	0.02	–0.05	0.04	0.29
	0.11	0.10	0.09	0.03	0.10	0.13	0.11	0.19	0.19	0.23	0.07	0.13	0.09	0.22	0.08
	127	26	4	5	4	27	21	23	16	11	9	44	2	6	4
23555	0.13	0.05	0.22	0.21	0.19	0.22	0.18	0.15	0.14	0.19	0.10	0.11	0.20	0.05	0.26
	0.11	0.10	0.09	0.05	0.03	0.11	0.11	0.18	0.17	0.23	0.07	0.14	0.17	0.22	0.07
	130	22	4	6	5	28	21	22	16	11	9	48	2	5	4
23941	–0.30	–0.31	–0.18	–0.19	–0.20	–0.20	–0.25	–0.25	–0.21	–0.32	–0.34	–0.36	–0.31	–0.37	–0.03
	0.13	0.09	0.08	0.06	0.04	0.06	0.12	0.06	0.14	0.17	0.06	0.15	0.00	0.22	0.08
	81	18	2	3	2	15	15	10	13	4	8	22	1	4	4
24829	0.06	0.02	0.14	0.17	0.09	0.13	0.15	0.08	0.11	0.04	0.03	0.00	0.01	0.23	0.46
	0.11	0.07	0.04	0.04	0.08	0.11	0.09	0.15	0.15	0.10	0.06	0.12	0.16	0.19	0.10
	139	28	4	7	6	32	22	25	17	11	9	51	2	7	4
26828	–0.37	–0.35	–0.16	–0.12	–0.16	–0.18	–0.21	–0.20	–0.13	–0.45	–0.36	–0.35	–0.25	–0.51	–0.24
	0.07	0.07	0.07	0.09	0.01	0.06	0.07	0.08	0.12	0.06	0.05	0.08	0.00	0.15	0.07
	58	15	4	3	2	13	9	6	6	3	5	21	1	4	4
29271	0.10	0.09	0.14	0.11	0.11	0.15	0.11	0.10	0.13	0.12	0.11	0.16	0.12	0.13	0.09
	0.11	0.12	0.05	0.05	0.04	0.07	0.06	0.22	0.15	0.09	0.08	0.09	0.04	0.32	0.05
	146	24	4	7	6	30	22	32	18	14	8	54	2	6	4
30480	0.19	0.14	0.29	0.25	0.30	0.23	0.18	0.15	0.17	0.17	0.12	0.22	0.24	0.35	0.28
	0.10	0.10	0.05	0.04	0.08	0.07	0.08	0.15	0.15	0.13	0.08	0.10	0.04	0.22	0.04
	146	27	3	7	5	32	22	29	18	14	9	53	2	7	4
30503	0.04	0.05	0.05	0.06	0.04	0.07	0.07	–0.01	0.07	0.06	0.00	0.02	0.08	0.10	0.16
	0.09	0.11	0.03	0.04	0.06	0.08	0.05	0.16	0.15	0.17	0.09	0.09	0.02	0.23	0.06
	147	26	4	6	6	32	22	31	18	14	9	53	2	7	4
36874	–0.07	–0.07	–0.13	0.00	0.04	–0.04	–0.05	–0.07	–0.06	–0.09	–0.03	–0.08	–0.01	–0.19	–0.04
	0.08	0.07	0.03	0.02	0.03	0.04	0.03	0.08	0.14	0.04	0.02	0.05	0.00	0.06	0.03
	88	19	4	4	6	15	8	10	9	6	6	35	1	4	4
37789	–0.67	–0.68	–0.63	–0.40	–0.53	–0.53	–0.58	–0.55	–0.49	–0.68	–0.66	–0.70	–0.61	–0.83	–0.66
	0.07	0.07	0.01	0.08	0.03	0.07	0.08	0.05	0.08	0.11	0.07	0.08	0.00	0.08	0.05
	77	15	4	3	3	15	9	10	8	4	6	32	1	4	4
40613	–0.63	–0.62	–0.50	–0.24	–0.30	–0.39	–0.37	–0.37	–0.31	–0.64	–0.61	–0.62	–0.47	–0.68	–0.71
	0.07	0.07	0.04	0.05	0.03	0.09	0.03	0.05	0.07	0.05	0.08	0.09	0.00	0.07	0.09
	71	16	4	4	5	16	10	10	8	3	5	30	1	4	4
44075	–0.91	–0.89	–0.83	–0.55	–0.57	–0.63	–0.67	–0.65	–0.59	–0.90	–0.90	–0.91	–0.78	–0.89	–0.81
	0.07	0.06	0.03	0.07	0.12	0.11	0.08	0.06	0.08	0.17	0.09	0.10	0.00	0.10	0.10
	67	16	4	4	3	15	10	9	8	4	5	26	1	4	4
44441	–0.28	–0.26	–0.20	–0.13	–0.23	–0.19	–0.19	–0.24	–0.20	–0.34	–0.27	–0.28	–0.36	–0.32	–0.06
	0.07	0.06	0.06	0.10	0.07	0.07	0.08	0.12	0.11	0.06	0.07	0.09	0.00	0.12	0.08
	65	14	4	4	3	14	10	7	6	2	4	28	1	4	4
44860	–0.45	–0.46	–0.36	–0.11	–0.15	–0.27	–0.21	–0.20	–0.19	–0.44	–0.43	–0.43	–0.25	–0.52	–0.51
	0.07	0.08	0.03	0.03	0.05	0.05	0.11	0.05	0.08	0.05	0.06	0.07	0.00	0.08	0.05
	77	16	4	4	6	15	10	11	8	6	5	32	1	4	4
72673	–0.62	–0.62	–0.44	–0.39	–0.42	–0.47	–0.47	–0.44	–0.45	–0.62	–0.66	–0.60	–0.52	–0.74	–0.50
	0.09	0.07	0.04	0.06	0.03	0.10	0.12	0.10	0.11	0.07	0.08	0.10	0.06	0.17	0.10
	118	23	4	5	3	28	21	21	18	7	9	40	2	6	4
75181	–0.34	–0.37	–0.28	–0.10	–0.11	–0.18	–0.22	–0.17	–0.15	–0.34	–0.37	–0.34	–0.19	–0.44	–0.35
	0.09	0.10	0.02	0.04	0.05	0.07	0.07	0.14	0.15	0.07	0.07	0.08	0.06	0.22	0.05
	145	25	4	6	6	31	22	30	18	13	9	51	2	7	3

Table B2: Abundances – Na, Mg, Al, Si, Ca, Ti, Cr, Fe, Ni, Zn, Y, and Ba - *continued*

HIP	Fe I	Fe II	Na I	Mg I	Al I	Si I	Ca I	Ti I	Ti II	Cr I	Cr II	Ni I	Zn I	Y II	Ba II
78955	0.33	0.28	0.41	0.38	0.41	0.37	0.35	0.36	0.36	0.33	0.28	0.40	0.26	0.30	0.29
	0.10	0.08	0.01	0.05	0.05	0.08	0.08	0.15	0.18	0.08	0.06	0.11	0.11	0.25	0.06
	146	27	4	7	6	32	22	30	18	14	9	53	2	8	4
79137	0.30	0.33	0.22	0.28	0.36	0.32	0.22	0.45	0.39	0.30	0.37	0.39	0.29	0.46	0.27
	0.16	0.18	0.07	0.07	0.07	0.10	0.08	0.32	0.24	0.18	0.20	0.21	0.01	0.42	0.18
	141	19	4	7	6	30	22	31	16	14	8	52	2	8	4
80337	0.03	0.03	–0.09	0.01	0.00	0.00	0.10	0.02	0.06	0.04	–0.01	–0.04	–0.14	0.19	0.43
	0.10	0.09	0.04	0.05	0.06	0.08	0.07	0.13	0.13	0.10	0.06	0.08	0.09	0.20	0.06
	147	26	4	7	6	32	22	30	18	14	9	54	2	7	4
80686	–0.06	–0.07	–0.14	–0.08	–0.08	–0.08	–0.01	–0.12	–0.06	–0.06	–0.06	–0.13	–0.17	0.01	0.23
	0.09	0.08	0.04	0.03	0.03	0.09	0.07	0.14	0.14	0.06	0.07	0.11	0.05	0.17	0.12
	139	26	4	6	6	32	22	27	18	12	9	49	2	7	4
81520	–0.48	–0.46	–0.50	–0.36	–0.38	–0.41	–0.43	–0.40	–0.36	–0.47	–0.46	–0.49	–0.47	–0.50	–0.33
	0.09	0.10	0.06	0.06	0.05	0.07	0.06	0.10	0.15	0.05	0.06	0.13	0.01	0.20	0.07
	140	25	4	7	6	31	22	28	17	12	9	51	2	7	4
82588	–0.02	–0.02	–0.12	–0.07	–0.02	–0.04	–0.02	–0.02	–0.01	0.02	0.01	–0.06	–0.11	0.08	0.19
	0.10	0.11	0.03	0.04	0.06	0.07	0.07	0.17	0.15	0.10	0.11	0.08	0.04	0.26	0.09
	143	23	4	7	6	31	22	30	17	14	9	54	2	7	4
83229	–0.57	–0.63	–0.46	–0.22	–0.22	–0.33	–0.36	–0.33	–0.34	–0.54	–0.56	–0.51	–0.34	–0.77	–0.66
	0.08	0.08	0.02	0.04	0.05	0.08	0.07	0.10	0.13	0.06	0.05	0.09	0.02	0.17	0.06
	138	25	4	6	6	29	22	28	18	12	9	50	2	7	4
83601	0.09	0.05	–0.02	0.07	0.08	0.06	0.12	0.07	0.07	0.13	0.03	–0.01	–0.01	0.09	0.33
	0.10	0.07	0.04	0.06	0.07	0.08	0.08	0.16	0.18	0.15	0.05	0.13	0.11	0.23	0.02
	142	26	4	4	5	30	22	27	17	12	9	49	2	6	4
84551	0.12	0.06	0.19	0.26	0.25	0.22	0.24	0.16	0.15	0.10	0.10	0.08	0.04	0.08	0.43
	0.11	0.13	0.06	0.05	0.06	0.14	0.13	0.17	0.19	0.13	0.14	0.13	0.11	0.19	0.09
	132	27	4	5	5	30	20	20	16	11	9	44	2	6	4
84636	0.23	0.19	0.47	0.33	0.39	0.34	0.26	0.23	0.21	0.22	0.19	0.32	0.29	0.09	0.15
	0.11	0.09	0.01	0.06	0.07	0.09	0.10	0.16	0.15	0.19	0.08	0.10	0.08	0.27	0.03
	144	28	4	7	5	32	22	29	18	14	9	52	2	7	4
84905	–0.57	–0.61	–0.52	–0.22	–0.22	–0.29	–0.35	–0.35	–0.33	–0.58	–0.59	–0.56	–0.44	–0.69	–0.55
	0.09	0.09	0.05	0.06	0.04	0.22	0.11	0.13	0.13	0.10	0.05	0.08	0.00	0.16	0.02
	132	24	4	7	5	29	22	28	18	12	9	48	1	7	4
85007	–0.39	–0.39	–0.33	–0.34	–0.38	–0.37	–0.37	–0.39	–0.37	–0.45	–0.44	–0.45	–0.34	–0.54	–0.24
	0.09	0.06	0.06	0.04	0.04	0.07	0.08	0.10	0.12	0.07	0.06	0.08	0.09	0.18	0.01
	132	23	4	6	6	32	22	23	18	11	9	50	2	7	4
85042	0.03	–0.01	0.00	0.06	0.11	0.05	0.04	0.04	0.07	0.05	–0.02	0.05	–0.06	0.00	0.03
	0.10	0.09	0.05	0.03	0.04	0.07	0.05	0.16	0.14	0.04	0.07	0.09	0.08	0.25	0.03
	147	26	4	7	5	32	22	32	18	14	9	54	2	8	4
86731	0.25	0.21	0.45	0.36	0.37	0.36	0.30	0.19	0.27	0.26	0.26	0.33	0.34	0.15	0.24
	0.10	0.08	0.03	0.03	0.07	0.10	0.13	0.22	0.19	0.09	0.07	0.15	0.12	0.23	0.05
	144	27	4	7	6	31	22	29	18	13	9	54	2	6	4
86796	0.32	0.30	0.41	0.34	0.37	0.36	0.30	0.35	0.38	0.33	0.31	0.40	0.31	0.28	0.30
	0.10	0.08	0.03	0.05	0.04	0.08	0.10	0.16	0.18	0.10	0.07	0.13	0.06	0.22	0.07
	149	26	4	7	6	32	22	31	18	14	9	53	2	8	4
87523	–0.40	–0.42	–0.25	–0.23	–0.31	–0.28	–0.30	–0.30	–0.28	–0.42	–0.42	–0.39	–0.40	–0.48	–0.23
	0.08	0.08	0.05	0.03	0.06	0.07	0.08	0.08	0.13	0.08	0.06	0.09	0.06	0.16	0.05
	138	26	4	6	6	32	22	24	18	11	9	50	2	7	4
88622	–0.46	–0.47	–0.38	–0.16	–0.20	–0.24	–0.31	–0.31	–0.27	–0.46	–0.44	–0.45	–0.26	–0.69	–0.51
	0.10	0.09	0.06	0.05	0.05	0.07	0.07	0.12	0.13	0.06	0.06	0.09	0.06	0.23	0.07
	137	24	4	6	6	27	22	30	17	12	8	49	2	7	4

Table B2: Abundances – Na, Mg, Al, Si, Ca, Ti, Cr, Fe, Ni, Zn, Y, and Ba - *continued*

HIP	Fe I	Fe II	Na I	Mg I	Al I	Si I	Ca I	Ti I	Ti II	Cr I	Cr II	Ni I	Zn I	Y II	Ba II
88945	–0.05	–0.03	–0.11	–0.09	–0.04	–0.07	0.03	–0.13	–0.10	–0.04	0.03	–0.17	–0.18	0.02	0.21
	0.09	0.06	0.07	0.13	0.06	0.06	0.07	0.11	0.11	0.03	0.06	0.08	0.00	0.08	0.14
	78	12	4	3	6	14	10	10	7	5	5	34	1	4	4
90485	0.12	0.10	0.20	0.17	0.21	0.18	0.19	0.09	0.15	0.16	0.09	0.11	0.07	0.07	0.25
	0.09	0.06	0.07	0.05	0.08	0.10	0.09	0.17	0.16	0.14	0.05	0.12	0.16	0.18	0.05
	144	28	4	5	5	31	22	26	17	12	9	52	2	7	4
91438	–0.24	–0.26	–0.26	–0.21	–0.19	–0.22	–0.20	–0.17	–0.19	–0.21	–0.25	–0.26	–0.27	–0.20	–0.10
	0.09	0.10	0.02	0.02	0.03	0.06	0.06	0.11	0.14	0.12	0.06	0.07	0.06	0.22	0.09
	144	25	4	7	6	32	22	30	18	14	9	54	2	8	4
92270	–0.06	–0.05	–0.03	–0.03	–0.05	–0.05	–0.03	–0.07	–0.04	–0.11	–0.05	–0.08	–0.19	–0.07	0.11
	0.06	0.07	0.04	0.11	0.05	0.07	0.06	0.07	0.10	0.05	0.03	0.09	0.00	0.12	0.07
	73	15	4	3	6	15	10	8	8	4	5	29	1	4	4
93185	–0.28	–0.29	–0.32	–0.24	–0.25	–0.25	–0.26	–0.28	–0.26	–0.31	–0.27	–0.33	–0.34	–0.28	–0.11
	0.07	0.07	0.02	0.05	0.05	0.05	0.06	0.07	0.08	0.04	0.03	0.06	0.00	0.09	0.08
	82	15	4	4	6	15	10	11	8	6	6	35	1	4	4
94645	0.16	0.15	0.16	0.17	0.18	0.21	0.18	0.05	0.15	0.13	0.14	0.11	0.06	0.16	0.25
	0.10	0.11	0.06	0.06	0.09	0.09	0.09	0.19	0.19	0.11	0.12	0.15	0.19	0.17	0.06
	139	27	4	4	5	32	22	22	17	12	8	48	2	5	4
95447	0.37	0.33	0.51	0.47	0.47	0.46	0.36	0.42	0.42	0.40	0.38	0.47	0.46	0.27	0.29
	0.11	0.12	0.04	0.06	0.05	0.08	0.10	0.22	0.21	0.11	0.10	0.11	0.09	0.29	0.09
	143	27	4	5	6	32	22	30	18	14	9	53	2	8	4
96124	–0.20	–0.20	–0.14	–0.01	0.02	–0.07	–0.13	–0.03	–0.04	–0.17	–0.20	–0.17	–0.07	–0.24	–0.22
	0.09	0.09	0.03	0.04	0.05	0.05	0.06	0.14	0.14	0.12	0.05	0.09	0.03	0.20	0.12
	147	25	4	7	6	32	22	31	18	14	9	52	2	8	4
96258	–0.02	–0.01	–0.05	0.04	–0.03	0.02	0.07	–0.03	0.03	–0.04	–0.03	–0.09	–0.18	0.01	0.24
	0.07	0.06	0.07	0.09	0.02	0.06	0.07	0.10	0.10	0.05	0.05	0.09	0.00	0.14	0.08
	68	15	4	3	4	13	10	7	7	4	5	27	1	3	4
96536	0.03	0.02	0.12	0.12	0.11	0.08	0.10	0.07	0.06	0.00	–0.03	0.00	–0.05	–0.02	0.22
	0.10	0.07	0.05	0.07	0.07	0.10	0.09	0.32	0.15	0.09	0.06	0.12	0.13	0.17	0.03
	139	27	4	6	5	32	22	24	17	12	9	51	2	7	4
98767	0.25	0.29	0.27	0.31	0.34	0.34	0.24	0.31	0.36	0.25	0.29	0.31	0.32	0.28	0.25
	0.11	0.13	0.01	0.05	0.04	0.07	0.08	0.22	0.21	0.10	0.11	0.11	0.11	0.27	0.14
	147	26	4	5	6	31	22	30	18	14	9	54	2	8	4
98785	0.03	–0.02	0.14	0.09	0.06	0.11	0.06	0.04	0.05	0.04	–0.03	–0.03	0.05	0.02	0.30
	0.14	0.11	0.02	0.05	0.03	0.12	0.10	0.18	0.12	0.11	0.07	0.15	0.05	0.22	0.10
	123	24	4	5	3	27	21	19	15	9	9	42	2	5	4
99240	0.37	0.37	0.44	0.37	0.43	0.44	0.34	0.39	0.39	0.38	0.34	0.44	0.41	0.31	0.30
	0.12	0.12	0.03	0.05	0.03	0.12	0.08	0.23	0.24	0.09	0.12	0.11	0.13	0.31	0.10
	147	26	4	6	6	30	18	31	17	14	9	53	2	7	4
100412	–0.32	–0.31	–0.28	–0.14	–0.18	–0.22	–0.20	–0.27	–0.22	–0.31	–0.33	–0.36	–0.26	–0.48	–0.22
	0.08	0.07	0.03	0.07	0.07	0.09	0.10	0.11	0.12	0.16	0.05	0.09	0.02	0.17	0.05
	137	25	4	6	6	32	22	27	18	13	9	52	2	8	4
102264	–0.22	–0.25	–0.27	–0.17	–0.19	–0.20	–0.19	–0.20	–0.21	–0.26	–0.26	–0.26	–0.15	–0.21	–0.02
	0.10	0.10	0.05	0.05	0.02	0.08	0.04	0.14	0.15	0.10	0.07	0.09	0.01	0.21	0.09
	149	26	4	7	6	32	22	31	18	13	9	54	2	7	4
103458	–0.65	–0.72	–0.59	–0.35	–0.38	–0.47	–0.48	–0.42	–0.46	–0.67	–0.69	–0.64	–0.51	–0.87	–0.71
	0.09	0.10	0.02	0.03	0.04	0.07	0.07	0.10	0.14	0.10	0.06	0.09	0.02	0.19	0.05
	142	25	4	7	4	32	22	30	18	12	9	51	2	6	4
103682	0.27	0.25	0.40	0.31	0.41	0.35	0.31	0.25	0.28	0.30	0.17	0.35	0.26	0.15	0.21
	0.11	0.07	0.06	0.04	0.05	0.12	0.10	0.19	0.19	0.12	0.32	0.11	0.11	0.19	0.04
	148	27	4	7	6	32	21	31	18	13	8	54	2	7	4

Table B2: Abundances – Na, Mg, Al, Si, Ca, Ti, Cr, Fe, Ni, Zn, Y, and Ba - *continued*

HIP	Fe I	Fe II	Na I	Mg I	Al I	Si I	Ca I	Ti I	Ti II	Cr I	Cr II	Ni I	Zn I	Y II	Ba II
105858	–0.73	–0.72	–0.54	–0.51	–0.56	–0.58	–0.63	–0.67	–0.63	–0.71	–0.73	–0.74	–0.65	–0.93	–0.64
	0.11	0.08	0.08	0.08	0.04	0.10	0.11	0.08	0.11	0.10	0.08	0.11	0.04	0.15	0.07
	127	24	4	7	4	31	22	24	17	9	9	47	2	7	4
107975	–0.53	–0.51	–0.39	–0.37	–0.49	–0.46	–0.46	–0.40	–0.39	–0.62	–0.52	–0.57	–0.57	–0.62	–0.23
	0.09	0.05	0.04	0.14	0.05	0.08	0.11	0.07	0.10	0.08	0.10	0.12	0.00	0.10	0.14
	67	15	4	2	3	15	9	8	8	2	4	24	1	4	4
108736	–0.38	–0.43	–0.28	–0.06	–0.06	–0.16	–0.18	–0.16	–0.15	–0.35	–0.40	–0.35	–0.19	–0.54	–0.44
	0.08	0.08	0.06	0.05	0.04	0.07	0.08	0.13	0.14	0.11	0.06	0.07	0.01	0.19	0.03
	143	27	4	7	6	32	22	31	18	13	9	50	2	7	4
109378	0.22	0.23	0.28	0.32	0.32	0.29	0.21	0.30	0.30	0.22	0.22	0.26	0.32	0.23	0.25
	0.10	0.11	0.05	0.03	0.05	0.06	0.06	0.22	0.20	0.10	0.12	0.10	0.05	0.27	0.12
	148	25	4	7	6	31	22	30	18	14	9	53	2	8	4
109450	–0.13	–0.12	–0.11	0.01	0.03	–0.07	–0.07	–0.14	–0.05	–0.11	–0.11	–0.16	–0.12	–0.21	–0.11
	0.10	0.07	0.03	0.05	0.07	0.09	0.07	0.10	0.14	0.05	0.06	0.09	0.08	0.26	0.06
	142	23	4	6	6	31	22	29	18	12	9	51	2	6	4
109821	–0.08	–0.14	–0.09	0.05	0.06	–0.06	–0.03	–0.03	–0.01	–0.09	–0.17	–0.10	–0.11	–0.19	–0.11
	0.09	0.07	0.04	0.03	0.03	0.06	0.04	0.15	0.13	0.06	0.05	0.08	0.03	0.21	0.09
	146	27	4	6	5	32	22	32	18	14	9	54	2	7	4
110341	–0.17	–0.18	–0.13	–0.08	–0.12	–0.09	–0.05	–0.07	–0.10	–0.14	–0.19	–0.24	–0.23	–0.19	0.09
	0.09	0.08	0.02	0.06	0.04	0.10	0.10	0.17	0.13	0.18	0.06	0.11	0.01	0.19	0.04
	124	25	3	5	2	30	22	23	15	10	9	39	2	6	4
110512	–0.30	–0.34	–0.24	–0.06	–0.04	–0.16	–0.18	–0.14	–0.11	–0.25	–0.32	–0.28	–0.14	–0.43	–0.28
	0.10	0.07	0.04	0.03	0.06	0.07	0.05	0.13	0.13	0.25	0.04	0.11	0.05	0.23	0.07
	135	24	4	6	5	31	22	30	18	13	8	50	2	6	4
112151	–0.42	–0.44	–0.37	–0.14	–0.09	–0.23	–0.22	–0.05	–0.16	–0.42	–0.41	–0.33	–0.30	–0.42	–0.52
	0.10	0.12	0.04	0.04	0.06	0.10	0.08	0.13	0.11	0.04	0.08	0.14	0.00	0.12	0.10
	86	14	4	4	6	17	10	11	8	6	5	37	1	4	4
113137	0.22	0.21	0.33	0.28	0.35	0.28	0.30	0.24	0.29	0.23	0.24	0.27	0.25	0.16	0.23
	0.13	0.08	0.05	0.04	0.08	0.10	0.13	0.19	0.21	0.11	0.08	0.10	0.18	0.22	0.05
	148	29	4	7	6	32	22	31	18	14	9	53	2	7	4
113174	–0.11	–0.08	–0.11	–0.12	0.00	–0.15	–0.06	–0.09	–0.02	–0.21	–0.06	–0.16	–0.20	–0.09	0.49
	0.07	0.06	0.09	0.05	0.00	0.08	0.12	0.03	0.08	0.08	0.06	0.08	0.00	0.00	0.15
	49	8	2	2	0	9	8	2	4	2	3	9	1	1	3
113357	0.20	0.20	0.31	0.20	0.29	0.23	0.22	0.21	0.25	0.20	0.19	0.26	0.24	0.18	0.24
	0.10	0.09	0.03	0.03	0.05	0.07	0.07	0.19	0.19	0.09	0.07	0.09	0.08	0.24	0.07
	147	24	4	6	6	32	22	30	18	14	9	53	2	7	4
113421	0.35	0.34	0.46	0.41	0.40	0.39	0.31	0.36	0.38	0.36	0.34	0.42	0.41	0.33	0.27
	0.12	0.11	0.03	0.04	0.06	0.08	0.09	0.21	0.21	0.09	0.10	0.10	0.04	0.28	0.10
	148	27	4	7	6	31	22	30	18	14	9	53	2	8	4
116421	–0.45	–0.44	–0.40	–0.13	–0.09	–0.23	–0.26	–0.17	–0.19	–0.43	–0.41	–0.40	–0.38	–0.48	–0.45
	0.08	0.08	0.03	0.03	0.02	0.06	0.07	0.07	0.11	0.04	0.04	0.12	0.00	0.08	0.05
	84	19	4	3	6	17	8	11	9	6	5	34	1	4	4
116740	0.05	0.07	0.10	0.21	0.17	0.09	0.16	–0.07	–0.01	0.06	0.05	–0.02	0.15	–0.09	0.19
	0.08	0.07	0.06	0.26	0.17	0.10	0.12	0.09	0.14	0.03	0.01	0.09	0.00	0.13	0.13
	66	9	4	3	6	14	10	8	7	2	4	28	1	3	4
117880	0.12	0.09	0.21	0.20	0.22	0.15	0.19	0.16	0.16	0.05	0.10	0.14	0.09	0.02	0.18
	0.10	0.08	0.04	0.04	0.05	0.10	0.09	0.12	0.19	0.16	0.10	0.10	0.06	0.20	0.06
	142	25	4	6	6	32	21	25	17	12	9	50	2	6	4
118010	–0.07	–0.09	–0.13	0.00	0.05	–0.05	0.01	–0.01	–0.01	–0.10	–0.12	–0.11	–0.05	–0.18	–0.05
	0.08	0.06	0.02	0.06	0.04	0.06	0.10	0.09	0.08	0.05	0.04	0.06	0.00	0.08	0.06
	84	16	4	4	4	15	10	11	8	6	5	35	1	4	4

Table B2: Abundances – Na, Mg, Al, Si, Ca, Ti, Cr, Fe, Ni, Zn, Y, and Ba - *continued*

HIP	Fe I	Fe II	Na I	Mg I	Al I	Si I	Ca I	Ti I	Ti II	Cr I	Cr II	Ni I	Zn I	Y II	Ba II
118115	–0.01	–0.01	–0.06	0.06	0.09	0.00	0.02	0.02	0.05	–0.01	–0.04	–0.04	–0.03	–0.15	0.04
	0.09	0.08	0.07	0.06	0.06	0.07	0.07	0.13	0.12	0.10	0.08	0.09	0.13	0.25	0.05
	147	25	4	7	6	32	22	29	18	13	9	53	2	7	4

Table B3: Abundances – Oxygen and Europium

OBJECT	[O/H]					NLTE-corr		[Eu/H]	
	6300	6363	7772	7774	7775	GCEG	P III	4129	6645
Sun	0.00	0.00	0.00	0.00	0.00	−0.05	−0.05	0.00	0.00
HIP 699								−0.08	
HIP 910	−0.21							−0.19	
HIP 2235								−0.03	
HIP 2787								−0.02	
HIP 3086	0.09		−0.03	−0.09	−0.05	−0.07	−0.07	0.11	0.10
HIP 3142	−0.25		−0.22	−0.28	−0.28	−0.12	−0.06	−0.21	−0.23
HIP 3170			−0.13	−0.16	−0.01	−0.09	−0.06	−0.16	
HIP 3185	−0.14	−0.21	−0.03	−0.11	−0.15	−0.04	−0.02	0.02	0.00
HIP 3497	−0.05	−0.01	0.05	0.00	0.05	−0.05	−0.02	−0.07	−0.03
HIP 3704	−0.08		−0.24	−0.31	−0.26	−0.07	−0.04	−0.19	
HIP 3909	−0.11							0.05	
HIP 5315	0.00	−0.01	−0.03	0.01	0.17	−0.03	−0.05	0.05	−0.06
HIP 5862	0.06						−0.10		
HIP 7276	0.14		0.09	0.05	0.05	−0.11	−0.12	0.19	0.21
HIP 9085			−0.08	−0.16	−0.13	−0.12	−0.06	−0.18	
HIP 10306								−0.06	
HIP 10798	−0.30		−0.37	−0.34	−0.30	−0.02	0.04	−0.25	
HIP 11309	0.02							−0.19	
HIP 12186	0.08		0.06	0.14	0.09	−0.08	−0.10	0.13	0.12
HIP 12306								−0.35	
HIP 12611		0.14	0.27	0.31	0.42	−0.06	−0.11	0.19	0.19
HIP 12653	0.04	0.06	0.12	0.10	0.17	−0.12	−0.09	0.11	0.42
HIP 14086	−0.16		−0.17	−0.20	−0.16	−0.03	−0.03	−0.22	−0.27
HIP 14954	0.11		0.14	0.06	0.02	−0.16	−0.13	0.11	0.21
HIP 15131	−0.26						−0.01		
HIP 15510	−0.01	−0.10					0.01		
HIP 16788	−0.27							−0.06	
HIP 17147	−0.32		−0.36	−0.36	−0.28	−0.06	0.02	−0.39	
HIP 17378	0.13	0.05	0.17	0.08	0.09	−0.02	−0.09	0.18	0.24
HIP 18235	−0.24							−0.32	
HIP 18833	−0.26							−0.22	
HIP 20242	−0.01							−0.07	
HIP 21832								−0.30	
HIP 22263			0.02	0.06	0.06	−0.06	−0.05	0.10	
HIP 22325	0.01		0.05	0.02	0.12	−0.19	−0.14	0.12	0.41
HIP 23555	0.06		0.08	0.10	0.15	−0.15	−0.11	0.09	
HIP 23941			−0.19	−0.17	−0.33	−0.22	−0.10	−0.15	
HIP 24829	0.03		0.00	0.03	−0.04	−0.21	−0.14	0.18	0.13
HIP 26828								−0.03	
HIP 29271	0.02		0.16	0.11	0.06	−0.09	−0.05	0.11	
HIP 30480	0.17	0.10	0.14	0.16	0.21	−0.08	−0.10	0.15	0.18
HIP 30503	0.02	0.00	0.01	0.04	0.09	−0.07	−0.06	0.10	0.15
HIP 36874	0.10							0.02	
HIP 37789	−0.18							−0.33	
HIP 40613								−0.32	
HIP 44075	−0.32							−0.48	
HIP 44441	−0.09							−0.10	
HIP 44860	−0.01							−0.07	
HIP 72673	−0.30		−0.39	−0.49	−0.45	−0.15	−0.05	−0.37	
HIP 75181	0.00		0.05	−0.04	0.03	−0.05	−0.02	−0.11	−0.03
HIP 78955	0.17	0.17	0.19	0.21	0.23	−0.07	−0.11	0.31	0.25
HIP 79137	0.20	0.13	0.31	0.38	0.45	−0.03	−0.09	0.32	0.23

Table B3: Abundances – Oxygen and Europium - *continued*

OBJECT	[O/H]					NLTE-corr		[Eu/H]	
	6300	6363	7772	7774	7775	GCEG	P III	4129	6645
HIP 80337	0.03		0.00	−0.08	−0.06	−0.06	−0.05	0.16	0.09
HIP 80686	−0.05	−0.09	0.00	−0.06	0.01	−0.08	−0.06	0.00	−0.03
HIP 81520			−0.21	−0.24	−0.20	−0.03	0.02	−0.24	−0.29
HIP 82588	0.01	0.00	0.05	0.02	−0.01	−0.02	−0.01	0.21	−0.02
HIP 83229		−0.23	−0.10	−0.12	−0.09	−0.05	−0.02	−0.24	−0.21
HIP 83601	0.07		0.03	−0.11	0.05	−0.10	−0.08	0.12	
HIP 84551	0.12		0.08	0.04	−0.02	−0.30	−0.17	0.18	0.26
HIP 84636	0.15		0.27	0.13	0.28	−0.01	−0.12	0.06	0.23
HIP 84905	−0.15		−0.15	−0.19	−0.20	−0.06	−0.03	−0.09	−0.12
HIP 85007	−0.26		−0.22	−0.37	−0.28	−0.07	−0.03	−0.31	
HIP 85042	0.00	0.06	−0.08	−0.01	−0.04	−0.04	−0.05	0.14	0.08
HIP 86731			0.21	0.22	0.16	−0.11	−0.14	0.16	0.16
HIP 86796	0.14		0.19	0.25	0.21	−0.07	−0.09	0.25	0.22
HIP 87523	−0.31	−0.31	−0.24	−0.24	−0.34	−0.09	−0.06	−0.26	−0.31
HIP 88622	−0.05	−0.09	0.04	−0.01	0.00	−0.06	−0.01	−0.19	−0.05
HIP 88945	−0.04							−0.02	
HIP 90485		0.06	0.15	0.05	0.13	−0.19	−0.13	0.12	0.26
HIP 91438	−0.18		−0.18	−0.24	−0.17	−0.02	−0.01	−0.10	−0.13
HIP 92270	0.01							0.03	
HIP 93185	−0.14							−0.29	
HIP 94645	0.06	0.11	0.20	0.13	0.13	−0.13	−0.10	0.12	
HIP 95447	0.20	0.23	0.36	0.31	0.41	−0.07	−0.10	0.25	0.23
HIP 96124	0.08	0.08	0.04	0.07	0.15	−0.03	−0.02	0.10	0.07
HIP 96258	0.01							0.11	
HIP 96536	0.05		0.07	−0.01	0.05	−0.21	−0.13	0.41	
HIP 98767	0.21	0.13	0.36	0.37	0.41	−0.05	−0.07	0.29	0.21
HIP 98785	0.11	0.01	0.08	−0.05	0.04	−0.21	−0.14	0.13	
HIP 99240	0.19	0.17	0.29	0.37	0.31	−0.05	−0.09	0.23	0.17
HIP 100412	−0.18		−0.08	−0.08	−0.05	−0.09	−0.06	−0.21	−0.08
HIP 102264	−0.12		−0.08	−0.17	−0.13	−0.03	−0.02	−0.20	−0.28
HIP 103458	−0.29		−0.23	−0.31	−0.30	−0.04	0.00	−0.33	−0.19
HIP 103682	0.14	0.12	0.13	0.18	0.19	−0.09	−0.10	0.21	
HIP 105858	−0.46		−0.33	−0.39	−0.36	−0.07	−0.01	−0.56	−0.36
HIP 107975	−0.26							−0.25	
HIP 108736	−0.01	−0.01	0.07	0.01	0.05	−0.07	−0.04	−0.15	−0.06
HIP 109378	0.16	0.16	0.21	0.28	0.26	−0.04	−0.06	0.30	0.33
HIP 109450	0.05	0.08	0.11	−0.03	0.05	−0.07	−0.06	−0.02	0.07
HIP 109821	0.10		−0.07	0.06	0.00	−0.06	−0.05	0.09	0.07
HIP 110341	−0.11	−0.12	−0.15	−0.17	−0.20	−0.21	−0.09	−0.07	
HIP 110512	0.00		0.07	−0.02	0.10	−0.07	−0.04	−0.07	0.08
HIP 112151	−0.01							−0.05	
HIP 113137	0.13	0.12	0.22	0.21	0.29	−0.08	−0.10	0.15	0.31
HIP 113174									
HIP 113357	0.10	0.24	0.10	0.09	0.07	−0.07	−0.08	0.13	0.17
HIP 113421	0.16		0.24	0.27	0.31	−0.05	−0.09	0.29	0.36
HIP 116421	−0.05							0.05	
HIP 116740								−0.02	
HIP 117880	0.05		0.06	0.14	0.09	−0.11	−0.10	0.08	
HIP 118010	0.04							0.12	
HIP 118115	0.04		0.02	−0.09	0.01	−0.06	−0.06	0.09	0.09

Appendix C
Atomic line data

This appendix consists of the following tables:

Table C1: Atomic line data The lines have been grouped according to their element and degree of ionozation. Column 1 gives the wavelength, col. 2 the lower excitation potential; col. 3 the correction factor to the classical Unsöld damping constant; col. 4 indicates if the broadening by collisions have been taken from Anstee & O'Mara (1995), Barklem & O'Mara (1997, 1998), and Barklem et al. (1998, 2000) (indicated by an "S") instead of the classical Unsöld broadening (indicated by an "U"). Column 5 gives the radiation damping constant; col. 6 gives the $\log gf$-values; col. 7 gives the references for the $\log gf$-values that in turn are given in Table C2

Table C2: References for $\log gf$-values in Table C1

Table C1: Atomic line data

λ (Å)	$\chi_{\rm l}$ (eV)	$\delta\gamma_6$	DMP	$\gamma_{\rm rad}$ (s^{-1})	$\log gf$	Ref.
Al I $\log\epsilon_\odot = 6.47$						
5557.070	3.140	2.50	U	3.0e+08	−2.21	*
6696.030	3.140	2.50	U	3.0e+08	−1.63	*
6698.670	3.140	2.50	U	3.0e+08	−1.92	*
7835.320	4.020	2.50	U	7.9e+07	−0.80	*
7836.130	4.020	2.50	U	7.9e+07	−0.65	*
8772.870	4.020	2.50	S	2.3e+08	−0.45	*
8773.900	4.020	2.50	S	2.3e+08	−0.32	*
Ca I $\log\epsilon_\odot = 6.36$						
4512.270	2.520	1.80	U	1.1e+07	−2.03	*
4526.934	2.710	1.80	U	2.8e+07	−0.80	*
4578.560	2.520	1.80	U	5.3e+07	−0.92	*
4685.268	2.930	1.80	U	2.5e+08	−0.94	*
5260.390	2.520	1.80	S	8.0e+07	−1.78	*
5261.710	2.520	1.80	S	8.0e+07	−0.45	*
5349.470	2.710	1.80	U	2.7e+06	−0.64	*
5512.980	2.930	1.80	U	2.8e+08	−0.56	*
5581.968	2.520	1.80	S	7.1e+07	−0.53	*
5590.117	2.520	1.80	S	7.1e+07	−0.52	*
5601.277	2.530	1.80	S	7.1e+07	−0.24	*
5867.570	2.930	1.80	U	2.6e+08	−1.61	*
6122.217	1.890	1.80	S	7.2e+07	−0.36	*
6161.300	2.520	1.80	S	1.9e+07	−1.26	*
6166.440	2.520	1.80	S	1.9e+07	−1.17	*
6169.040	2.520	1.80	S	2.0e+07	−0.84	*
6169.562	2.520	1.80	S	1.9e+07	−0.63	*
6439.080	2.520	1.80	S	4.5e+07	0.30	*
6455.610	2.520	1.80	S	4.6e+07	−1.30	*
6471.670	2.520	1.80	S	4.4e+07	−0.65	*
6493.790	2.520	1.80	S	4.4e+07	−0.19	*
6499.650	2.520	1.80	S	4.4e+07	−0.73	*
6798.470	2.710	1.80	U	1.9e+07	−2.46	*
Cr I $\log\epsilon_\odot = 5.67$						
4511.900	3.090	2.50	S	6.7e+07	−0.39	*
4545.945	0.940	2.50	S	1.6e+07	−1.31	*
4708.019	3.168	2.50	S	7.9e+07	−0.09	*
5238.960	2.710	2.50	S	2.5e+08	−1.43	*
5296.691	0.983	2.50	S	5.3e+08	−1.41	*
5297.390	2.900	2.50	S	1.1e+08	0.00	*
5304.180	3.460	2.50	S	2.5e+08	−0.78	*
5318.770	3.440	2.50	S	2.5e+08	−0.77	*
5480.510	3.500	2.50	U	7.4e+07	−0.92	*
5574.390	4.450	2.50	U	6.7e+07	−0.72	*

Table C1: Atomic line data - *continued*

λ (Å)	χ_1 (eV)	$\delta\gamma_6$	DMP	$\gamma_{\rm rad}$ (s^{-1})	$\log gf$	Ref.
5783.073	3.232	2.50	S	1.0e+08	−0.48	*
5783.866	3.322	2.50	S	1.0e+08	−0.26	*
5787.930	3.320	2.50	S	1.0e+08	−0.15	*
6330.090	0.940	2.50	S	2.4e+07	−2.90	*
6630.030	1.030	2.50	S	2.4e+07	−3.60	*
Cr II $\log\epsilon_\odot = 5.67$						
4588.199	4.070	2.50	U	2.6e+08	−0.74	*
4616.628	4.073	2.50	U	2.6e+08	−1.21	*
4848.252	3.865	2.50	U	2.6e+08	−1.14	*
5237.320	4.070	2.50	U	2.6e+08	−1.18	*
5305.860	3.830	2.50	U	2.6e+08	−2.06	*
5308.420	4.070	2.50	U	2.6e+08	−1.79	*
5310.690	4.070	2.50	U	2.6e+08	−2.24	*
5313.580	4.070	2.50	U	2.6e+08	−1.55	*
5502.092	4.168	2.50	U	2.6e+08	−1.97	*
Fe I $\log\epsilon_\odot = 7.50$						
4517.525	3.071	1.40	S	1.1e+08	−1.86	OWL
4547.847	3.546	1.40	S	4.8e+07	−1.01	OWL
4566.520	3.300	1.40	S	2.0e+08	−2.38	OWL
4587.128	3.573	1.40	S	3.8e+07	−1.74	OWL
4602.000	1.610	1.20	S	1.2e+08	−3.15	BL1
4630.130	2.280	1.20	S	4.0e+08	−2.59	OWL
4635.850	2.840	1.40	S	5.8e+07	−2.36	OWL
4683.560	2.832	1.40	S	7.9e+07	−2.32	OWL
4690.138	3.687	1.40	S	2.2e+08	−1.64	OWL
4733.592	1.485	1.10	U	1.7e+08	−2.99	OWL
4741.529	2.830	1.40	S	1.4e+08	−1.76	OWL
4745.800	3.654	1.40	U	1.2e+08	−1.27	OWL
4779.439	3.415	1.40	S	7.9e+07	−2.02	OWL
4787.827	2.998	1.40	S	6.0e+07	−2.60	OWL
4788.757	3.237	1.40	S	1.9e+07	−1.76	OWL
4802.880	3.642	1.40	U	7.8e+07	−1.51	OWL
4839.520	3.270	1.40	S	3.7e+07	−1.82	OWL
4844.014	3.547	1.40	S	5.8e+07	−2.05	OWL
4882.144	3.420	1.40	S	6.3e+07	−1.64	GK
4946.385	3.370	1.40	S	6.3e+07	−1.17	WBW
4961.920	3.635	1.40	S	8.9e+07	−2.19	MRW
4962.570	4.180	1.40	U	2.1e+08	−1.18	OWL
5044.212	2.850	1.40	S	1.0e+08	−2.06	BK2
5054.643	3.640	1.40	S	4.0e+07	−1.92	OWL
5067.160	4.220	1.40	S	2.1e+08	−0.97	GK,RW
5083.340	0.960	1.10	S	1.5e+07	−2.96	BL2
5088.160	4.150	1.40	S	2.6e+08	−1.68	MRW
5090.780	4.260	1.40	S	2.1e+08	−0.40	BK3

Table C1: Atomic line data - *continued*

λ (Å)	χ_1 (eV)	$\delta\gamma_6$	DMP	$\gamma_{\rm rad}$ (s^{-1})	$\log gf$	Ref.
5104.440	4.280	1.40	S	2.1e+08	−1.59	MRW
5109.660	4.300	1.40	S	2.1e+08	−0.98	RW
5127.370	0.910	1.10	S	1.7e+07	−3.31	BL2
5141.750	2.420	1.20	S	1.5e+08	−2.24	OWL
5145.094	2.198	1.20	S	1.6e+08	−2.88	OWL
5187.914	4.143	1.40	U	1.2e+08	−1.37	OWL
5198.711	2.220	1.20	S	1.0e+08	−2.14	BL3
5223.180	3.630	1.40	S	7.9e+07	−1.78	OWL
5225.525	0.110	1.00	S	4.4e+03	−4.79	BL4
5242.491	3.635	1.40	S	5.8e+07	−0.97	OWL
5253.033	2.279	1.40	S	1.6e+08	−3.84	MRW
5288.530	3.680	1.40	S	6.0e+07	−1.51	OWL
5294.553	3.640	1.40	S	1.4e+08	−2.76	MRW
5295.321	4.416	1.40	S	1.8e+08	−1.59	MRW
5307.361	1.610	1.20	S	2.0e+06	−2.99	BL1
5308.690	4.260	1.40	S	2.1e+08	−2.50	GK
5320.030	3.640	1.40	U	3.1e+08	−2.44	MRW
5321.110	4.430	1.40	S	1.7e+08	−0.95	OWL
5322.040	2.280	1.20	S	1.0e+08	−2.80	OWL
5365.399	3.573	1.40	U	2.5e+07	−1.02	OWL
5373.698	4.470	1.40	S	1.1e+08	−0.76	MRW
5376.836	4.295	1.40	S	1.5e+08	−2.21	MRW
5379.573	3.700	1.40	S	5.8e+07	−1.51	OWL
5386.340	4.150	1.40	S	2.3e+08	−1.67	MRW
5395.220	4.440	1.40	S	1.8e+08	−2.07	MRW
5398.280	4.440	1.40	S	1.9e+08	−0.63	MRW
5417.042	4.416	1.40	S	1.8e+08	−1.58	MRW
5436.596	2.279	1.20	S	1.7e+08	−2.96	OWL
5441.347	4.313	1.40	S	1.8e+08	−1.63	MRW
5461.559	4.446	1.40	S	1.9e+08	−1.80	MRW
5464.280	4.143	1.40	U	8.7e+07	−1.40	OWL
5466.988	3.573	1.40	U	3.0e+07	−2.23	OWL
5483.100	4.150	1.40	S	2.6e+08	−1.41	OWL
5501.465	0.958	1.10	S	1.5e+07	−3.05	OWL
5522.454	4.209	1.40	S	8.9e+07	−1.45	MRW
5546.514	4.372	1.40	S	1.8e+08	−1.21	MRW
5560.207	4.430	1.40	S	1.6e+08	−1.09	MRW
5576.100	3.430	1.40	S	7.5e+07	−0.90	MRW
5577.020	5.030	1.40	U	6.9e+08	−1.55	GK
5618.633	4.209	1.40	S	1.0e+08	−1.28	OWL
5619.609	4.387	1.40	S	1.8e+08	−1.60	MRW
5635.831	4.257	1.40	S	1.9e+08	−1.79	MRW
5651.477	4.474	1.40	S	1.6e+08	−1.90	MRW
5652.327	4.261	1.40	S	8.2e+07	−1.85	MRW
5667.518	4.178	1.40	U	3.0e+08	−1.58	OWL
5679.025	4.650	1.40	S	1.4e+08	−0.82	MRW

Table C1: Atomic line data - *continued*

λ (Å)	χ_1 (eV)	$\delta\gamma_6$	DMP	$\gamma_{\rm rad}$ (s^{-1})	$\log gf$	Ref.
5701.550	2.560	1.50	S	1.5e+08	−2.12	BK2
5705.473	4.302	1.40	S	2.0e+08	−1.50	MRW
5731.772	4.257	1.40	S	2.0e+08	−1.20	MRW
5741.848	4.257	1.40	S	2.1e+08	−1.85	OWL
5753.130	4.260	1.40	S	9.7e+07	−0.69	OWL
5775.080	4.220	1.40	U	1.9e+08	−1.30	OWL
5778.463	2.588	1.50	S	1.5e+08	−3.49	MRW
5793.922	4.221	1.40	S	2.1e+08	−1.60	MRW
5809.220	3.880	1.40	S	5.1e+07	−1.74	MRW
5849.690	3.690	1.40	S	5.5e+07	−2.89	MRW
5852.220	4.550	1.40	S	1.9e+08	−1.23	MRW
5855.080	4.610	1.40	S	1.9e+08	−1.48	BK2
5856.090	4.290	1.40	S	5.6e+07	−1.33	OWL
5858.780	4.220	1.40	S	2.7e+08	−2.16	MRW
5859.590	4.550	1.40	U	1.9e+08	−0.30	MFW
5861.110	4.280	1.40	S	2.1e+08	−2.45	GK
5862.360	4.550	1.40	U	1.9e+08	−0.06	VALD
5956.710	0.860	1.10	S	2.7e+04	−4.61	BL2
6027.051	4.076	1.40	U	8.9e+07	−1.09	OWL
6065.490	2.610	1.50	S	1.0e+08	−1.53	BL5
6082.720	2.220	1.20	S	7.7e+06	−3.57	BL3
6085.259	2.759	1.40	S	1.4e+08	−2.71	OWL
6093.649	4.608	1.40	S	2.0e+08	−1.40	MRW
6094.377	4.652	1.40	S	2.0e+08	−1.84	MRW
6096.671	3.984	1.40	S	4.6e+07	−1.83	MRW
6127.904	4.140	1.40	U	9.3e+07	−1.40	OWL
6151.620	2.180	1.30	S	1.6e+08	−3.27	BK2
6157.730	4.080	1.40	U	5.0e+07	−1.16	MRW
6159.380	4.610	1.40	S	1.9e+08	−1.97	GK
6165.370	4.140	1.40	U	8.8e+07	−1.47	OWL
6173.340	2.220	1.30	S	1.7e+08	−2.88	BL3
6180.203	2.730	1.40	S	1.5e+08	−2.59	BK2
6187.990	3.940	1.40	S	4.6e+07	−1.62	MRW
6200.320	2.610	1.50	S	1.0e+08	−2.44	BL5
6213.437	2.220	1.30	S	1.6e+08	−2.48	OWL
6219.280	2.200	1.30	S	1.6e+08	−2.42	BK2
6226.740	3.884	1.40	S	5.4e+07	−2.12	MRW
6229.230	2.840	1.40	S	1.4e+08	−2.87	MRW
6240.646	2.223	1.20	S	1.6e+07	−3.17	OWL
6246.330	3.600	1.40	S	8.0e+07	−0.88	OWL
6252.560	2.400	1.30	S	8.7e+07	−1.69	BL3
6265.140	2.180	1.30	S	1.7e+08	−2.55	BL3
6270.230	2.860	1.40	S	1.4e+08	−2.61	OWL
6297.800	2.220	1.30	S	1.5e+08	−2.73	BK2
6322.690	2.590	1.50	S	1.0e+08	−2.43	BL5
6335.340	2.200	1.30	S	1.7e+08	−2.18	OWL

Table C1: Atomic line data - *continued*

λ (Å)	χ_l (eV)	$\delta\gamma_6$	DMP	$\gamma_{\rm rad}$ (s^{-1})	$\log gf$	Ref.
6344.148	2.430	1.30	S	8.7e+07	−2.92	BL3
6380.750	4.190	1.40	U	1.3e+07	−1.38	OWL
6393.610	2.430	1.30	S	9.3e+07	−1.58	OWL
6411.650	3.640	1.40	S	8.0e+07	−0.72	OWL
6430.850	2.180	1.30	S	1.6e+08	−2.01	BL3
6436.410	4.190	1.40	U	3.0e+07	−2.46	GK
6481.880	2.280	1.20	S	1.5e+08	−2.96	BK2
6498.940	0.960	1.10	S	4.3e+04	−4.70	BL2
6518.370	2.830	1.40	S	1.5e+08	−2.45	BK2
6574.250	0.990	1.10	U	3.4e+04	−5.02	OWL
6592.913	2.730	1.40	S	1.0e+08	−1.47	OWL
6593.868	2.430	1.30	S	8.6e+07	−2.42	BL3
6627.560	4.550	1.40	S	1.8e+08	−1.58	MRW
6633.760	4.560	1.40	S	2.4e+08	−0.80	OWL
6677.990	2.680	1.40	S	1.0e+08	−1.42	OWL
6696.320	4.830	1.40	S	2.4e+08	−1.67	V
6699.130	4.590	1.40	S	1.4e+08	−2.10	BK2
6703.570	2.760	1.40	S	1.0e+08	−3.06	MRW
6704.500	4.220	1.40	S	1.0e+08	−2.66	GK
6710.320	1.480	1.20	S	1.7e+07	−4.88	GK
6713.740	4.790	1.40	S	2.4e+08	−1.50	MRW
6750.152	2.420	1.20	S	7.7e+06	−2.62	BL3
6796.120	4.140	1.40	S	1.4e+08	−2.53	GK
6806.850	2.730	1.40	S	1.0e+08	−3.21	GK
6810.260	4.610	1.40	S	2.3e+08	−0.99	OWL
6855.162	4.559	1.40	U	2.4e+08	−0.74	OWL
6858.150	4.608	1.40	S	1.9e+08	−0.93	OWL
7107.460	4.190	1.40	U	4.8e+07	−1.34	OWL
7127.570	4.990	1.40	U	4.9e+08	−1.36	GK
7130.920	4.220	1.40	S	2.1e+08	−0.69	MRW
7132.986	4.076	1.40	U	5.5e+07	−1.63	OWL
7401.685	4.187	1.40	U	7.1e+07	−1.35	OWL
7418.330	4.140	1.40	U	5.5e+07	−2.93	VALD
7418.670	4.140	1.40	S	1.1e+08	−1.38	OWL
7421.550	4.640	1.40	S	2.5e+08	−1.80	GK
7583.788	3.018	1.40	S	1.0e+08	−1.89	OWL
7710.365	4.221	1.40	U	1.7e+08	−1.11	OWL
7745.520	5.080	1.40	U	6.4e+08	−1.29	GK
7746.600	5.060	1.40	U	6.3e+08	−1.33	MFW
7748.269	2.949	1.40	S	8.0e+08	−1.75	OWL
7751.110	4.990	1.40	S	6.4e+08	−0.72	MFW
7802.510	5.080	1.40	U	6.3e+08	−1.40	MFW
7941.090	3.270	1.40	S	1.4e+08	−2.58	GK
7955.710	5.030	1.40	U	6.4e+08	−1.19	MFW
7959.140	5.030	1.40	U	6.4e+08	−1.32	VALD
8239.128	2.424	1.20	U	6.8e+06	−3.18	OWL

Table C1: Atomic line data - *continued*

λ (Å)	χ_1 (eV)	$\delta\gamma_6$	DMP	$\gamma_{\rm rad}$ (s^{-1})	$\log gf$	Ref.
8365.634	3.251	1.40	U	1.5e+08	−1.91	OWL
8515.108	3.018	1.40	U	7.6e+07	−2.07	OWL
8526.669	4.913	1.40	U	4.8e+08	−0.76	OWL
8582.257	2.991	1.40	U	7.9e+07	−2.13	OWL
8598.830	4.387	1.40	U	1.3e+08	−1.09	OWL
8611.804	2.845	1.40	S	6.9e+06	−1.85	OWL
8621.601	2.949	1.40	U	8.7e+07	−2.32	OWL
8674.747	2.832	1.40	S	7.8e+06	−1.68	OWL
8713.200	2.950	1.40	U	9.3e+07	−2.47	V
8747.440	3.020	1.40	U	8.0e+07	−3.36	V
8757.190	2.840	1.40	S	7.7e+06	−1.91	OWL
Fe II $\log \epsilon_\odot = 7.50$						
4508.290	2.850	2.50	U	4.1e+08	−2.35	RU
4576.339	2.840	2.50	U	4.1e+08	−2.98	RU
4582.833	2.840	2.50	U	3.1e+08	−3.22	RU
4620.520	2.830	2.50	U	4.1e+08	−3.31	RU
4629.339	2.810	2.50	U	3.0e+08	−2.48	RU
4635.311	5.960	2.50	U	5.4e+08	−1.58	RU
4656.981	2.890	2.50	U	4.1e+08	−3.64	RU
4670.173	2.580	2.50	U	3.5e+08	−4.07	RU
4720.133	3.200	2.50	U	3.4e+08	−4.82	RU
4993.347	2.810	2.50	U	3.0e+08	−3.52	RU
5100.660	2.810	2.50	U	3.4e+08	−4.20	RU
5132.657	2.810	2.50	U	3.5e+08	−4.09	RU
5197.576	3.230	2.50	U	3.0e+08	−2.35	RU
5234.630	3.220	2.50	U	3.1e+08	−2.28	RU
5284.098	2.890	2.50	U	3.5e+08	−3.20	RU
5325.559	3.220	2.50	U	3.1e+08	−3.32	RU
5414.046	3.220	2.50	U	4.1e+08	−3.64	RU
5425.260	3.200	2.50	U	3.0e+08	−3.39	RU
5534.834	3.250	2.50	U	3.0e+08	−2.86	RU
5991.368	3.150	2.50	U	3.5e+08	−3.65	RU
6084.099	3.200	2.50	U	3.5e+08	−3.88	RU
6149.230	3.890	2.50	U	3.4e+08	−2.84	RU
6179.388	5.570	2.50	U	3.1e+08	−2.80	RU
6239.948	3.890	2.50	U	3.4e+08	−3.57	RU
6247.545	3.890	2.50	U	3.4e+08	−2.43	RU
6369.464	2.890	2.50	U	2.9e+08	−4.23	RU
6383.710	5.550	2.50	U	4.1e+08	−2.41	RU
6416.930	3.890	2.50	U	3.4e+08	−2.88	RU
6432.680	2.890	2.50	U	2.9e+08	−3.69	RU
6446.400	6.220	2.50	U	5.2e+08	−2.08	RU
6456.390	3.900	2.50	U	3.4e+08	−2.19	RU
6516.080	2.890	2.50	U	2.9e+08	−3.43	RU
7222.397	3.89	2.50	U	4.2e+08	−3.40	RU

Table C1: Atomic line data - *continued*

λ (Å)	$\chi_{\rm l}$ (eV)	$\delta\gamma_6$	DMP	$\gamma_{\rm rad}$ (s^{-1})	$\log gf$	Ref.
7224.464	3.89	2.50	U	4.2e+08	−3.36	RU
7479.694	3.89	2.50	U	3.1e+08	−3.63	RU
7515.837	3.90	2.50	U	4.1e+08	−3.55	RU
7711.731	3.90	2.50	U	4.1e+08	−2.68	RU
Mg I $\log \epsilon_\odot = 7.58$						
4571.100	0.000	2.50	U	1.1e+03	−5.55	*
5711.090	4.330	2.50	U	5.1e+08	−1.87	*
7387.69	5.753	2.50	U	1.0e+08	−1.27	*
7691.55	5.753	2.50	U	1.0e+08	−1.00	*
8473.663	5.933	2.50	U	1.0e+08	−2.02	*
8712.690	5.930	2.50	U	1.4e+07	−1.27	*
8717.820	5.930	2.50	U	1.4e+07	−1.04	*
8736.02	5.95	2.50	U	1.0e+08	−0.64	*
Na I $\log \epsilon_\odot = 6.33$						
5682.650	2.100	1.40	S	1.0e+08	−0.71	LW
5688.219	2.100	1.40	S	1.0e+08	−0.40	LW
6154.220	2.100	1.40	U	6.4e+07	−1.57	LW
6160.750	2.100	1.40	U	6.6e+07	−1.27	LW
Ni I $\log \epsilon_\odot = 6.25$						
4686.220	3.600	2.50	S	1.1e+08	−0.58	WL
4831.180	3.610	2.50	S	1.2e+08	−0.32	WL
4857.395	3.740	2.50	U	1.0e+08	−0.83	*
4866.27	3.539	2.50	U	1.1e+08	−0.21	WL
4904.420	3.540	2.50	S	1.8e+08	−0.25	*
4953.21	3.740	2.50	S	1.2e+08	−0.58	WL
4998.22	3.606	2.50	S	1.2e+08	−0.69	WL
5082.350	3.660	2.50	S	1.8e+08	−0.54	*
5084.110	3.680	2.50	S	1.3e+08	−0.06	*
5088.540	3.850	2.50	U	1.6e+08	−1.08	*
5088.960	3.680	2.50	S	1.3e+08	−1.29	*
5094.420	3.830	2.50	S	1.2e+08	−1.11	*
5102.970	1.680	2.50	S	1.3e+08	−2.66	*
5115.400	3.830	2.50	S	7.3e+07	−0.14	*
5392.330	4.150	2.50	S	2.0e+08	−1.32	*
5468.110	3.850	2.50	S	1.6e+08	−1.66	*
5578.729	1.677	2.50	S	5.4e+07	−2.57	*
5587.870	1.930	2.50	S	1.3e+03	−2.44	*
5593.746	3.899	2.50	S	1.3e+08	−0.78	*
5748.360	1.680	2.50	S	4.3e+07	−3.24	*
5754.670	1.930	2.50	S	1.6e+08	−1.85	*
5805.22	4.168	2.50	S	2.2e+08	−0.62	*
5847.000	1.680	2.50	S	7.4e+07	−3.44	*
5996.740	4.236	2.50	S	1.9e+08	−1.01	*

Table C1: Atomic line data - *continued*

λ (Å)	χ_1 (eV)	$\delta\gamma_6$	DMP	$\gamma_{\rm rad}$ (s^{-1})	$\log gf$	Ref.
6007.317	1.677	2.50	S	9.3e+06	−3.41	*
6086.288	4.266	2.50	S	2.6e+08	−0.46	*
6108.120	1.680	2.50	S	4.9e+07	−2.43	*
6111.080	4.090	2.50	S	1.5e+08	−0.82	*
6128.984	1.677	2.50	S	1.2e+07	−3.36	*
6130.140	4.270	2.50	S	2.8e+08	−0.88	*
6133.980	4.090	2.50	S	1.4e+08	−1.91	*
6175.370	4.090	2.50	S	2.3e+08	−0.50	*
6176.820	4.090	2.50	S	1.5e+08	−0.26	WL
6177.250	1.830	2.50	U	4.3e+07	−3.55	*
6186.717	4.106	2.50	S	2.0e+08	−0.88	*
6204.610	4.090	2.50	S	1.8e+08	−1.10	WL
6223.98	4.106	2.50	S	2.1e+08	−0.91	WL
6314.668	1.936	2.50	S	5.4e+07	−2.00	*
6322.169	4.154	2.50	S	2.0e+08	−1.21	*
6327.600	1.680	2.50	S	7.2e+07	−3.06	*
6378.25	4.154	2.50	S	2.1e+08	−0.81	WL
6482.810	1.930	2.50	S	8.1e+07	−2.76	*
6598.611	4.236	2.50	S	1.9e+08	−0.91	*
6635.130	4.420	2.50	S	1.5e+08	−0.72	*
6643.650	1.680	2.50	S	1.0e+08	−1.91	*
6767.780	1.830	2.50	U	1.0e+08	−2.10	*
6772.321	3.658	2.50	S	1.5e+08	−0.94	*
6813.610	5.340	2.50	U	8.2e+08	−0.33	*
6842.043	3.658	2.50	S	1.5e+08	−1.50	*
7110.900	1.940	2.50	S	5.2e+07	−2.88	*
7715.591	3.700	2.50	U	5.9e+07	−1.01	*
7748.890	3.710	2.50	U	9.5e+07	−0.33	*
7788.930	1.950	2.50	S	1.0e+08	−1.75	*
7797.580	3.900	2.50	U	1.0e+08	−0.32	*
7826.77	3.700	2.50	U	6.0e+07	−2.05	*
O I $\log \epsilon_\odot = 8.83$						
6363.776	0.020	2.50	U	1.0e+05	−10.303	WSG
7771.944	9.140	2.50	S	4.8e+07	0.37	BZ,HBGV
7774.166	9.140	2.50	S	4.7e+07	0.22	BZ,HBGV
7775.388	9.140	2.50	S	4.5e+07	0.00	BZ,HBGV
Si I $\log \epsilon_\odot = 7.55$						
5645.61	4.930	1.30	U	2.0e+08	−2.04	G,BZH
5665.55	4.930	1.30	U	2.0e+08	−1.94	G,BZH
5684.48	4.954	1.30	U	1.8e+08	−1.55	G,BZH
5690.43	4.930	1.30	U	2.0e+08	−1.77	G,BZH
5701.120	4.930	1.30	U	2.0e+08	−1.95	G,BZH
5772.148	5.080	1.30	U	2.2e+08	−1.65	G,BZH
5793.080	4.930	1.30	U	1.9e+08	−1.96	G,BZH

Table C1: Atomic line data - *continued*

λ (Å)	χ_1 (eV)	$\delta\gamma_6$	DMP	$\gamma_{\rm rad}$ (s^{-1})	$\log gf$	Ref.
5797.86	4.954	1.30	U	1.8e+08	−1.95	G,BZH
5948.545	5.080	1.30	U	2.0e+08	−1.13	G,BZH
6125.030	5.610	1.30	U	1.1e+06	−1.52	*
6142.490	5.620	1.30	U	8.4e+05	−1.50	*
6145.020	5.610	1.30	U	9.6e+05	−1.46	*
6155.140	5.620	1.30	U	3.6e+06	−0.72	*
6237.328	5.614	1.30	U	1.0e+08	−1.05	*
6243.823	5.616	1.30	U	1.0e+08	−1.30	*
6244.476	5.616	1.30	U	1.0e+08	−1.32	*
6741.63	5.984	1.30	U	2.7e+07	−1.65	G,BZH
7034.90	5.871	1.30	U	1.4e+08	−0.78	G,BZH
7405.77	5.614	1.30	U	1.4e+08	−0.72	G,BZH
7415.960	5.610	1.30	S	1.0e+08	−0.85	*
7423.520	5.620	1.30	S	1.3e+08	−0.65	*
7680.27	5.863	1.30	U	4.6e+07	−0.59	G,BZH
7760.640	6.200	1.30	U	6.6e+05	−1.37	*
7800.000	6.180	1.30	U	3.3e+06	−0.72	*
7849.984	6.191	1.30	U	1.0e+08	−0.82	*
7918.38	5.954	1.30	U	3.4e+07	−0.51	G,BZH
7932.35	5.964	1.30	U	3.7e+07	−0.37	G,BZH
7944.00	5.984	1.30	U	2.6e+08	−0.21	G,BZH
8595.968	6.191	1.30	U	1.0e+08	−0.89	*
8728.010	6.180	1.30	U	6.6e+06	−0.47	*
8742.450	5.870	1.30	U	8.2e+07	−0.53	*
8752.025	5.871	1.30	U	1.0e+08	−0.49	*
Ti I $\log\epsilon_\odot = 5.02$						
4512.733	0.840	1.50	S	1.2e+08	−0.42	BL7,GBP
4518.023	0.830	1.50	S	1.2e+08	−0.27	BL7,GBP
4555.485	0.850	1.50	S	1.2e+08	−0.43	BL7,GBP
4562.640	0.020	1.50	S	6.9e+05	−2.60	BL6,GBP
4617.280	1.750	1.50	S	1.1e+08	0.45	BL9,GBP
4623.100	1.740	1.50	S	1.1e+08	0.17	BL9,GBP
4758.120	2.250	1.50	S	1.1e+08	0.48	BL9,GBP
4778.258	2.236	1.50	S	1.6e+08	−0.22	K
4820.410	1.500	1.50	S	1.4e+08	−0.39	BL9,GBP
4840.880	0.900	1.50	S	2.8e+07	−0.45	BL7,GBP
4858.14	4.102	1.50	S	1.3e+08	−0.14	NWL
4874.88	3.320	1.50	S	4.2e+08	−0.39	NWL
4913.616	1.870	1.50	S	6.5e+07	0.22	BL9,GBP
5016.162	0.850	1.50	S	7.8e+07	−0.52	BL7,GBP
5022.871	0.830	1.50	S	7.7e+07	−0.38	BL7,GBP
5024.850	0.820	1.50	S	7.7e+07	−0.55	BL7,GBP
5087.060	1.430	1.50	S	3.3e+07	−0.78	K
5113.450	1.440	1.50	S	3.6e+07	−0.73	BL9,GBP
5186.33	2.117	1.50	U	6.8e+07	−0.77	NWL

Table C1: Atomic line data - *continued*

λ (Å)	$\chi_{\rm l}$ (eV)	$\delta\gamma_6$	DMP	$\gamma_{\rm rad}$ (s^{-1})	$\log gf$	Ref.
5219.700	0.020	1.50	S	6.0e+06	−2.24	BL6,GBP
5299.980	1.050	1.50	S	3.4e+06	−1.47	K
5426.260	0.020	1.50	S	1.7e+06	−2.95	BL6,GBP
5471.200	1.440	1.50	S	1.1e+08	−1.40	K
5474.230	1.460	1.50	U	8.4e+07	−1.23	K
5474.460	2.340	1.50	S	1.1e+08	−0.85	VALD
5490.150	1.460	1.50	S	1.5e+08	−0.88	BL9,GBP
5866.460	1.070	1.50	S	6.4e+07	−0.78	BL7,GBP
5953.170	1.890	1.50	S	8.6e+06	−0.27	BL9,GBP
6126.220	1.070	1.50	S	7.1e+06	−1.37	BL8,GBP
6258.110	1.440	1.50	S	1.7e+08	−0.30	BL9,GBP
6261.110	1.430	1.50	S	1.7e+07	−0.42	BL9,GBP
6303.760	1.440	1.50	S	1.7e+08	−1.51	BL9,GBP
6743.13	0.899	1.50	S	8.7e+05	−1.63	K
7949.150	1.500	1.50	S	2.0e+06	−1.46	BK
Ti II $\log \epsilon_\odot = 5.02$						
4562.03	5.692	2.50	U	6.8e+08	−1.78	PTP
4563.770	1.220	2.50	U	1.6e+08	−0.69	PTP
4583.415	1.165	2.50	U	1.6e+08	−2.92	PTP
4636.32	1.165	2.50	U	2.8e+08	−3.02	PTP
4657.204	1.243	2.50	U	1.6e+08	−2.24	PTP
4705.62	5.648	2.50	U	6.0e+08	−1.83	PTP
4708.672	1.237	2.50	U	1.6e+08	−2.34	PTP
4749.55	5.638	2.50	U	6.0e+08	−1.78	PTP
4798.537	1.080	2.50	U	1.9e+08	−2.68	PTP
4865.61	1.116	2.50	U	1.9e+08	−2.79	PTP
4874.014	3.095	2.50	U	2.0e+08	−0.80	PTP
4911.200	3.120	2.50	U	2.0e+08	−0.61	PTP
5005.16	1.566	2.50	U	3.0e+08	−2.72	PTP
5145.69	5.424	2.50	U	5.8e+08	−1.18	PTP
5154.080	1.570	2.50	U	1.7e+08	−1.75	PTP
5185.910	1.890	2.50	U	2.3e+08	−1.49	PTP
5211.53	2.590	2.50	U	3.0e+08	−1.16	PTP
5336.781	1.580	2.50	U	1.6e+08	−1.59	PTP
5381.018	1.570	2.50	U	1.6e+08	−1.92	PTP
5418.770	1.580	2.50	U	1.6e+08	−2.00	PTP
5490.69	1.566	2.50	U	2.7e+07	−2.43	PTP
6606.979	2.061	2.50	U	1.7e+08	−2.76	PTP
Zn I $\log \epsilon_\odot = 4.60$						
4722.16	4.030	2.50	U	1.0e+08	−0.41	*
4810.537	4.080	2.50	U	1.0e+08	−0.29	*
6362.350	5.790	2.50	U	1.0e+08	0.09	*

Table C1: Atomic line data - *continued*

λ (Å)	$\chi_{\rm l}$ (eV)	$\delta\gamma_6$	DMP	$\gamma_{\rm rad}$ (s^{-1})	$\log gf$	Ref.
Y II $\log\epsilon_\odot = 2.24$						
4854.87	0.99	2.50	U	1.0e+08	−0.11	PN
4883.68	1.08	2.50	U	1.0e+08	0.23	PN
4900.12	1.03	2.50	U	1.0e+08	0.05	PN
5087.43	1.08	2.50	U	1.3e+07	−0.17	PN
5200.41	0.99	2.50	U	1.0e+08	−0.49	PN
5402.78	1.84	2.50	U	1.0e+08	−0.63	PN
5662.93	1.94	2.50	U	1.0e+08	0.20	PN
Ba II $\log\epsilon_\odot = 2.13$						
4554.03	0.00	3.00	S	1.0e+08	0.17	SMP/G67
5853.68	0.60	3.00	S	6.4e+07	−1.01	SMP/G67
6141.73	0.70	3.00	S	7.3e+07	−0.07	SMP/G67
6496.91	0.60	3.00	S	1.0e+08	−0.38	SMP/G67
SYNTHESIZED LINES						
[**O** I] $\log\epsilon_\odot = 8.83$						
6300.304	0.00	2.50	U	1.0e+05	−9.819	WSG
Ni I $\log\epsilon_\odot = 6.25$						
6300.335	4.27	2.50	U	2.7e+08	−2.275	JLLZ
6300.355	4.27	2.50	U	2.7e+08	−2.695	JLLZ
Eu II $\log\epsilon_\odot = 0.51$						
4129.610	0.00	2.50	U	1.0e+05	−1.833	LWDS
4129.613	0.00	2.50	U	1.0e+05	−1.356	LWDS
4129.627	0.00	2.50	U	1.0e+05	−1.637	LWDS
4129.632	0.00	2.50	U	1.0e+05	−1.298	LWDS
4129.635	0.00	2.50	U	1.0e+05	−1.833	LWDS
4129.652	0.00	2.50	U	1.0e+05	−1.578	LWDS
4129.657	0.00	2.50	U	1.0e+05	−1.168	LWDS
4129.652	0.00	2.50	U	1.0e+05	−1.637	LWDS
4129.674	0.00	2.50	U	1.0e+05	−1.614	LWDS
4129.679	0.00	2.50	U	1.0e+05	−1.795	LWDS
4129.681	0.00	2.50	U	1.0e+05	−1.017	LWDS
4129.682	0.00	2.50	U	1.0e+05	−1.318	LWDS
4129.686	0.00	2.50	U	1.0e+05	−1.598	LWDS
4129.687	0.00	2.50	U	1.0e+05	−1.578	LWDS
4129.689	0.00	2.50	U	1.0e+05	−1.259	LWDS
4129.692	0.00	2.50	U	1.0e+05	−1.795	LWDS
4129.696	0.00	2.50	U	1.0e+05	−1.539	LWDS
4129.700	0.00	2.50	U	1.0e+05	−1.129	LWDS
4129.703	0.00	2.50	U	1.0e+05	−1.598	LWDS
4129.711	0.00	2.50	U	1.0e+05	−1.576	LWDS
4129.714	0.00	2.50	U	1.0e+05	−0.979	LWDS
4129.716	0.00	2.50	U	1.0e+05	−1.801	LWDS

Table C1: Atomic line data - *continued*

λ (Å)	χ_l (eV)	$\delta\gamma_6$	DMP	$\gamma_{\rm rad}$ (s^{-1})	$\log gf$	Ref.
4129.717	0.00	2.50	U	1.0e+05	−1.539	LWDS
4129.723	0.00	2.50	U	1.0e+05	−0.866	LWDS
4129.729	0.00	2.50	U	1.0e+05	−1.614	LWDS
4129.732	0.00	2.50	U	1.0e+05	−1.762	LWDS
4129.733	0.00	2.50	U	1.0e+05	−0.828	LWDS
4129.735	0.00	2.50	U	1.0e+05	−1.576	LWDS
4129.757	0.00	2.50	U	1.0e+05	−0.683	LWDS
4129.758	0.00	2.50	U	1.0e+05	−1.762	LWDS
4129.773	0.00	2.50	U	1.0e+05	−0.722	LWDS
4129.780	0.00	2.50	U	1.0e+05	−1.801	LWDS
6645.068	1.38	2.50	U	1.0e+05	−0.837	LWDS
6645.069	1.38	2.50	U	1.0e+05	−2.106	LWDS
6645.070	1.38	2.50	U	1.0e+05	−0.799	LWDS
6645.071	1.38	2.50	U	1.0e+05	−3.750	LWDS
6645.074	1.38	2.50	U	1.0e+05	−2.144	LWDS
6645.082	1.38	2.50	U	1.0e+05	−3.787	LWDS
6645.084	1.38	2.50	U	1.0e+05	−0.875	LWDS
6645.086	1.38	2.50	U	1.0e+05	−1.911	LWDS
6645.091	1.38	2.50	U	1.0e+05	−3.431	LWDS
6645.093	1.38	2.50	U	1.0e+05	−0.955	LWDS
6645.094	1.38	2.50	U	1.0e+05	−0.913	LWDS
6645.098	1.38	2.50	U	1.0e+05	−1.866	LWDS
6645.101	1.38	2.50	U	1.0e+05	−1.037	LWDS
6645.101	1.38	2.50	U	1.0e+05	−1.949	LWDS
6645.104	1.38	2.50	U	1.0e+05	−3.359	LWDS
6645.106	1.38	2.50	U	1.0e+05	−1.121	LWDS
6645.107	1.38	2.50	U	1.0e+05	−1.917	LWDS
6645.108	1.38	2.50	U	1.0e+05	−3.470	LWDS
6645.111	1.38	2.50	U	1.0e+05	−1.204	LWDS
6645.112	1.38	2.50	U	1.0e+05	−2.112	LWDS
6645.113	1.38	2.50	U	1.0e+05	−3.528	LWDS
6645.115	1.38	2.50	U	1.0e+05	−0.955	LWDS
6645.123	1.38	2.50	U	1.0e+05	−1.904	LWDS
6645.130	1.38	2.50	U	1.0e+05	−3.397	LWDS
6645.134	1.38	2.50	U	1.0e+05	−1.075	LWDS
6645.141	1.38	2.50	U	1.0e+05	−1.955	LWDS
6645.147	1.38	2.50	U	1.0e+05	−3.566	LWDS
6645.149	1.38	2.50	U	1.0e+05	−1.159	LWDS
6645.155	1.38	2.50	U	1.0e+05	−2.150	LWDS
6645.160	1.38	2.50	U	1.0e+05	−1.242	LWDS

Table C2: References for $\log gf$-values in Table C1

Abbr. in Table C1	Reference
BK:	Bachor & Kock (1980)
BK2:	Bard & Kock (1994)
BZH:	Becker et al. (1980)
BL1:	Blackwell et al. (1980)
BL2:	Blackwell et al. (1979b)
BL3:	Blackwell et al. (1982c)
BL4:	Blackwell et al. (1979a)
BL5:	Blackwell et al. (1982d)
BL6:	Blackwell et al. (1982b)
BL7:	Blackwell et al. (1982a)
BL8:	Blackwell et al. (1983)
BL9:	Blackwell et al. (1986)
BBP:	Booth et al. (1984)
BK3:	Bridges & Kornblith (1974)
BZ:	Biémont & Zeippen (1992)
G:	Garz (1971)
GBP:	Grevesse et al. (1989)
G67:	Gallagher (1967)
GK:	Gurtovenko & Kostik (1981)
HBGV:	Hibbert et al. (1991)
JLLZ:	Johansson et al. (2003)
K:	Kostyk (1981)
LW:	Lambert & Warner (1968)
LD:	Lawler & Dakin (1989)
LWDS:	Lawler et al. (2001)
MRW:	May et al. (1974)
MFW:	Meylan et al. (1993)
NWL:	Nitz et al. (1998)
OWL:	O'Brian et al. (1991)
PN:	Pitts & Newsom (1986)
PTP:	Pickering et al. (2001)
RU:	Raassen & Uylings (1998) The atomic data are available on: http://www.science.uva.nl/pub/orth/iron/FeII.E1
RW:	Richter & Wulff (1970)
SMP:	Sneden et al. (1996)
VALD:	Piskunov et al. (1995); Kupka et al. (1999)
WSG:	Wiese et al. (1966)
WL:	Wickliffe & Lawler (1997)
WBW:	Wolnik et al. (1971)
$*$ (asterisk):	Astrophysical values from this work.

Appendix D
HIP 99240 from 4500 to 8800 Å

The fully reduced and normalized 1-D spectrum of HIP 99240 is here shown as observed with the ESO 1.5 m telescope and the FEROS spectrograph. All spectral lines in Table C1 have been marked out. It should be noted that Hip 99240 is a metal-rich star having [Fe/H] $= +0.37$.

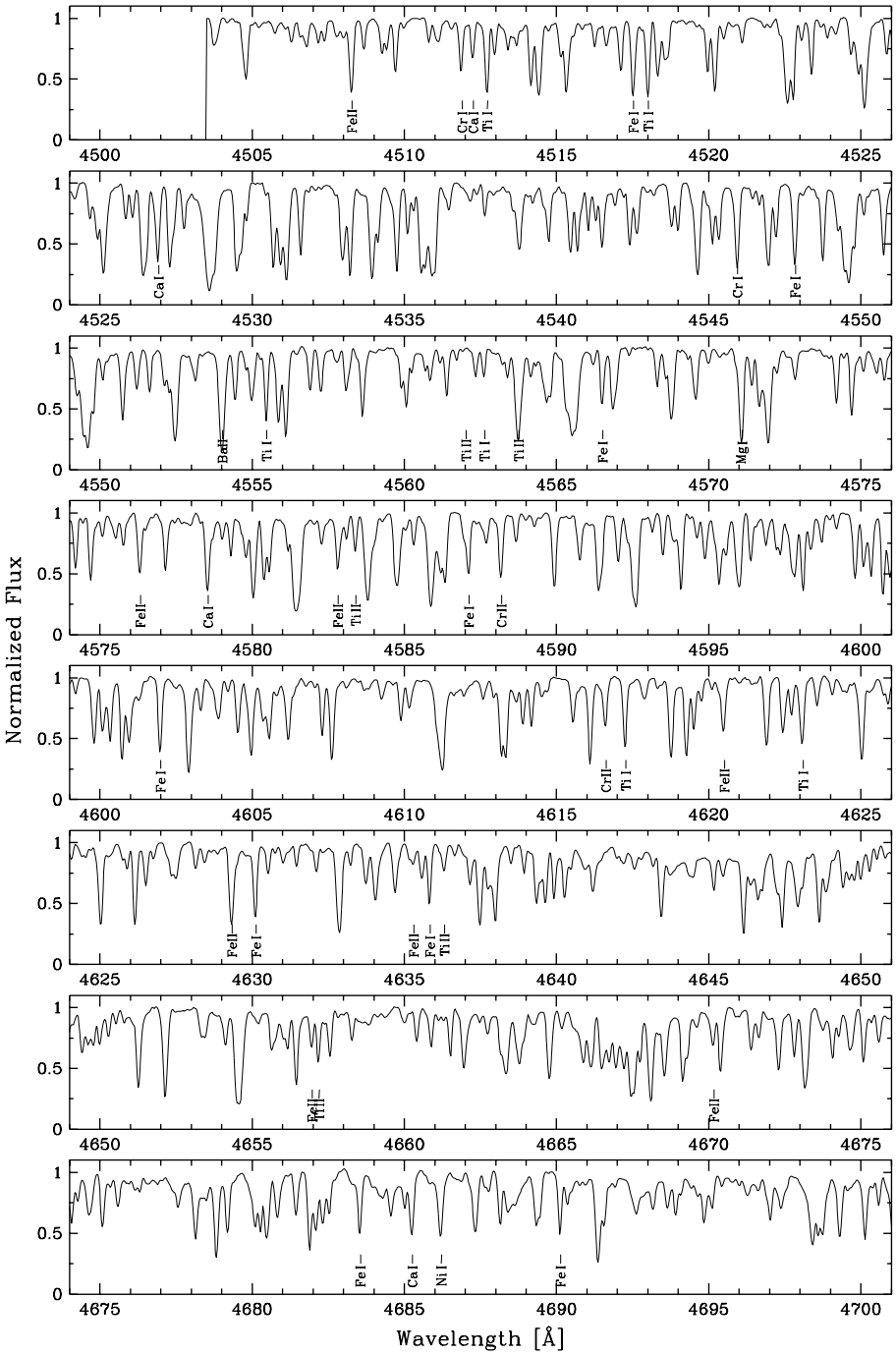
Normalized Flux
Wavelength [Å]
FeII
CrI
CaI
TiI
FeI
TiII
CaI
BaII
TiI
TiII
MgI
CrII
NiI

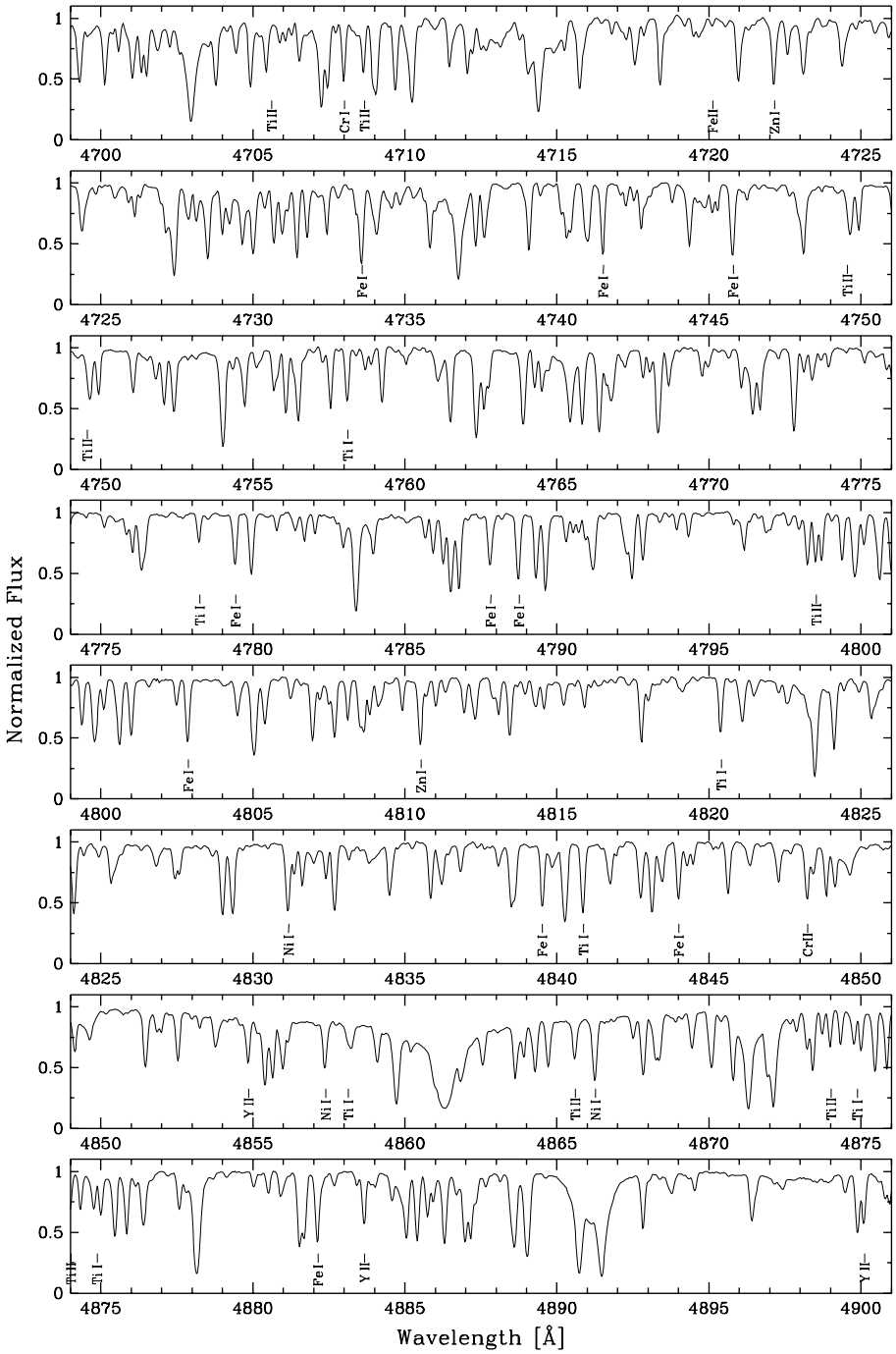
Normalized Flux
Wavelength [Å]
Ti II
Cr I
Ti II
Fe II
Zn I
Fe I
Fe I
Fe I
Ti II
Ti II
Ti I
Ti I
Fe I
Fe I
Fe I
Ti II
Fe I
Zn I
Ti I
Ni I
Fe I
Ti I
Fe I
Cr II
Y II
Ni I
Ti I
Ti II
Ni I
Ti II
Ti I
Fe I
Y II
Y II

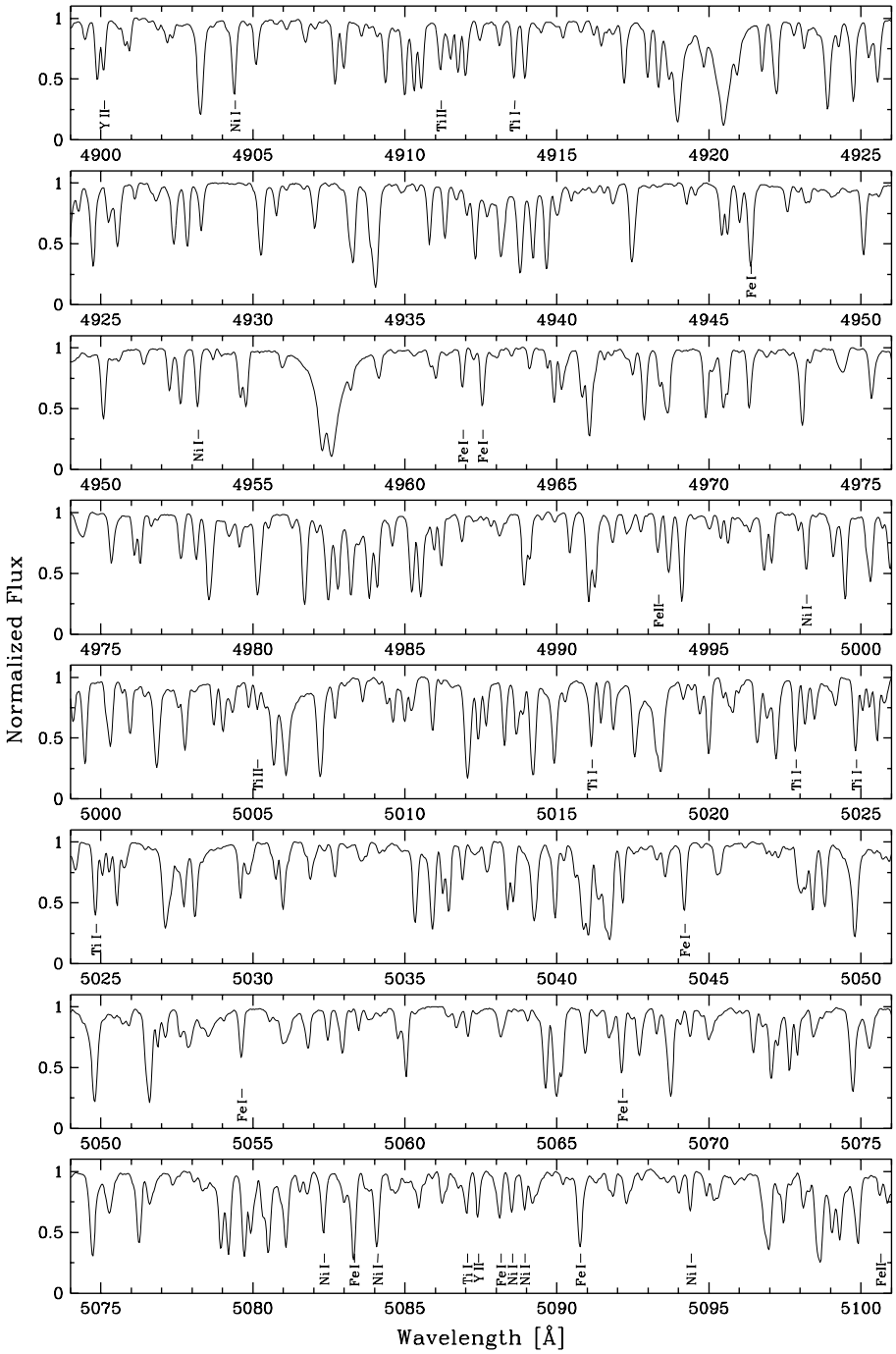
Normalized Flux
Wavelength [Å]
Y II
Ni I
Ti II
Ti I
Fe I
Ni I
Fe I
Fe I
Fe II
Ni I
Ti II
Ti I
Ti I
Ti I
Ti I
Fe I
Fe I
Fe I
Ni I
Fe I
Ni I
Ti II
Fe I
Ni I
Ni I
Fe I
Ni I
Fe II

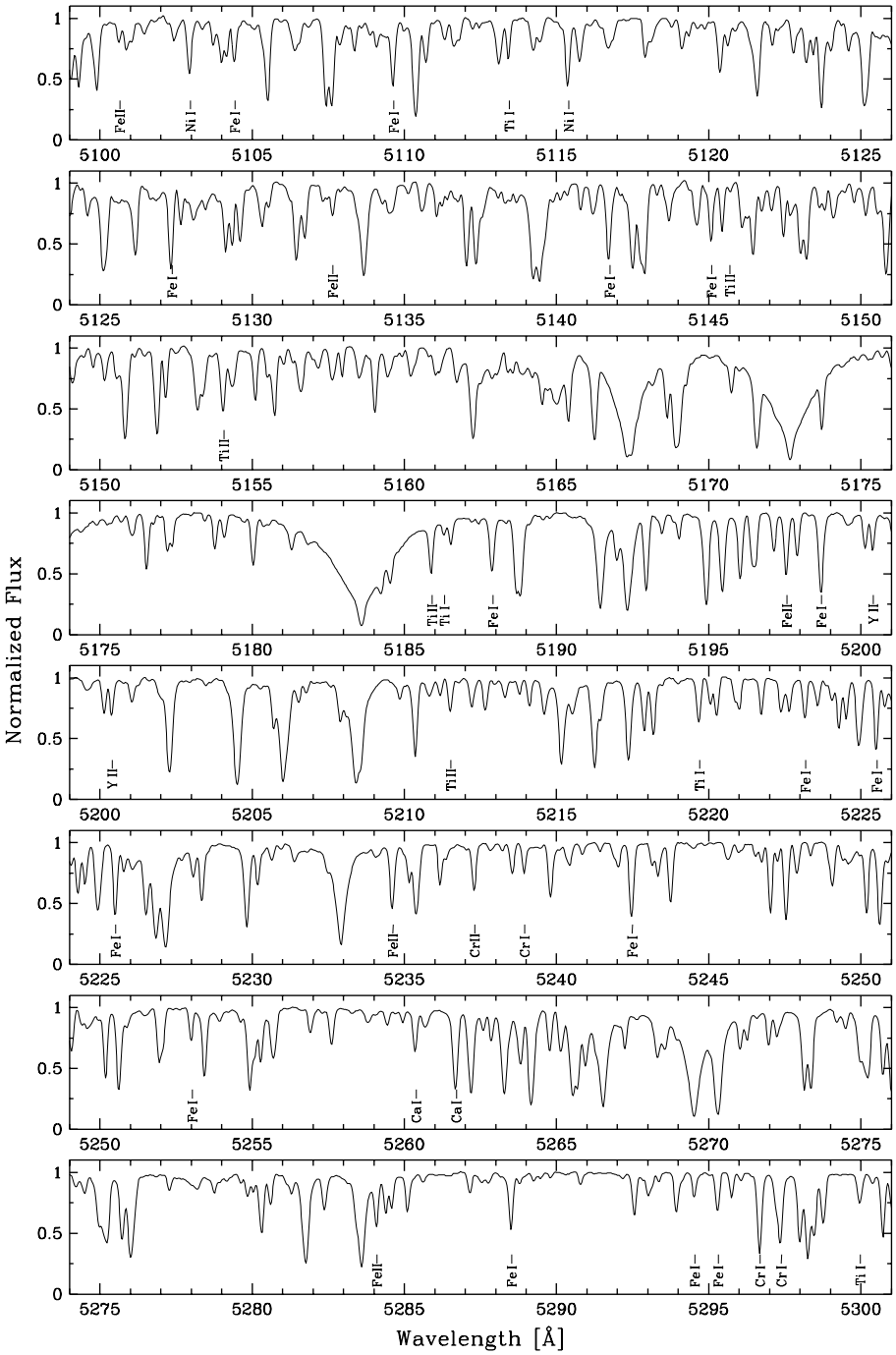
Normalized Flux
Wavelength [Å]
Fe II
Ni I
Fe I
Ti I
Ti II
Y II
Cr I
Ca I

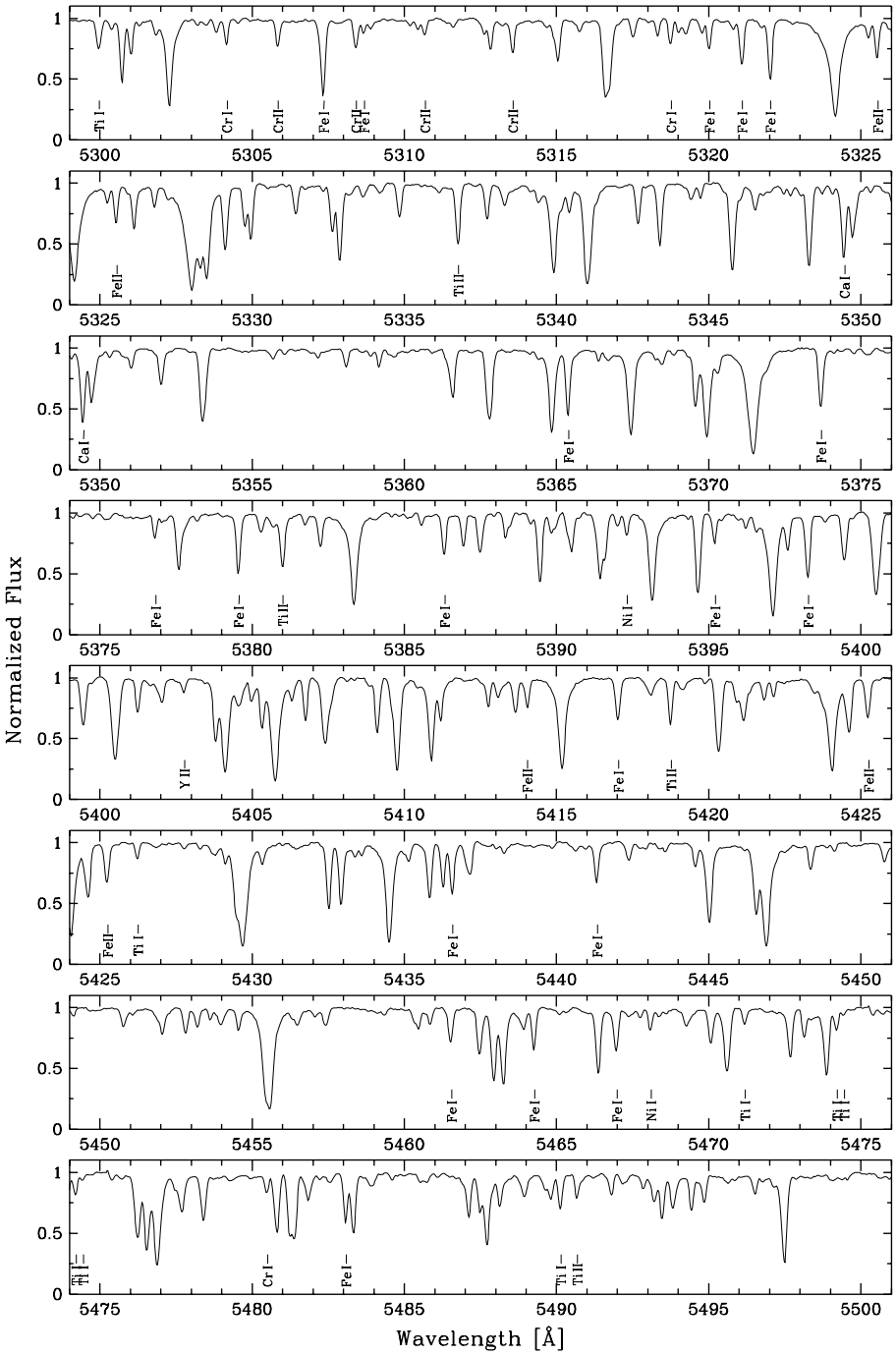
Normalized Flux
Wavelength [Å]
Ti I
Cr I
Cr II
Fe I
Fe II
Ti II
Ca I
Y II
Ni I

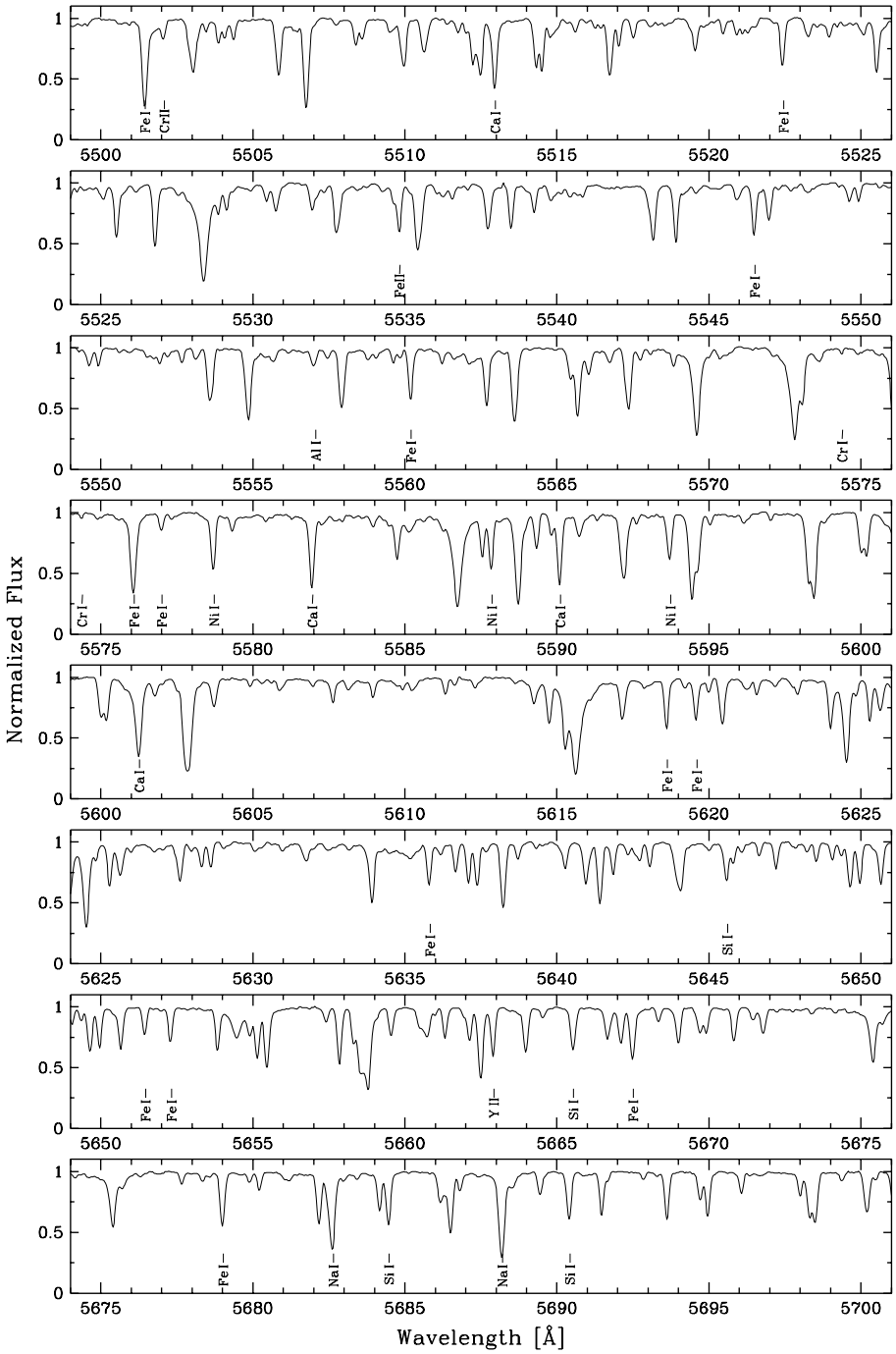
Normalized Flux
Wavelength [Å]
Fe I
Cr II
Ca I
Fe I
Fe II
Fe I
Al I
Fe I
Cr I
Cr I
Fe I
Fe I
Ni I
Ca I
Ni I
Ca I
Ni I
Ca I
Fe I
Fe I
Fe I
Si I
Fe I
Fe I
Y II
Si I
Fe I
Fe I
Na I
Si I
Na I
Si I

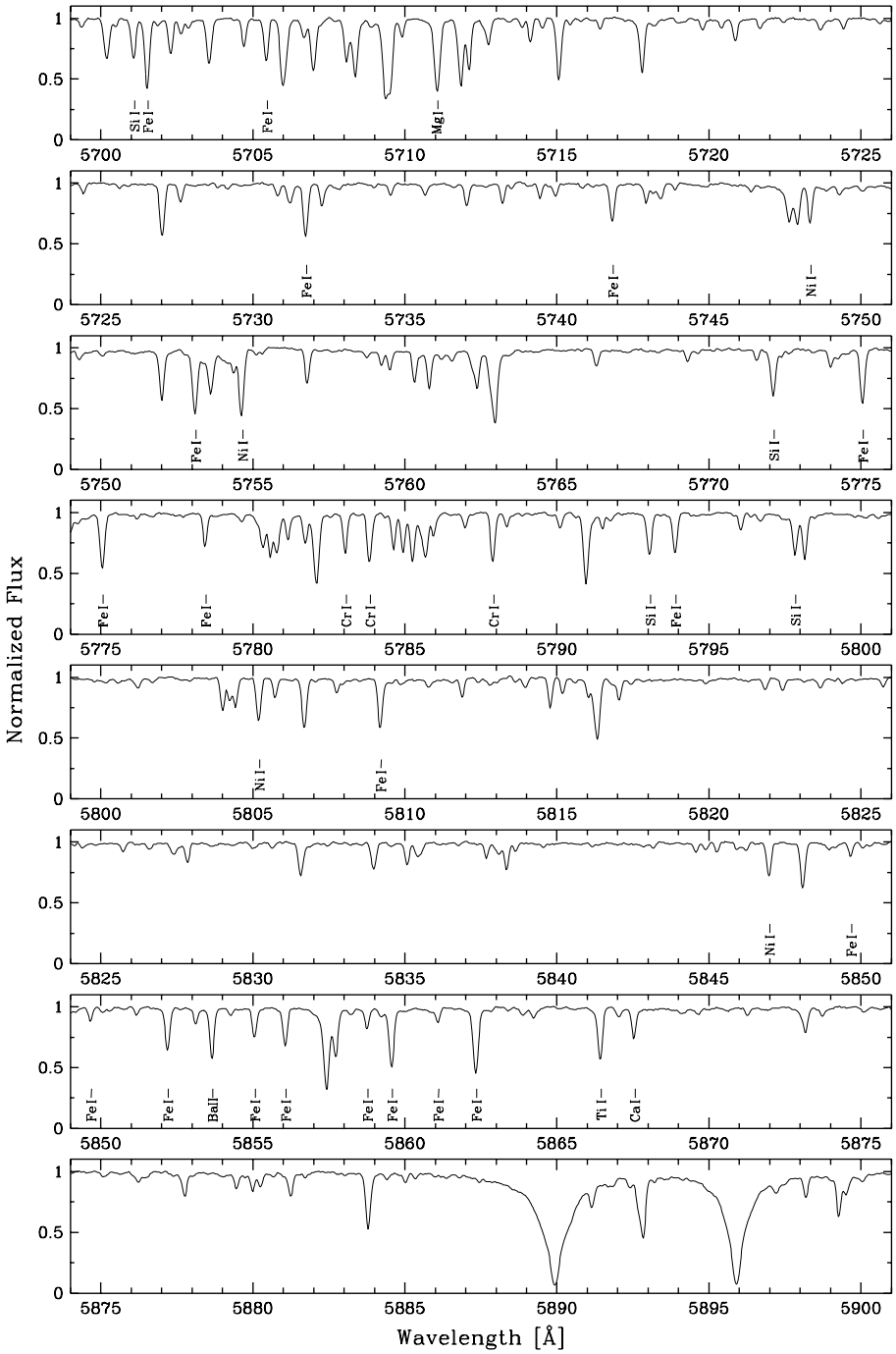
Normalized Flux
Wavelength [Å]
Si I
Fe I
Mg I
Ni I
Cr I
Ti I
Ca I
Ba II

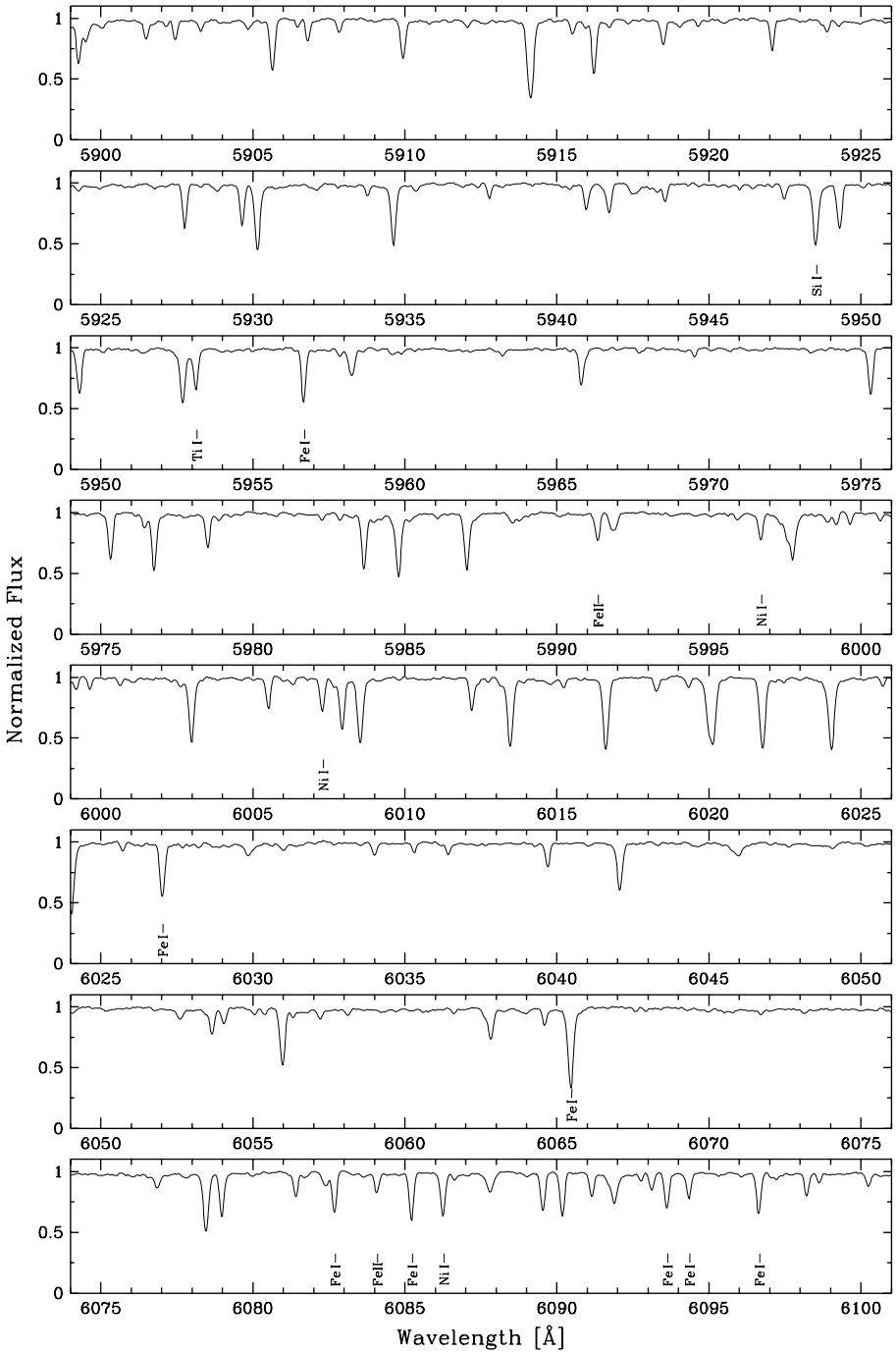
Normalized Flux
Wavelength [Å]
Si I
Ti I
Fe I
Fe II
Ni I

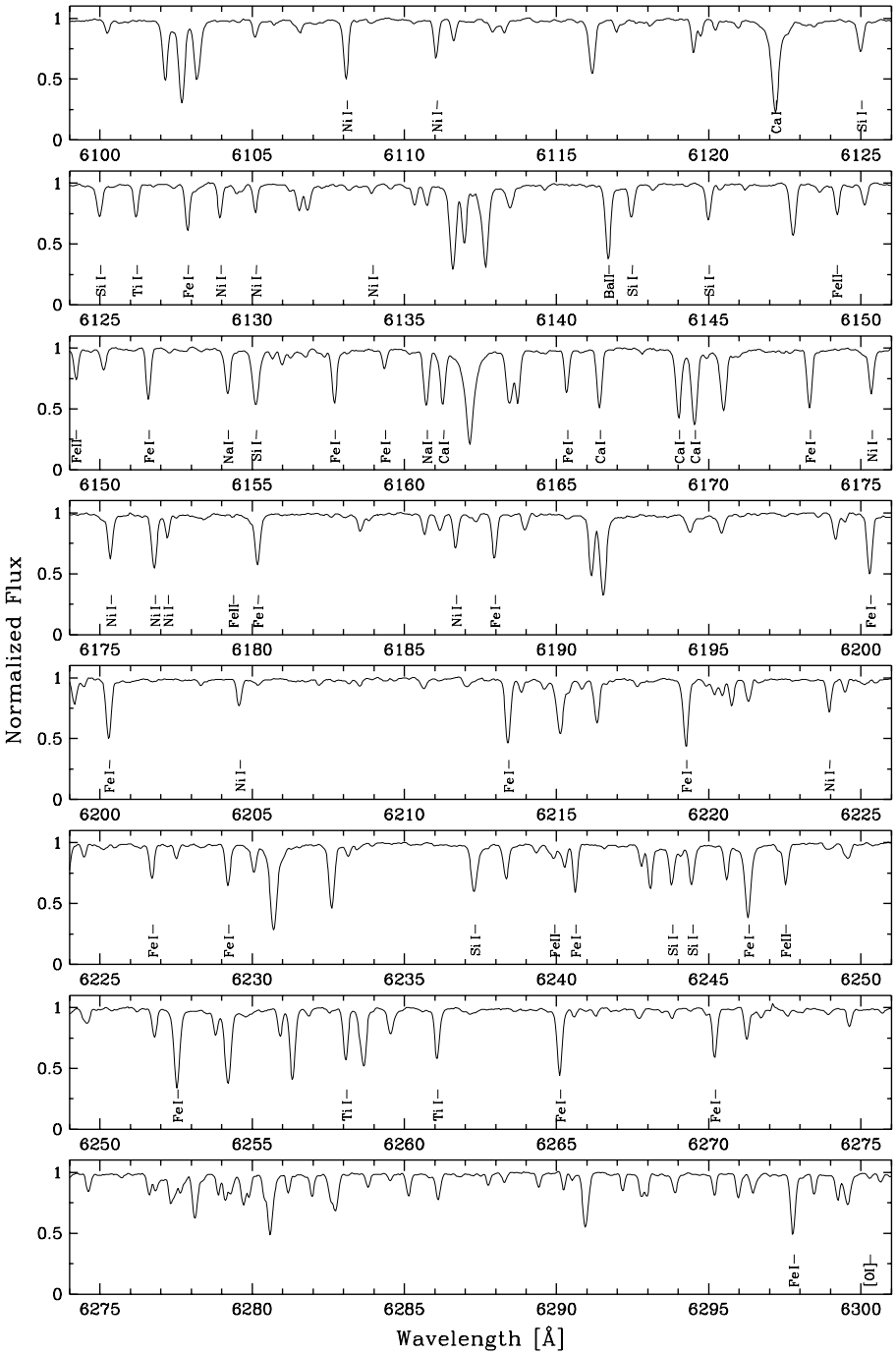
Normalized Flux
Wavelength [Å]
Ni I
Ni I
Ca I
Si I
Si I
Ti I
Fe I
Ni I
Ni I
Ni I
Ba II
Si I
Si I
Fe II
Fe II
Fe I
Na I
Si I
Fe I
Fe I
Na I
Ca I
Fe I
Ca I
Ca I
Ca I
Fe I
Ni I
Ni I
Ni I
Ni I
Fe II
Fe I
Ni I
Fe I
Fe I
Ni I
Fe I
Fe I
Ni I
Fe I
Fe I
Si I
Fe II
Fe I
Si I
Si I
Fe I
Fe II
Fe I
Ti I
Ti I
Fe I
Fe I
Fe I
[O I]

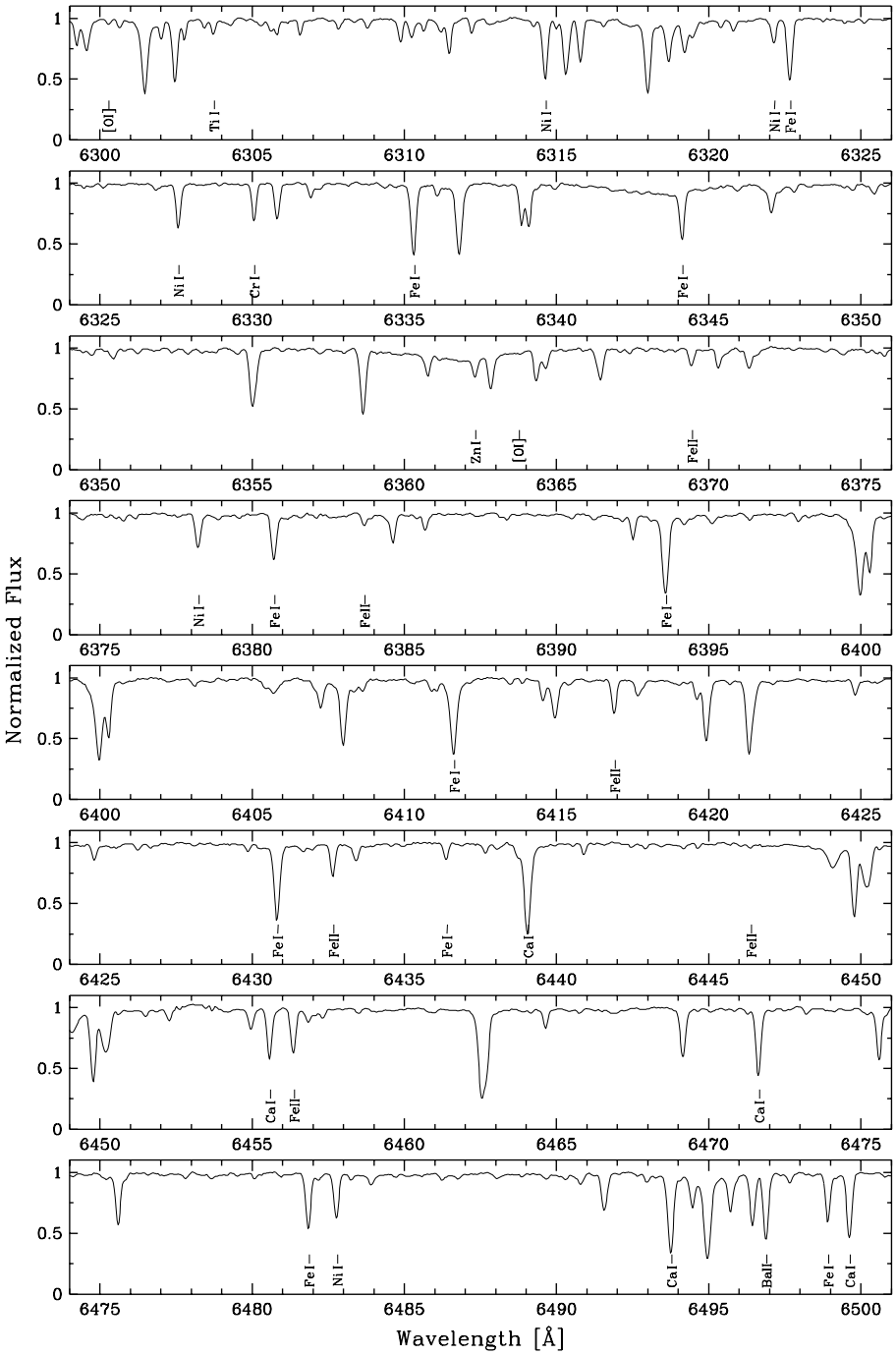
Normalized Flux
Wavelength [Å]
[OI]
TiI
NiI
NiI
FeI
NiI
CrI
FeI
FeI
ZnI
[OI]
FeII
NiI
FeI
FeII
FeI
FeI
FeII
FeI
CaI
FeII
CaI
FeII
CaI
FeI
NiI
CaI
BaII
FeI
CaI

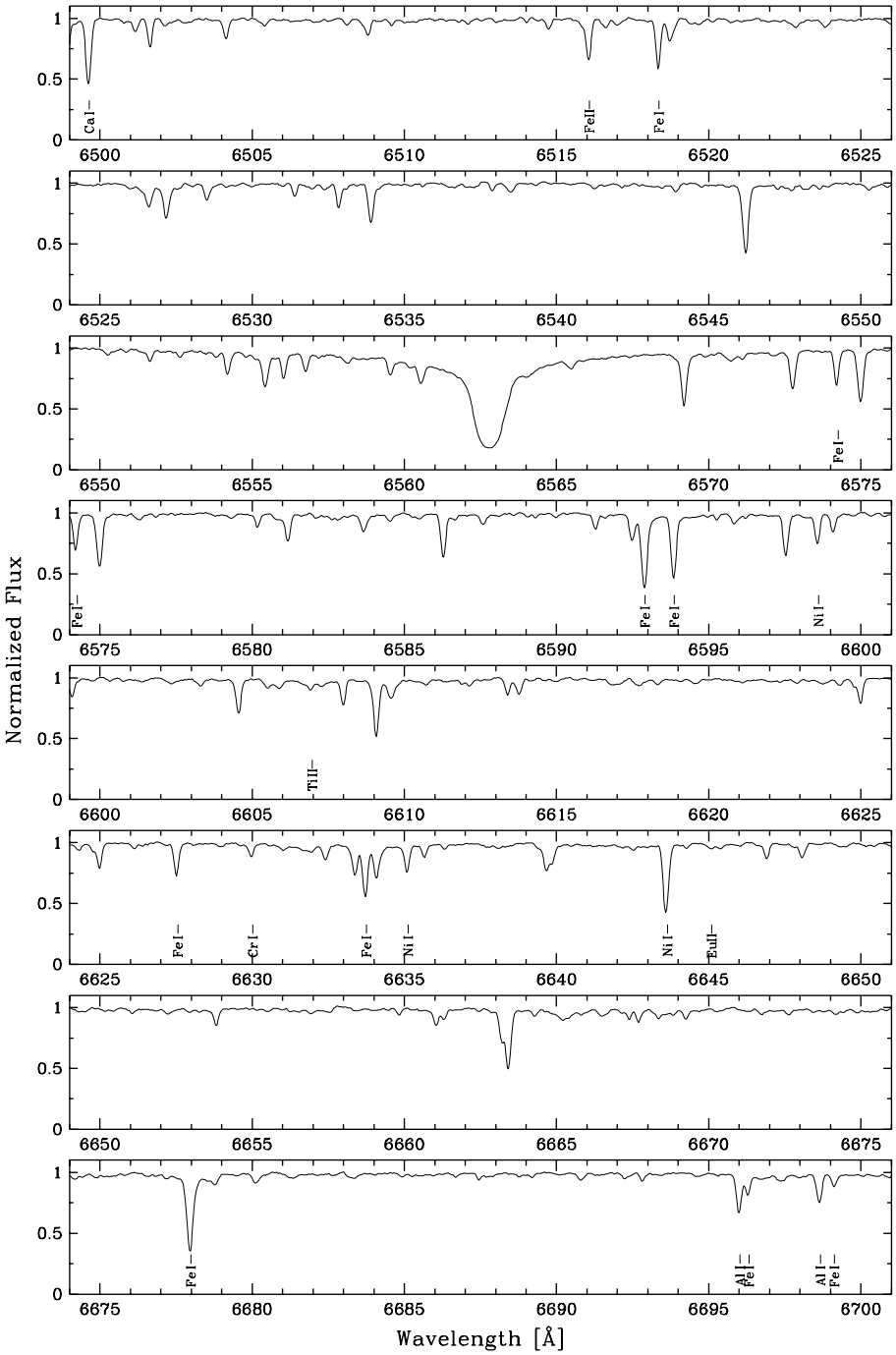
Normalized Flux
Wavelength [Å]
CaI
FeII
FeI
TiII
CrI
NiI
EuII
AlI

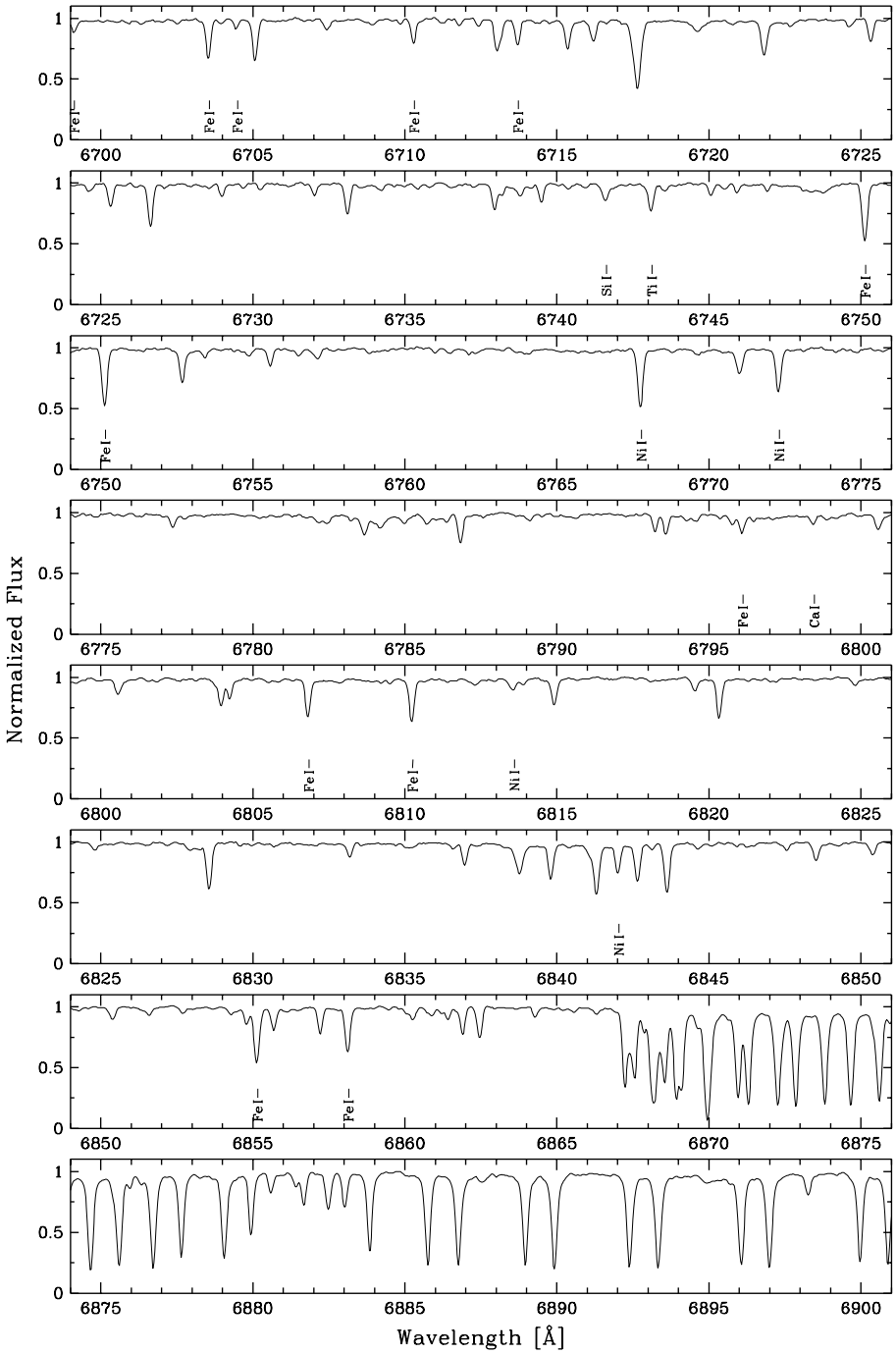
Normalized Flux
Wavelength [Å]
Fe I
Si I
Ti I
Ni I
Ca I

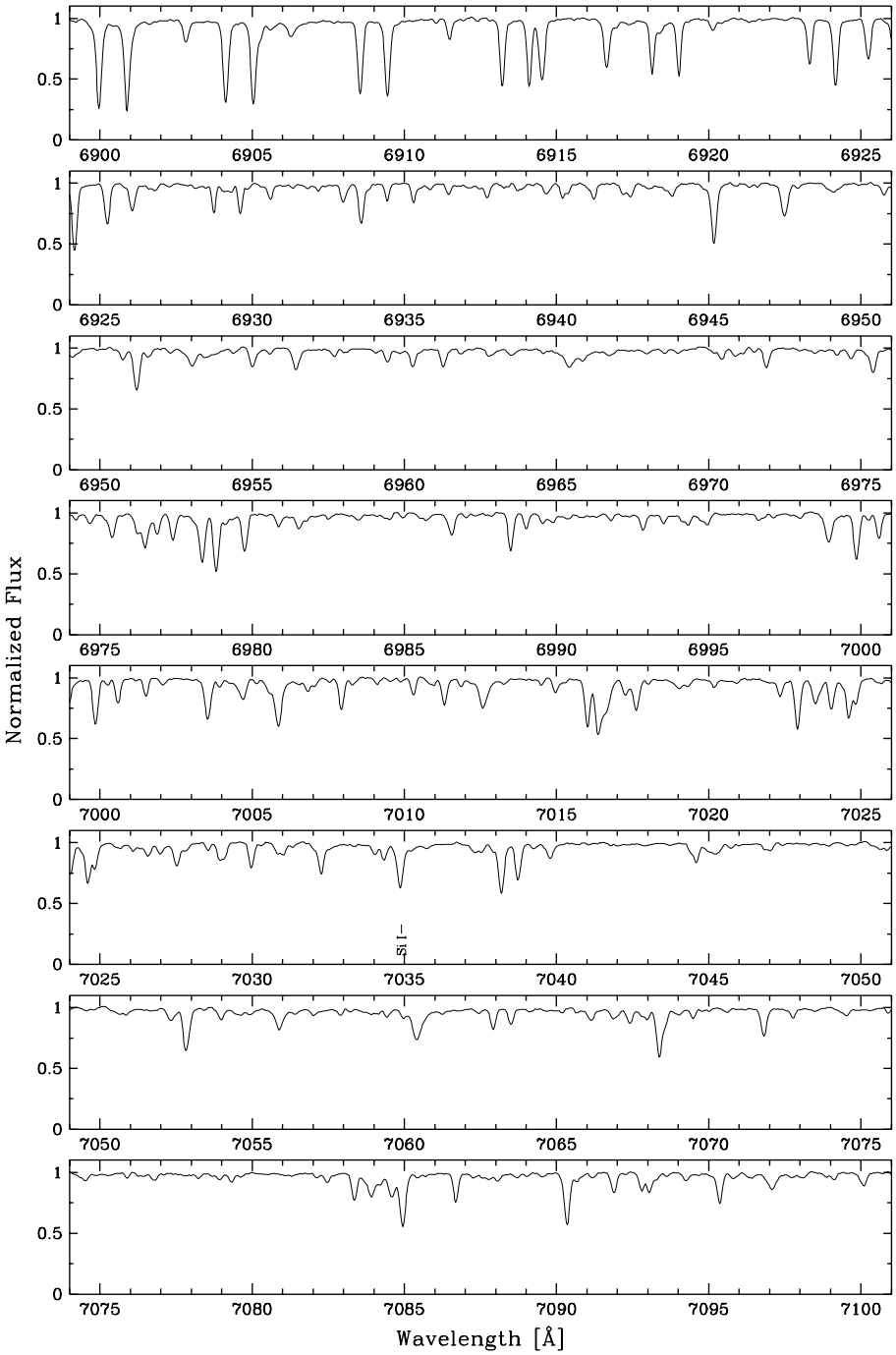
Normalized Flux
Wavelength [Å]
Si I

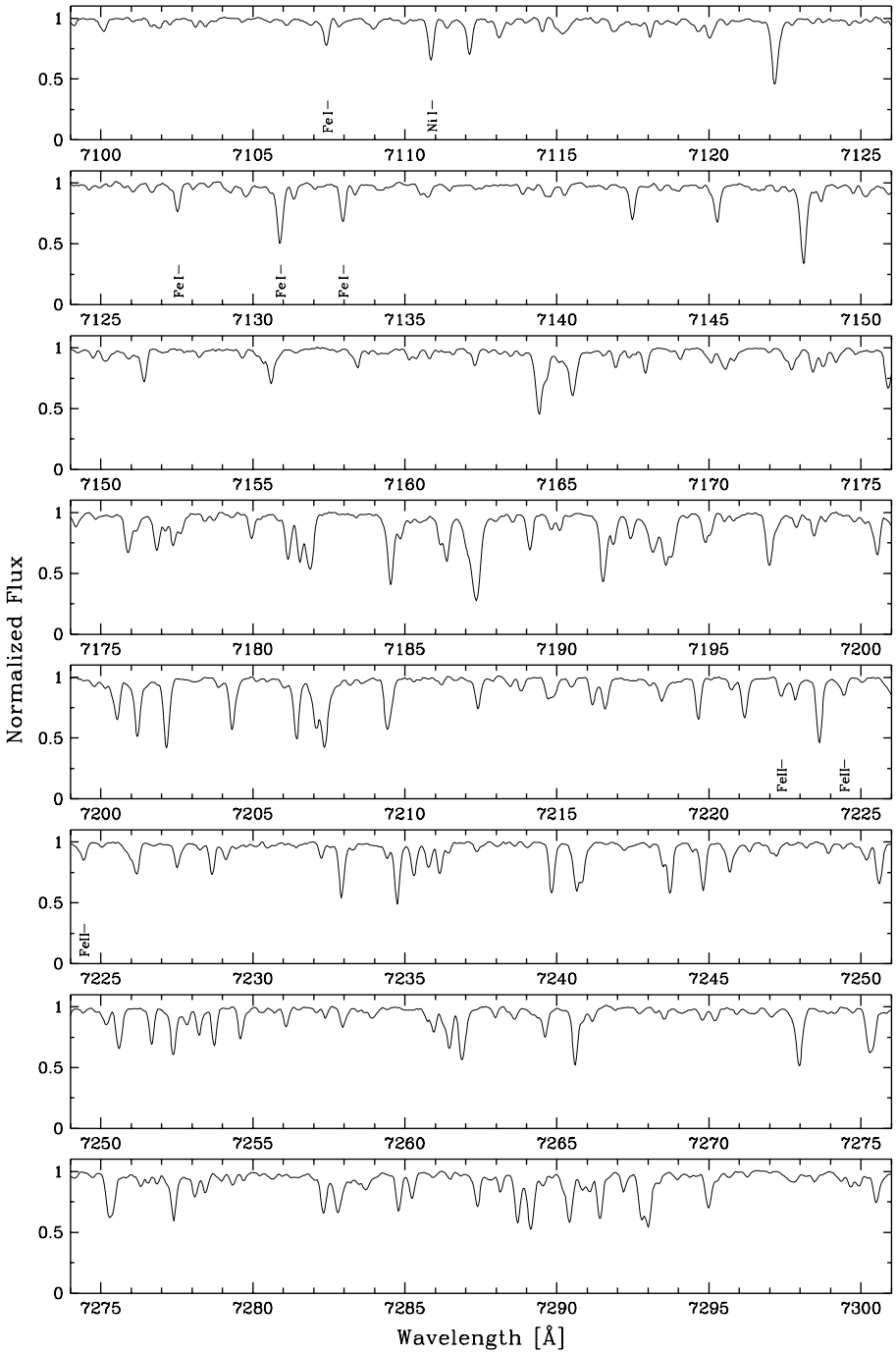
Normalized Flux
Wavelength [Å]
FeI
NiI
FeI
FeI
FeI
FeII
FeII
FeII

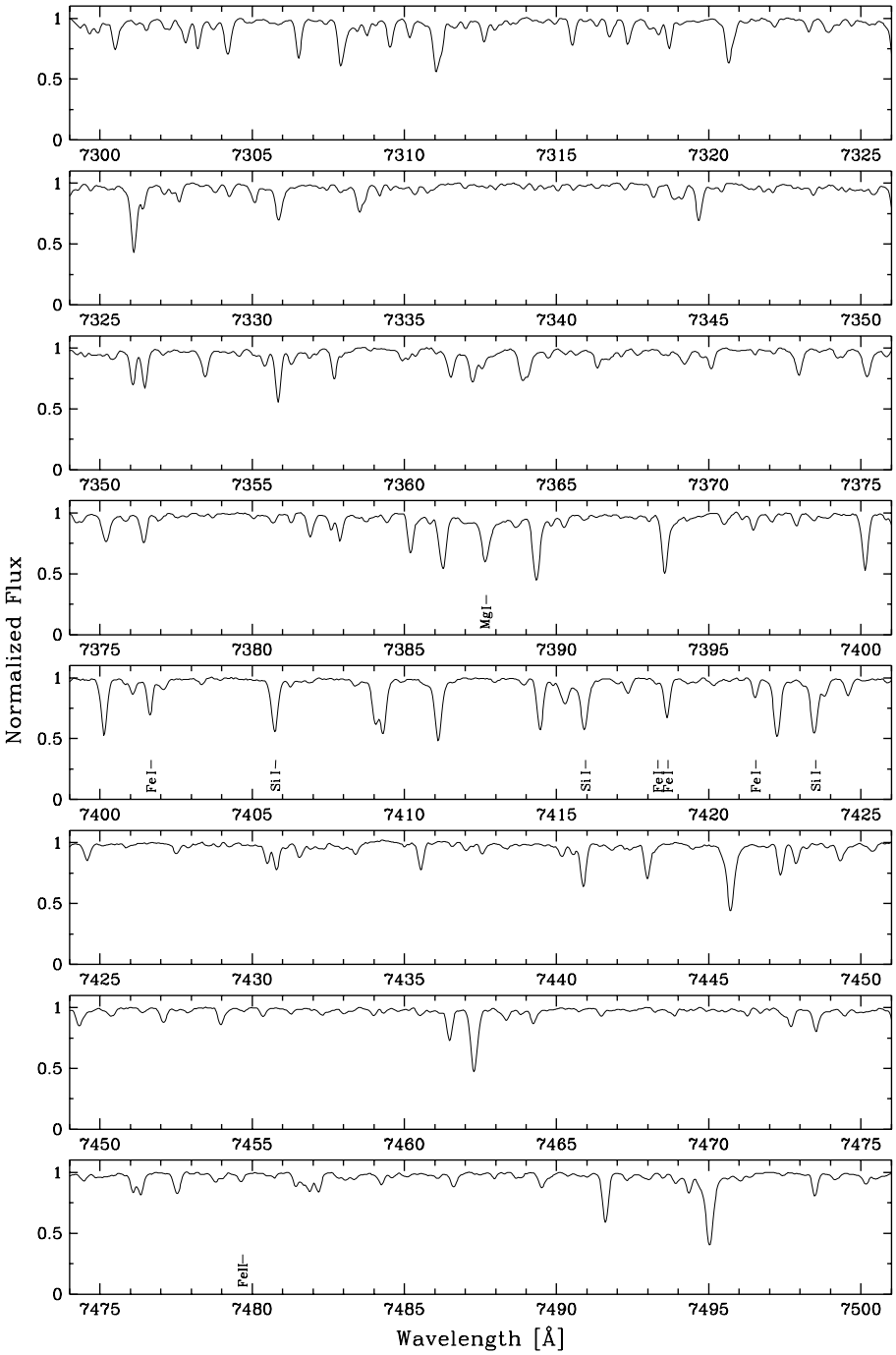
Normalized Flux
Wavelength [Å]
Mg I
Fe I
Si I
Si I
Fe I
Fe I
Fe I
Si I
Fe II

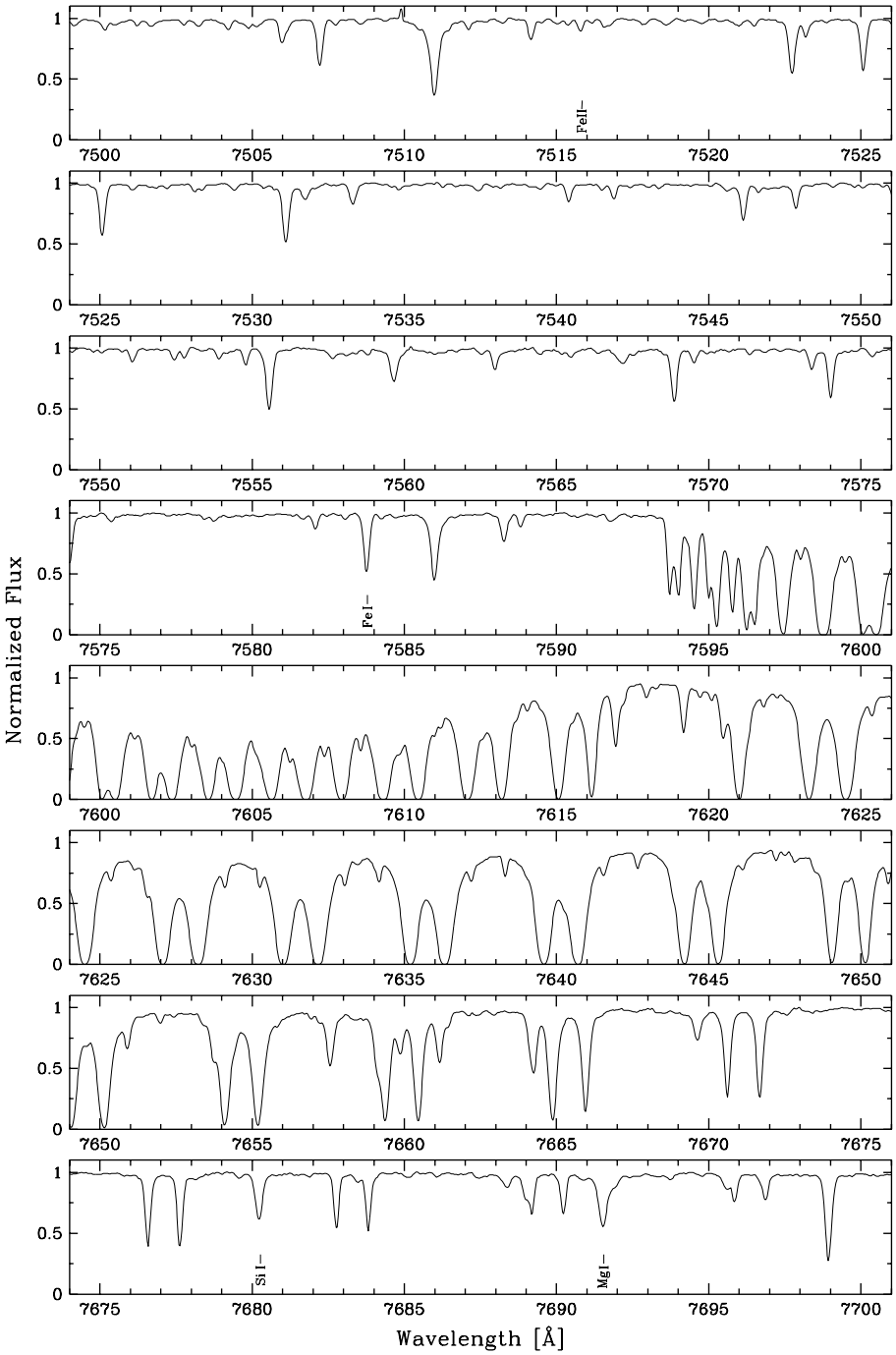
Normalized Flux
Wavelength [Å]
FeII
FeI
SiI
MgI

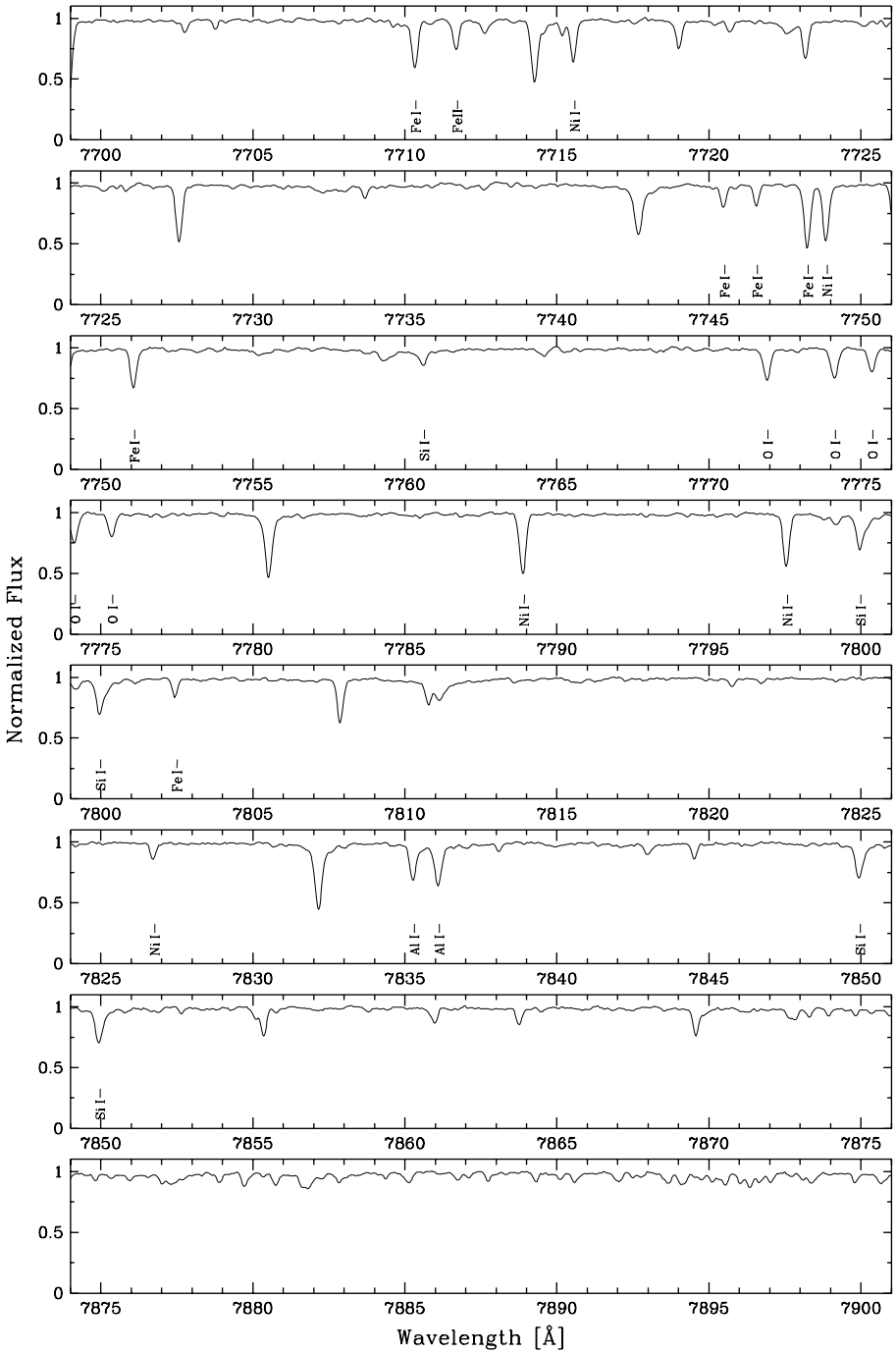
Normalized Flux
Wavelength [Å]
Fe I
Fe II
Ni I
Si I
Al I
O I

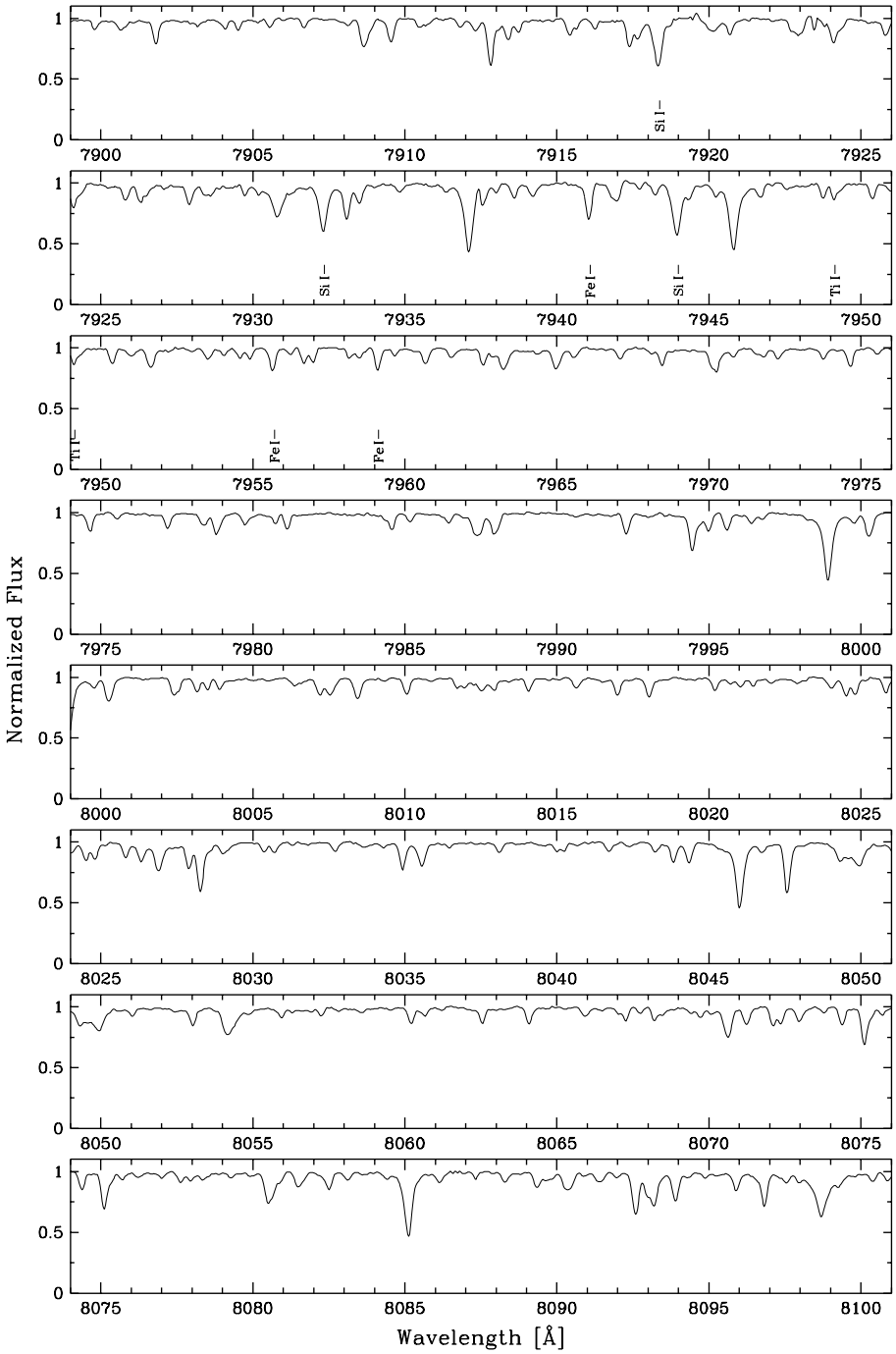
Normalized Flux
Wavelength [Å]
Si I
Si I
Fe I
Si I
Ti I
Ti I
Fe I
Fe I

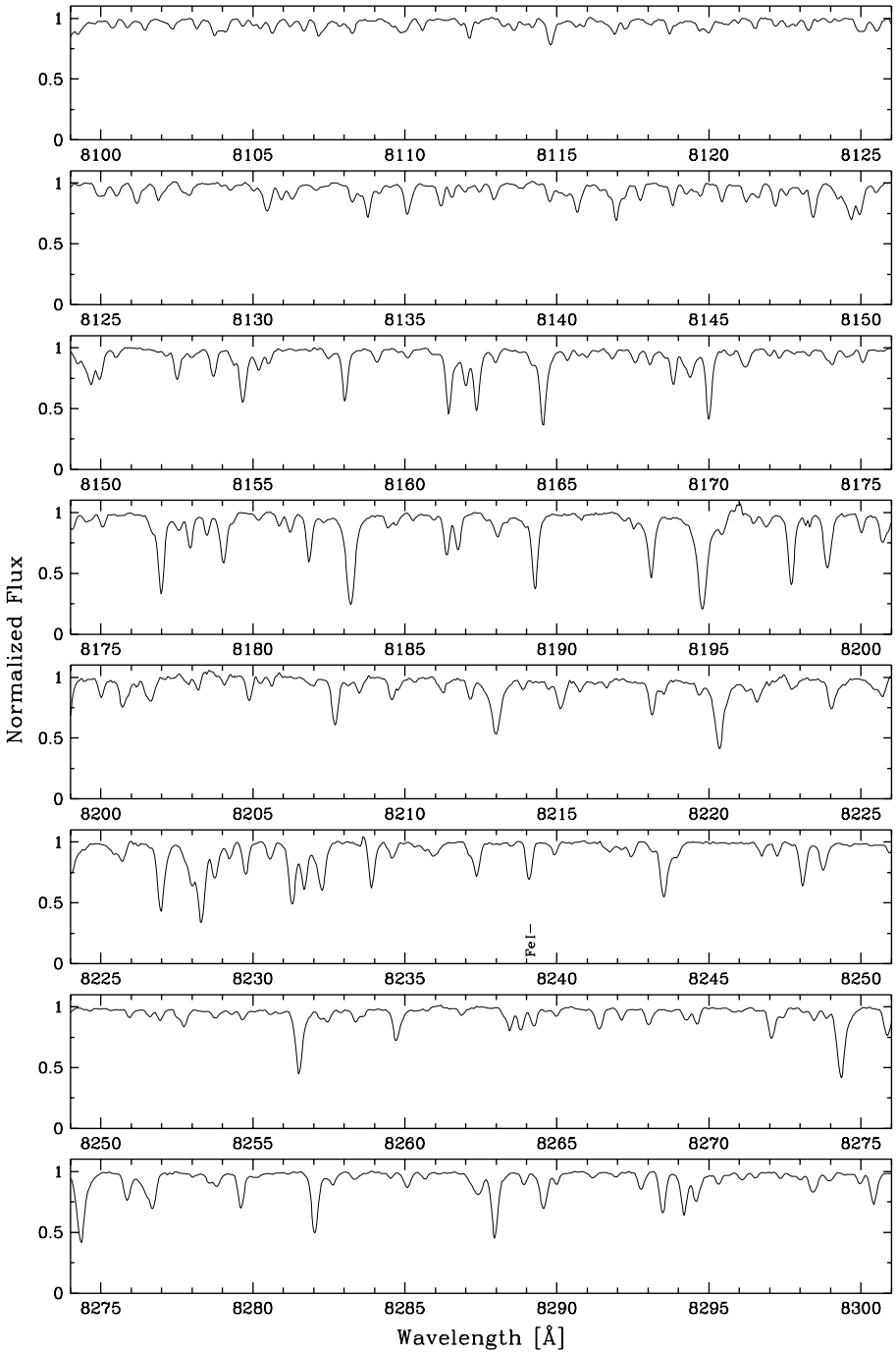
Normalized Flux
Wavelength [Å]
Fe I

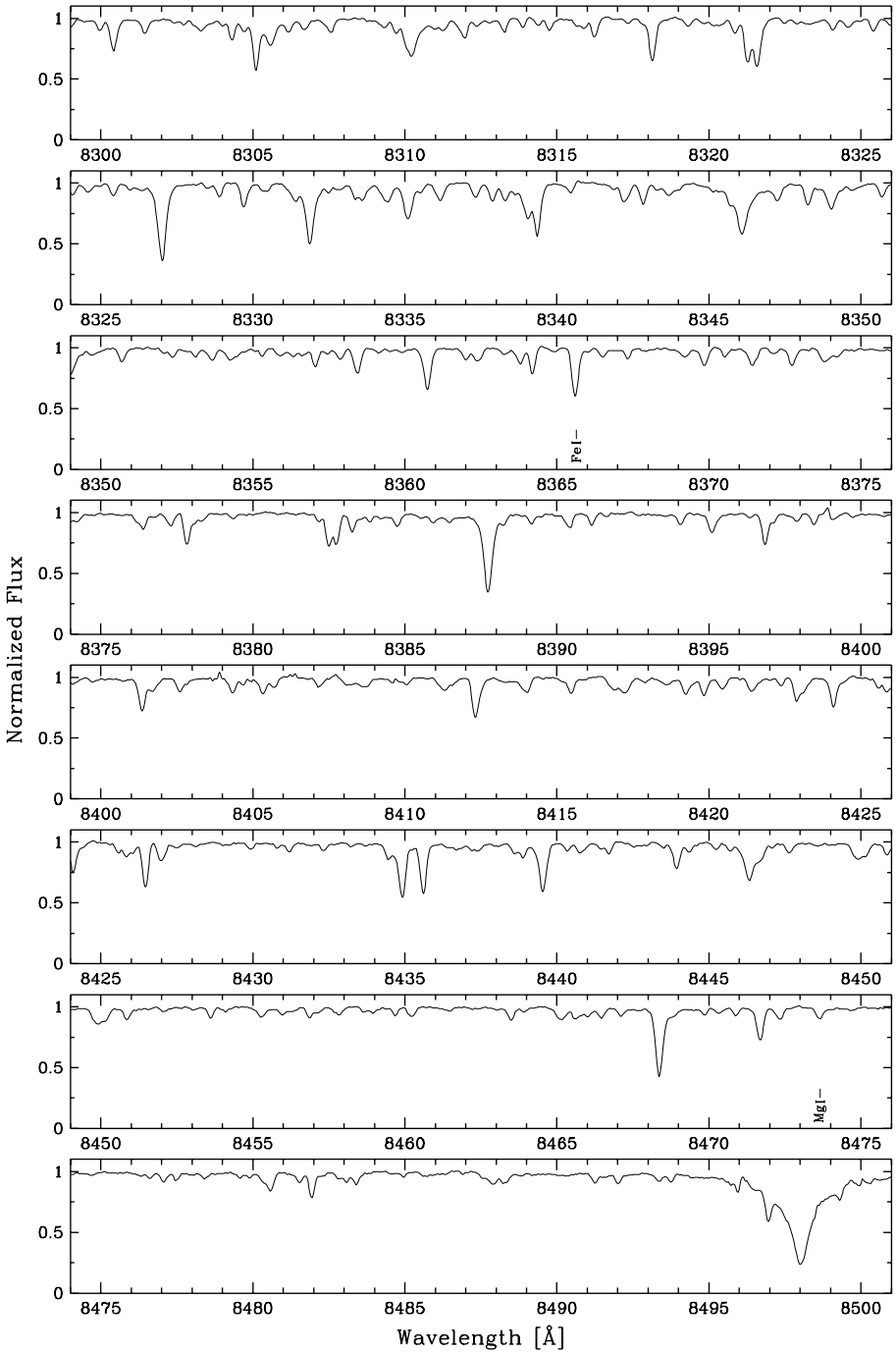
Normalized Flux
Wavelength [Å]
Fe I
Mg I

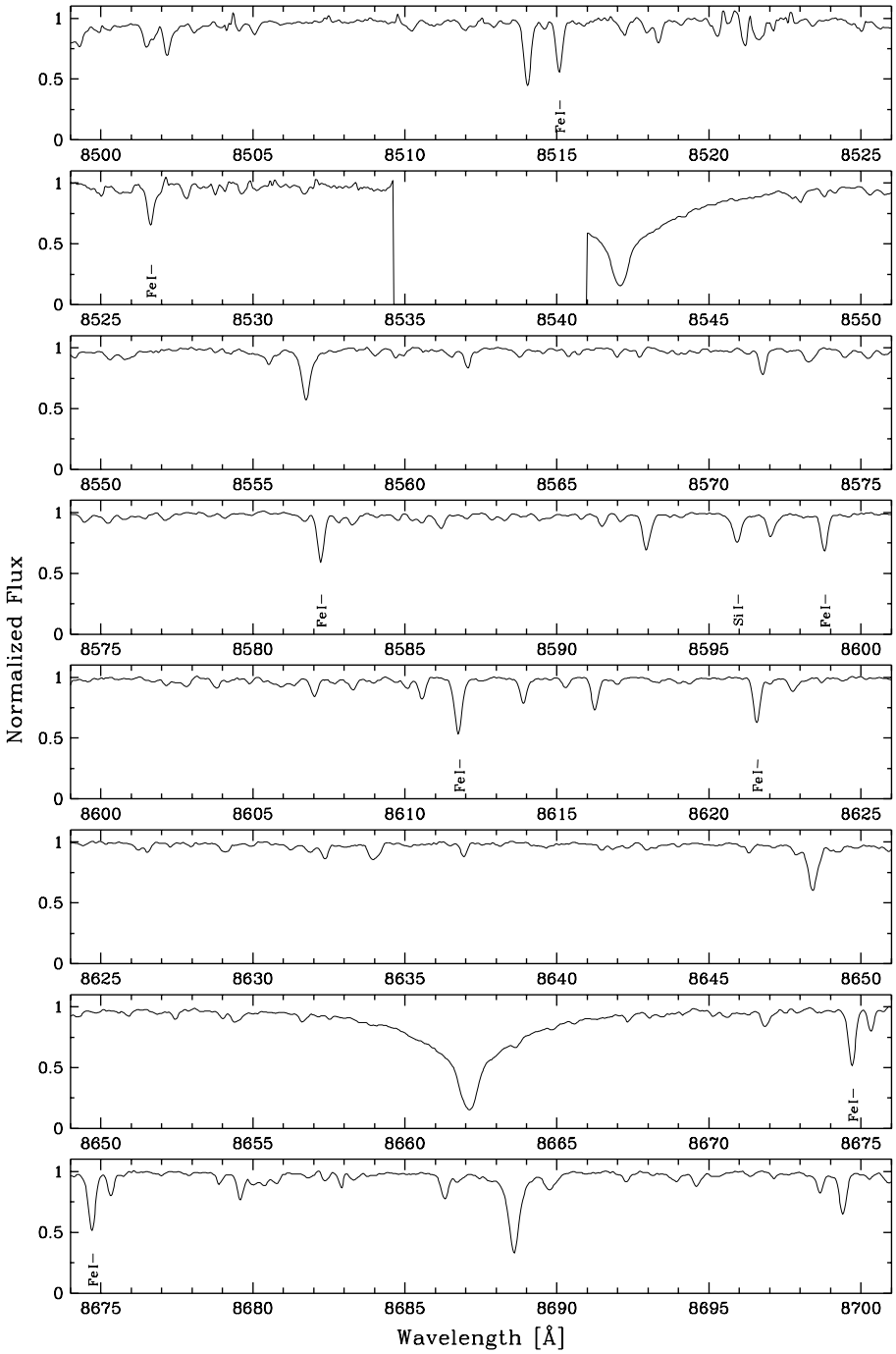
Normalized Flux
Wavelength [Å]
Fe I
Si I

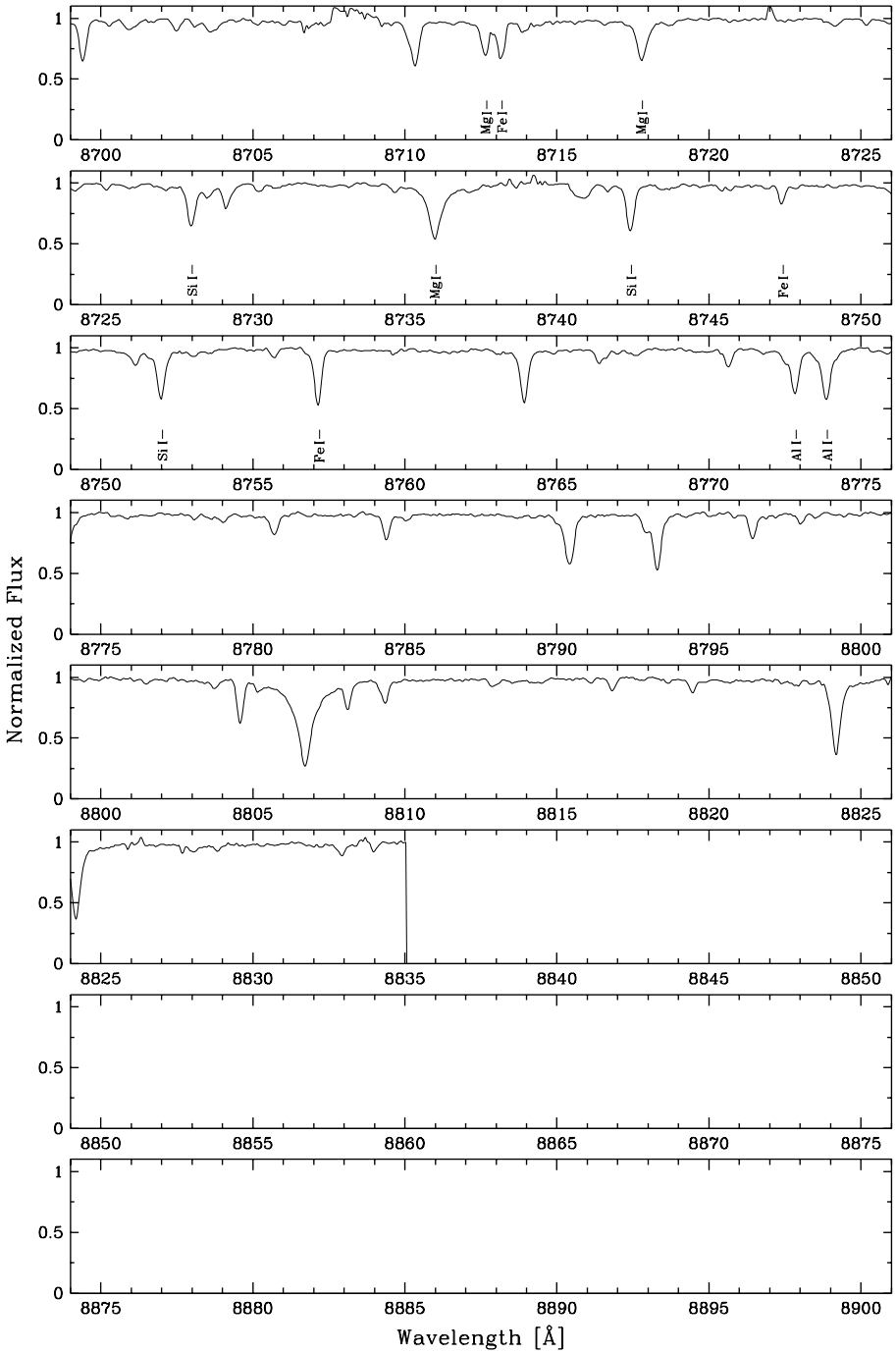
Normalized Flux
Wavelength [Å]
Mg I
Fe I
Mg I
Si I
Mg I
Si I
Fe I
Si I
Fe I
Al I
Al I

References

Alonso, A., Arribas, S., & Martinez-Roger, C. 1995, A&A, 297, 197

Anstee, S. D., & O'Mara, B. J. 1995, MNRAS, 276, 859

Arnett, D. 1996, Supernovae and nucleosynthesis. an investigation of the history of matter, from the Big Bang to the present (Princeton series in astrophysics, Princeton, NJ: Princeton University Press)

Asplund, M., Gustafsson, B., Kiselman, D., & Eriksson, K. 1997, A&A, 318, 521

Bachor, H. A., & Kock, M. 1980, Journal of Physics B Atomic Molecular Physics, 13, 2497

Ballester, P., Boitquin, O., Modigliani, A., & Wolf, S. 2003, UVES Pipeline User's Manual, Doc. No. VLT-MAN-ESO-19500-2964, Issue 5 (UVES Pipeline V2.0.0) (European Southern Observatory)

Barbier-Brossat, M., Petit, M., & Figon, P. 1994, A&AS, 108, 603

Bard, A., & Kock, M. 1994, A&A, 282, 1014

Barklem, P. S., & O'Mara, B. J. 1997, MNRAS, 290, 102

—. 1998, MNRAS, 300, 863

Barklem, P. S., O'Mara, B. J., & Ross, J. E. 1998, MNRAS, 296, 1057

Barklem, P. S., Piskunov, N., & O'Mara, B. J. 2000, A&AS, 142, 467

Becker, U., Zimmermann, P., & Holweger, H. 1980, Geochim. Cosmoch. Acta, 44, 2145

Biémont, E., & Zeippen, C. J. 1992, A&A, 265, 850

Binney, J., & Merrifield, M. 1998, Galactic astronomy (Princeton series in astrophysics, Princeton University Press)

Blackwell, D. E., Booth, A. J., Menon, S. L. R., & Petford, A. D. 1986, MNRAS, 220, 289

Blackwell, D. E., Ibbetson, P. A., Petford, A. D., & Shallis, M. J. 1979a, MNRAS, 186, 633

Blackwell, D. E., Menon, S. L. R., & Petford, A. D. 1983, MNRAS, 204, 883

Blackwell, D. E., Menon, S. L. R., Petford, A. D., & Shallis, M. J. 1982a, MNRAS, 201, 611

Blackwell, D. E., Petford, A. D., & Shallis, M. J. 1979b, MNRAS, 186, 657

Blackwell, D. E., Petford, A. D., Shallis, M. J., & Leggett, S. 1982b, MNRAS, 199, 21

Blackwell, D. E., Petford, A. D., Shallis, M. J., & Simmons, G. J. 1980, MNRAS, 191, 445

—. 1982c, MNRAS, 199, 43

Blackwell, D. E., Petford, A. D., & Simmons, G. J. 1982d, MNRAS, 201, 595

Boesgaard, A. M., & Steigman, G. 1985, ARA&A, 23, 319

Booth, A. J., Blackwell, D. E., Petford, A. D., & Shallis, M. J. 1984, MNRAS, 208, 147

Bridges, J. M., & Kornblith, R. L. 1974, ApJ, 192, 793

Burkert, A., Truran, J. W., & Hensler, G. 1992, ApJ, 391, 651

Buser, R. 2000, Science, 287, 69

Busso, M., Gallino, R., & Wasserburg, G. J. 1999, ARA&A, 37, 239

Cayrel, R., Hill, V., Beers, T. C., Barbuy, B., Spite, M., Spite, F., Plez, B., Andersen, J., Bonifacio, P., François, P., Molaro, P., Nordström, B., & Primas, F. 2001, Nature, 409, 691

Chiappini, C., Romano, D., & Matteucci, F. 2003, MNRAS, 339, 63

Christlieb, N., Bessell, M. S., Beers, T. C., Gustafsson, B., Korn, A., Barklem, P. S., Karlsson, T., Mizuno-Wiedner, M., & Rossi, S. 2002, Nature, 419, 904

Dalcanton, J. J., & Bernstein, R. A. 2002, AJ, 124, 1328

Dehnen, W., & Binney, J. J. 1998, MNRAS, 298, 387

Edvardsson, B., Andersen, J., Gustafsson, B., Lambert, D. L., Nissen, P. E., & Tomkin, J. 1993, A&A, 275, 101

ESA. 1997, The HIPPARCOS and TYCHO catalogues. (Noordwijk, Netherlands: ESA Publications Division, Series: ESA SP Series vol no: 1200)

Feltzing, S., & Holmberg, J. 2000, A&A, 357, 153

Feltzing, S., Holmberg, J., & Hurley, J. R. 2001, A&A, 377, 911

Freeman, K., & Bland-Hawthorn, J. 2002, ARA&A, 40, 487

Fuhrmann, K. 1998, A&A, 338, 161

—. 2002, New Astronomy, 7, 161

Gallagher, A. 1967, Physical Review, 157, 24

Garz, T. 1971, A&A, 10, 175

Gilmore, G. 2003, in Revista Mexicana de Astronomia y Astrofisica Conference Series, 149–157

Gilmore, G., & Reid, N. 1983, MNRAS, 202, 1025

Gilmore, G., Wyse, R. F. G., & Jones, J. B. 1995, AJ, 109, 1095

Gilmore, G., Wyse, R. F. G., & Kuijken, K. 1989, ARAA, 27, 555

Gilmore, G., Wyse, R. F. G., & Norris, J. E. 2002, ApJL, 574, L39

Girardi, L., Bressan, A., Bertelli, G., & Chiosi, C. 2000, A&AS, 141, 371

Gratton, R. G., Carretta, E., Eriksson, K., & Gustafsson, B. 1999, A&A, 350, 955

Gray, D. F. 1992, The observation and analysis of stellar photospheres, 2nd ed. (Cambridge Astrophysics Series, Cambridge: Cambridge University Press)

Grevesse, N., Blackwell, D. E., & Petford, A. D. 1989, A&A, 208, 157

Grevesse, N., & Sauval, A. J. 1998, Space Science Reviews, 85, 161

Gurtovenko, E. A., & Kostik, R. I. 1981, A&AS, 46, 239

Gustafsson, B., Bell, R. A., Eriksson, K., & Nordlund, A. 1975, A&A, 42, 407

Hänninen, J., & Flynn, C. 2002, MNRAS, 337, 731

Hauck, B., & Mermilliod, M. 1998, A&AS, 129, 431

Herschel, W. 1785, Philosophical Transactions of the Royal Society of London, 75, 213

Hibbert, A., Biemont, E., Godefroid, M., & Vaeck, N. 1991, Journal of Physics B Atomic Molecular Physics, 24, 3943

Huang, S., & Carlberg, R. G. 1997, ApJ, 480, 503

Ilyin, I. V. 2000, Ph.D. Thesis, University of Oulo, Finland

Johansson, S., Litzén, U., Lundberg, H., & Zhang, Z. 2003, ApJL, 584, L107

Kim, Y., Demarque, P., Yi, S. K., & Alexander, D. R. 2002, ApJS, 143, 499

Kostyk, R. I. 1981, Astrometriia i Astrofizika, 45, 3

Kroupa, P. 2002, MNRAS, 330, 707

Kupka, F., Piskunov, N., Ryabchikova, T. A., Stempels, H. C., & Weiss, W. W. 1999, A&AS, 138, 119

Laird, J. B., Carney, B. W., Rupen, M. P., & Latham, D. W. 1988, AJ, 96, 1908

Lambert, D. L., & Warner, B. 1968, MNRAS, 138, 181

Lawler, J. E., Wickliffe, M. E., den Hartog, E. A., & Sneden, C. 2001, ApJ, 563, 1075

Lawler, W., & Dakin, J. T. 1989, Optical Society of America Journal B Optical Physics, 6, 1457

Livio, M. 2001, in Supernovae and Gamma-Ray Bursts: the Greatest Explosions since the Big Bang, (eds) M. Livio, N. Panagia, K. Sahu., STScI symp. ser. Vol. 13,, Cambridge University Press, p. 334

Maeder, A. 2000, New Astronomy Review, 44, 291

Majewski, S. R. 1993, ARA&A, 31, 575

Mateo, M. L. 1998, ARA&A, 36, 435

Matteucci, F. 2001, The chemical evolution of the Galaxy (Astrophysics and space science library, Volume 253, Dordrecht: Kluwer Academic Publishers)

May, M., Richter, J., & Wichelmann, J. 1974, A&AS, 18, 405

McWilliam, A. 1997, ARA&A, 35, 503

McWilliam, A., & Rich, R. M. 1994, ApJS, 91, 749

Meylan, T., Furenlid, I., Wiggs, M. S., & Kurucz, R. L. 1993, ApJS, 85, 163

Nissen, P. E., Primas, F., Asplund, M., & Lambert, D. L. 2002, A&A, 390, 235

Nitz, D. E., Wickliffe, M. E., & Lawler, J. E. 1998, ApJS, 117, 313

O'Brian, T. R., Wickliffe, M. E., Lawler, J. E., Whaling, J. W., & Brault, W. 1991, Optical Society of America Journal B Optical Physics, 8, 1185

Ortolani, S., Renzini, A., Gilmozzi, R., Marconi, G., Barbuy, B., Bica, E., & Rich, R. M. 1995, Nature, 377, 701

Pickering, J. C., Thorne, A. P., & Perez, R. 2001, ApJS, 132, 403

Piskunov, N. E., Kupka, F., Ryabchikova, T. A., Weiss, W. W., & Jeffery, C. S. 1995, A&AS, 112, 525

Pitts, R. E., & Newsom, G. H. 1986, J. Quant. Spectrosc. Radiat. Transfer, 35, 383

Pompéia, L., Barbuy, B., & Grenon, M. 2002, ApJ, 566, 845

Quinn, P. J., Hernquist, L., & Fullagar, D. P. 1993, ApJ, 403, 74

Raassen, A. J. J., & Uylings, P. H. M. 1998, A&A, 340, 300

Reshetnikov, V., & Combes, F. 1997, A&A, 324, 80

Richter, J., & Wulff, P. 1970, A&A, 9, 37

Salasnich, B., Girardi, L., Weiss, A., & Chiosi, C. 2000, A&A, 361, 1023

Schwarzkopf, U., & Dettmar, R.-J. 2000, A&A, 361, 451

Silk, J., & Wyse, R. F. G. 1993, Physics Reports, 231, 295

Sneden, C., McWilliam, A., Preston, G. W., Cowan, J. J., Burris, D. L., & Armosky, B. J. 1996, ApJ, 467, 819

Spergel, D. N., Verde, L., Peiris, H. V., Komatsu, E., Nolta, M. R., Bennett, C. L., Halpern, M., Hinshaw, G., Jarosik, N., Kogut, A., Limon, M., Meyer, S. S., Page, L., Tucker, G. S., Weiland, J. L., Wollack, E., & Wright, E. L. 2003, ApJS, 148, 175

Thévenin, F., & Idiart, T. P. 1999, ApJ, 521, 753

Thielemann, F.-K., Argast, D., Brachwitz, F., Martinez-Pinedo, G., Rauscher, T., Liebendörfer, M., Mezzacappa, A., Höflich, P., & Nomoto, K. 2002, ApSS, 281, 25

Tinsley, B. M. 1979, ApJ, 229, 1046

Unavane, M., Wyse, R. F. G., & Gilmore, G. 1996, MNRAS, 278, 727

Velázquez, H., & White, S. D. M. 1999, MNRAS, 304, 254

Walker, I. R., Mihos, J. C., & Hernquist, L. 1996, ApJ, 460, 121

Wallerstein, G., Iben, I. J., Parker, P., Boesgaard, A. M., Hale, G. M., Champagne, A. E., Barnes, C. A., Käppeler, F., Smith, V. V., Hoffman, R. D., Timmes, F. X., Sneden, C., Boyd, R. N., Meyer, B. S., & Lambert, D. L. 1997, Reviews of Modern Physics, 69, 995

Wickliffe, M. E., & Lawler, J. E. 1997, ApJS, 110, 163

Wiese, W. L., Smith, M. W., & Glennon, B. M. 1966, Atomic transition probabilities. Vol.: Hydrogen through Neon. A critical data compilation (NSRDS-NBS 4, Washington, D.C.: US Department of Commerce, National Buereau of Standards, 1966)

Wolnik, S. J., Berthel, R. O., & Wares, G. W. 1971, ApJL, 166, L31

Wyse, R. F. G., & Gilmore, G. 1992, AJ, 104, 144

—. 1995, AJ, 110, 2771

Wyse, R. F. G., Gilmore, G., & Franx, M. 1997, ARA&A, 35, 637

Yi, S., Demarque, P., Kim, Y., Lee, Y., Ree, C. H., Lejeune, T., & Barnes, S. 2001, ApJS, 136, 417

Yi, S. K., Kim, Y., & Demarque, P. 2003, ApJS, 144, 259